Properties of ionic liquids for spinning of cellulose and recycling via freeze crystallization

Liu, Yanrong

Publication date:
2017

Document Version
Publisher's PDF, also known as Version of record

Properties of ionic liquids for spinning of cellulose and recycling via freeze crystallization

Yanrong Liu (刘艳荣)

Ph.D. Thesis

December 2017

DTU Chemical Engineering

Department of Chemical and Biochemical Engineering

Properties of ionic liquids for spinning of cellulose and recycling via freeze crystallization

This thesis was prepared by

Yanrong Liu (刘艳荣)

Supervised by

Professor Anne S. Meyer (main supervisor, DTU)

Professor Suojiang Zhang (main supervisor, IPE)

Associate professor Kaj Thomsen (co-supervisor, DTU)

Professor Yi Nie (co-supervisor, IPE)

December 2017

Center for Bioprocess Engineering & Center for Energy Resources Engineering

Department for Chemical and Biochemical Engineering

Technical University of Denmark

PREFACE

This thesis is submitted in partial fulfillment of the requirements for the Doctorate (PhD) degree at the Technical University of Denmark (DTU). The work displayed in this thesis was conducted during my PhD study at the Department of Chemical and Biochemical Engineering, DTU and Beijing Key Laboratory of Ionic Liquids Clean Process (ILC), Institute of Process Engineering (IPE) from January 1th, 2015 until December 31th, 2017. The PhD study was supervised by:

Main supervisor; Professor, PhD, Anne S. Meyer (BioEng, DTU)
Main supervisor; Professor, PhD, Suojiang Zhang (ILC, IPE)
Co-supervisor; Associate professor, PhD, Kaj Thomsen (CERE, DTU)
Co-supervisor; Professor, PhD, Yi Nie (ILC, DTU)

The PhD thesis work was funded by grants jointly provided by the Institute of Process Engineering, Chinese Academy of Sciences, China and Dept. of Chemical and Biochemical Engineering, DTU, Denmark.

Prediction screening of ionic liquids for dissolving cellulose by COSMO-RS and experimental verification were performed at ILC, IPE and BioEng, and CERE, DTU. Freezing point measurement and determination of water-ionic liquid (IL) mixtures was finished at CERE and BioEng, DTU. Low energy recycling of ionic liquids via freeze crystallization during cellulose spinning was performed at CERE and BioEng, DTU, and ILC, IPE. Wet-spinning conductive cellulose fiber base on ionic liquids as solvent manufacturing and fiber properties analysis were carried out at ILC, IPE. The enzymatic modification for conductive MWCNTs-cellulose fiber was done at BioEng and CERE, DTU.

Yanrong Liu

Yanrong Liu

DTU, 31th of December, 2017

ACKNOWLEDGEMENTS

I sincerely thank my main supervisors Anne S. Meyer and Suojiang Zhang, and my co-supervisors Kaj Thomsen and Yi Nie for accepting me as a joint PhD student at DTU and IPE. I am very grateful to them for the valuable comments in my PhD study and precious time to supervise my study, and special thanks to my supervisors for continuous support and encouragement. I also wish to thank Michael Krogsgaard Nielsen (BioEng, DTU) and Zacarias Tecle (CERE, DTU) for assisting me with handling the experimental facilities. And I am grateful to Philip L. Fosbøl (CERE, DTU), Ming Liu (BioEng, DTU) and Yuhong Huang (BioEng, DTU) for sharing knowledge, access to facilities, and valuable comments.

I would like to thank Hariklia N. Gavala, Thi Thuy Hang Cao and Anna Burniol Figols, with whom I shared an office, for their valuable help and sharing of laughs and thoughts.

Special thanks go to Xiaochun Zhang, Feng Huo and Yongsheng Zhao for many helpful suggestion in the COSMO-RS calculation. Wenjun Wang, Liangyu Ma, Zhaoqing Kang and Xue Liu are thanked for helping with synthesis of ionic liquids, cellulose solubility measurement and partly analytical work. And many thanks to Line Munk and Demi Tristan Djajadi for providing the enzyme to me.

Finally, I wish to thank my family, in particular my parents for their continuous support and never ending love.

ABSTRACT

The overall hypotheses underlying this PhD work were that: a) It is possible to produce conductive carbon nano-tube-cellulose based fibers with improved strength using ionic liquids (ILs) and enzymes in the spinning process. b) It is possible to predict the cellulose solubilisation properties of ILs via thermodynamic modeling of the cellulose and IL properties using COSMO-RS. c) Freeze crystallization of water is an energy saving way to separate IL+H_2O mixtures for ILs recycling in cellulose spinning processes as compared to separation by evaporation. In turn, the main work objectives were: (1) Identify the best ILs for dissolving cellulose. (2) Assess energy-use via freeze crystallization for recycling of the ILs to reduce the cost. (3) Prepare conductive fibers based on spinning of cellulose and carbon nano-tubes using ILs for dissolution and assess enzymatic improvement of fiber tensile strength by use of laccase. Due to strong the hydrogen bonds (H-bonds) in its supra-molecular structure, cellulose is insoluble in water and in most organic solvents. Traditional cellulose spinning processes (e.g. for textile manufacture) therefore often involve use of strong acid or alkali, which in turn poses an environmental burden. As outlined above, this study was based on that ionic liquids might be useful for cellulose dissolution. For this, the following research parts were completed:

First, 375 ILs candidates were screened by COSMO-RS modelling for cellulose dissolution properties. As a part of this, a comparison of cellulose models in COSMO-RS was performed, identifying the mid-monomer in cellotriose as best, and enthalpy calculations of cellulose dissolution in 7 relevant, selected ILs was accomplished, and the cellulose dissolution experimentally verified. COSMO-RS excess enthalpy predictions indicated that the cellulose dissolution process is mostly anion dependent and the main forces in the cellulose dissolution in ILs are H-bonds: Ac^-, Cl^-, DEP^-, and Br^- were the most promising anions for cellulose dissolution. Cations with ethyl, allyl, 2-hydroxylethyl, 2-methoxyethyl and acryl-oyloxypropyl functional groups exhibited particularly good properties for cellulose dissolution.

Second, recycling ILs from water mixtures by freeze crystallization was conducted. Six ILs, EmimAc, EmimDep, AmimCl, HOEtpyBr, HOEtmimBr, and EtOMmimCl, which had been found to have high cellulose solubility in phase one, were selected for freezing point measurements alone and in ILs+H_2O mixtures. The results illustrated that the ILs exhibit similar features as inorganic salts of $MgCl_2$ and $MgSO_4$ in depressing the freezing point of water. Ice starts forming when the IL aqueous solutions are cooled to their freezing points in the dilute region. At higher IL concentrations, the solid phases formed were presumed to be solid IL or hydrates of the form IL·$n$$H_2O$. The HOEtpyBr+$H_2O$ and HOEtmimBr+H_2O systems formed simple eutectic systems and the freeing points of these two system were higher than those of the other four ILs. This result indicated that these two bromide ILs could be separated from water directly by freeze crystallization of the water. From the experimental results it was moreover determined that the freezing points of IL+H_2O systems were affected by the nature of both the cations and the anions of the ILs.

Third, separation of IL+H_2O by freeze crystallization was applied to recycling EmimAc and EmimDep, respectively, in the cellulose spinning process, and the methodology was named as the freeze crystallization method. The energy requirement for EmimAc and EmimDep recycling after cellulose spinning by the freeze crystallization method followed by evaporation was calculated and compared to the energy use in a traditional (patented) evaporation method. It was found that to fabricate 1 kg dry cellulose fiber using freeze crystallization+evaporation rather than evaporation, 21.5 MJ can be saved for EmimAc and 37.3 MJ for EmimDep recycling. It was also shown that significantly less H_2O is required in the cellulose spinning process with ILs than with N-methylmorpholine oxide.

Finally, the production of multiwall carbon nanotubes (MWCNTs)-cellulose conductive fibers using a selected IL with good cellulose dissolution properties, namely EmimDep, was studied: The material used was cotton pulp and MWCNTs. The work verified that EmimDep can dissolve cellulose and disperse MWCNTs. The fiber electrical conductivity increased with increasing mass ratio of MWCNTs relative to the

cellulose. The highest electrical conductivity measured was 760 S/m at a spinning extrusion flow of 1 mL/min, spinneret diameter of 0.46 mm and a ratio of 5:1 of MWCNTs versus cellulose. Thermogravimetric analysis and surface area results gave evidence that the fiber was more stable at the spinneret diameter of 0.46 mm than at 0.98 mm. The surface area of the conductive fiber reached 188 m^2/g. The SEM data also revealed pore structures in the fiber surface and hinted that the alignment of MWCNTs in the fiber decreases the fiber electrical conductivity. Tensile strength measurements showed that the fiber tensile strength could be increased by laccase enzyme treatment, provided that phenols were added to the spun cotton pulp-CNTs fiber bath solution. The data obtained verified the hypotheses formulated for the PhD work and provided new knowledge of: ILs cellulose solubility properties, COSMO-RS modelling of cellulose, freezing points and freeze thermodynamics properties of ILs and ILs+H_2O mixtures, energy saving for ILs recycling by freeze crystallization, and finally indicated the promising potential of using ILs and enzymes in the production of conductive CNT-cellulose based fibers.

DANSK SAMMENFATNING

De overordnede hypoteser, der ligger til grund for dette ph.d.-arbejde, var følgende: a) Det er muligt at fremstille ledende carbon nano-rør-cellulose baserede fibre med forbedret styrke ved anvendelse af ioniske væske (IL) og enzymer i spinding processen. b) Det er muligt at forudsige opløsningen af cellulose med IL via termodynamisk modellering af cellulose- og IL-egenskaberne ved anvendelse af COSMO-RS. c) Frysekrystallisation af vand er en energibesparende måde at adskille IL+H_2O-blandinger til ILs-genanvendelse i cellulosespinningsprocesser sammenlignet med separering ved fordampning. Til gengæld var hovedmålene for arbejdet: (1) Identificer de bedste IL'er til opløsning af cellulose. (2) Vurdere energiforbruget via frysekrystallisation til genbrug af IL'er for at reducere omkostningerne. (3) Fremstille ledende fibre baseret på spinning af cellulose og carbon nano-rør ved anvendelse af IL'er til opløsning samt laccase behandling. Derefter vurderes den enzymatiske forbedring af fiberstrækstyrken. På grund af stærke hydrogenbindinger i sin supramolekylære struktur er cellulose uopløselig i vand og i de fleste organiske opløsningsmidler. Traditionelle cellulosespinningsprocesser (for eksempel tekstilfremstilling) involverer derfor ofte stærk syre eller base, der udgør en miljøbelastning. Som beskrevet ovenfor var denne undersøgelse baseret på, at IL kan være nyttige til celluloseopløsning. Til dette blev følgende forskningsarbejde udført:

Først blev 375 IL-typer screenet ved COSMO-RS-modellering for celluloseopløsningsegenskaber. Som en del af dette blev en sammenligning af cellulosemodeller i COSMO-RS udført ved identifikation af cellotriose centermonomeren, og enthalpiberegninger af celluloseopløsning i 7 relevante udvalgte IL'er blev opnået, og celluloseopløsningen blev eksperimentelt verificeret. COSMO-RS overskydende entalpibaserede forudsigelser viste, at celluloseopløsningen for det meste er anionsafhængig, og hovedkræfterne i celluloseopløsningen i IL'er er hydrogenbindinger: Ac^-, Cl^-, DEP^- og Br^- var de mest lovende anioner til celluloseopløsning. Kationer med ethyl-, allyl-, 2-hydroxylethyl-, 2-methoxyethyl- og

acryl-oyloxypropylfunktionelle grupper udviste særligt gode egenskaber til celluloseopløsning.

For det andet blev genanvendelse af IL separeret fra H_2O-blandinger ved frysekrystallisation udført. Seks IL'er: EmimAc, EmimDep, AmimCI, HOEtpyBr, HOEmimBr og EtOMmimCI, som viste sig at have høj celluloseopløselighed i fase 1, blev valgt til frysepunktsmålinger alene og i (IL+H_2O)-blandinger. Resultaterne viste, at IL'erne udviser lignende træk som uorganiske salte af $MgCl_2$ og $MgSO_4$ ved frysepunktssænkning i vand. Is begynder at blive dannet, når IL+H_2O opløsninger afkøles til deres frysepunkter i den fortyndede region. Ved højere IL-koncentrationer antages de dannede faste faser at være fast IL eller hydrater af formen IL·nH_2O. HOEtpyBr+H_2O- og HOEtmimBr+H_2O-systemer dannede enkle eutektiske systemer, og frigivelsespunkterne for disse to systemer var højere end for de fire andre IL'er. Dette resultat viste, at disse to bromid-IL'er kunne separeres fra vand direkte ved frysekrystallisation af vandet. Ud fra de eksperimentelle resultater blev det desuden fastslået, at frysepunkterne for IL+H_2O-systemer var påvirket af egenskaberne af både kationerne og anionerne i IL.

For det tredje blev adskillelse af IL+H_2O ved frysekrystallisation udført til recirkulering af henholdsvis EmimAc og EmimDep i cellulosespinningsprocessen, og fremgangsmåden blev betegnet som frysekrystallisationsfremgangsmåden. Energikravet til regenerering af EmimAc og EmimDep efter cellulose spinning ved frysekrystallisationsmetoden efterfulgt af fordampning blev beregnet og sammenlignet med en traditionel (patenteret) fordampningsmetode. Det blev konstateret, at 21,5 MJ kan spares ved EmimAc og 37,3 MJ ved EmimDep-regenerering ved fremstilling af 1 kg tør cellulosefiber ved anvendelse af frysekrystallisation+fordampning frem for inddampning. Det blev også vist, at der kræves signifikant mindre H_20 i cellulosespinningsprocessen med IL'er end med N-methylmorpholinoxid.

Endelig blev produktionen af flerlags kulstof nanorør (MWCNT)-cellulose ledende fibre under anvendelse af et udvalgt IL med gode celluloseopløsningsegenskaber,

nemlig EmimDep, undersøgt: Det anvendte materiale var bomuldsmasse og MWCNT'er. Arbejdet bekræftede, at EmimDep kan opløse cellulose og sprede MWCNT'er. Fiberens elektriske ledningsevne øgedes med stigende masseforhold MWCNT'er i forhold til cellulose. Den højeste elektriske ledningsevne målt var 760 S/m ved et spin-ekstrusionsstrøm på 1 mL/min, spinnerdiameter på 0,46 mm og et forhold på 5:1 MWCNT'er versus cellulose. Termogravimetrisk analyse og overfladeareal resultater viste, at fiberen var mere stabil ved spindeldiameteren 0,46 mm end ved 0,98 mm. Overfladearealet af den ledende fiber nåede 188 m^2/g. SEM-dataene afslørede også porestrukturer i fiberoverfladen og antydede, at justeringen af MWCNT'er i fiberen reducerer fiberens elektriske ledningsevne. Trækstyrke målinger viste, at fiberens trækstyrke kunne forøges ved laccase-enzymbehandling, forudsat at phenoler blev tilsat til den spinde bomuldsmasse-CNT fiberbadopløsning. De opnåede data bekræftede hypoteserne formuleret til ph.d.-arbejdet og gav ny viden om: IL'er celluloseopløselighedsegenskaber, COSMO-RS-modellering af cellulose, frysepunkter og frysetermodynamiske egenskaber af ILs og IL+H_2O-blandinger, energibesparelse til IL-genvinding ved frysekrystallisation og endelig angav det lovende potentiale ved anvendelse af IL'er og enzymer til fremstilling af ledende CNT-cellulosebaserede fibre.

LIST OF PUBLICATIONS

This PhD thesis is based on the following papers, which will be referred to by their roman numerals in the text:

I Yan-Rong Liu, Kaj Thomsen, Yi Nie, Suo-Jiang Zhang and Anne S. Meyer

Predictive screening of ionic liquids for dissolving cellulose and experimental verification

Green Chemistry, 2016, 18, 624−625.

II Yanrong Liu, Anne S. Meyer, Yi Nie, Suojiang Zhang, Yongsheng Zhao, Philip L. Fosbøl, Kaj Thomsen

Freezing point determination of water-ionic liquid mixtures

Journal of Chemical & Engineering Data, 2017, 62, 2374−2383.

III Yanrong Liu, Anne S. Meyer, Yi Nie, Suojiang Zhang, Kaj Thomsen

Low energy recycling of ionic liquids via freeze crystallization during cellulose spinning

Green Chemistry, 2017, DOI: 10.1039/C7GC02880F.

IV Yanrong Liu, Yi Nie, Kaj Thomsen, Suojiang Zhang, Anne S. Meyer

Wet-spinning conductive cellulose fiber base on ionic liquids as solvent and enzymatic modification

Yet to be submitted

TABLE OF CONTENTS

CHAPTER I−Introduction

1.1 Motivation of study

Electrically conductive polymer fibers may bring desirable applications to the electrochemical and biomedical fields, such as electronic devices, capacitor electrodes, neural probes, biosensors and bio-actuators, and shielding materials [1-3]. The conductive fillers are carbon black (CB), carbon nanotubes (CNTs) and graphene nanoplatelets (GNP). It has been evidenced that CNTs is a remarkable candidate as a conductive filler, better than CB and GNP [3]. Moreover, CNTs have many merits of unique tubular structures, nanometer diameter, a large length/diameter ratio [4], high mechanical property and excellent thermal stability [5].

Spinning and dip-drying are the main fabrication methods for CNT conductive fiber.[6] And wet spinning has been reported to be a flexible method to manufacture any type of conductive fiber [7]. Cellulose-based composites are of great importance because of the low cost of cellulose and its biodegradability. Cellulose, combined with CNTs can offer a good biocompatibility, electrical conductivity, and the ability to easily spin into fiber [8]. However, there are three challenges in achieving excellent conductivity cellulose/CNTs fiber: 1) dissolving cellulose by green solvent, 2) avoiding the CNTs entanglement in a solvent. 3) dispersing CNTs uniformly in cellulose solution [9]. To overcome these three challenges, dissolving and dispersing green solvent is the key factor. This potential and desirable green solvent is ionic liquids (ILs).

1.1.1 Aims of study

It has been indicated that dozens to hundreds of ILs were studied to dissolve cellulose. However, none of them has been employed in industry and the efficient type ILs for dissolving cellulose still needs to be determined. Hence, a rapid and a priori screening method to predict the cellulose solubility capacity for numerous ILs is needed in

chemical engineering research and industry. In addition, recycling ILs after the fiber fabrication is one of the key factors for successful IL application in industry because of its environmental friendliness and economic viability.

For the manufacturing the conductive fiber, the CNT is an excellent conductive material. With the increase of the amount of CNTs, the conductivity is increased with the decrease of the fiber tensile strength. Understanding the properties of cellulose conductive fiber and designing an efficient method to improve the tensile strength of the conductive fiber will greatly help to apply the cellulose conductive fiber. This Ph.D. study was conducted to realize the above purpose and expedite the cellulose conductive fiber application.

1.1.2 Hypotheses

Cotton pulp, MWCNTs and EmimDep were selected as the material for the production the cellulose conductive fiber in this study. The hypotheses of the Ph.D. study are as follows:

- Cellulose mode and the cation and anion structure of ILs both affect the COSMO-RS prediction results of cellulose solubility.
- Freezing point depression measurement values can be used for recycling the ILs from water mixture.
- Freeze crystallization recycling method will save energy for recycling ILs from water mixture in the cellulose fiber production process by wet spinning.
- Conductivity will increase with the increased amount of CNTs in cellulose, but the tensile strength will decrease.
- Enzymatic modification treatment method (Laccase+phenol) for cellulose or cellulose conductive fiber will increase the tensile strength of the fiber.

1.1.3 Objectives

The main objective of this study was to verify the above hypotheses. The Ph.D. project will be conducted with the following objectives.

- To establish a cellulose's model, ILs structures and screen potential ILs for dissolving the cellulose by COSMO-RS.
- To explain the hydrogen bonding capacity of cations and anions of ionic liquids for dissolving cellulose via COSMO-RS simulations.
- To synthesize several kinds of potential ionic liquids and do experiments for validating the COSMO-RS calculation results.
- To establish a new ILs recycling method from ILs+H_2O mixtures.
- To predict the energy requirement base on the new recycling method for recycling ILs form water after cellulose spinning.
- To develop a conductive spinning solution of cellulose using MWCNTs as conductive material and IL as a solvent.
- To fabricate the cellulose conductive fiber by wet spinning and analyze the properties of the fiber.
- To treat the cellulose or cellulose conductive fiber by enzyme modification and to evaluate enzymatic modification by fiber tensile strength.

1.2 Structure of cellulose

Cellulose notable has properties such as biocompatibility, biodegradability, and thermal and chemical stability [10], and is widely used in textiles, coatings, composites, paper products, optical film and other applications. The average cellulose amount in plants is about 33%. For example, the cellulose amount in wood is approximately 40–50% and that of cotton is 90% [11]. Cellulose is a linear polymer consisting of from several hundred to over ten thousand β-(1→4)-linked glucose repeating units, together with numerous intermolecular and intramolecular H-bonds [12,13], as illustrated in **Figure 1.1** [12]. The inter- and intra-chain hydrogen bonding network makes cellulose a stable polymer, and gives the cellulose fibrils their high axial stiffness. Cellulose chains are arranged in highly ordered crystalline regions, and regions that are amorphous or disordered (shown in **Figure 1.2)** [14]. These highly ordered crystalline regions and disordered regions make cellulose insoluble in water and common organic solvents [15].

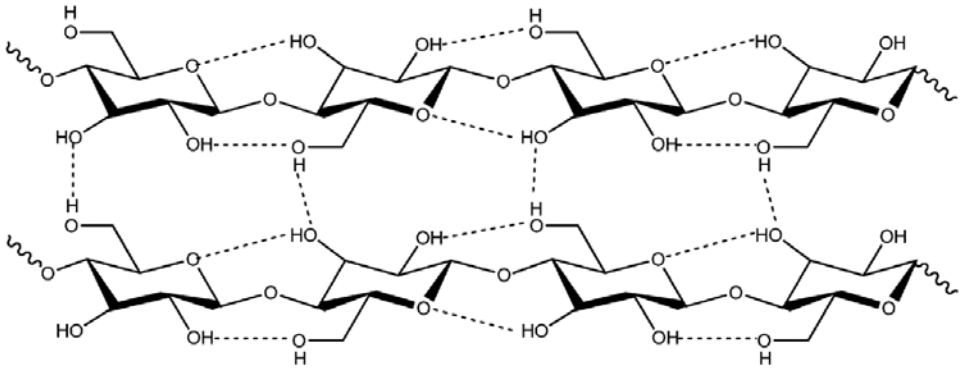

Figure 1.1 Intermolecular and intramolecular hydrogen bonds in cellulose [12].

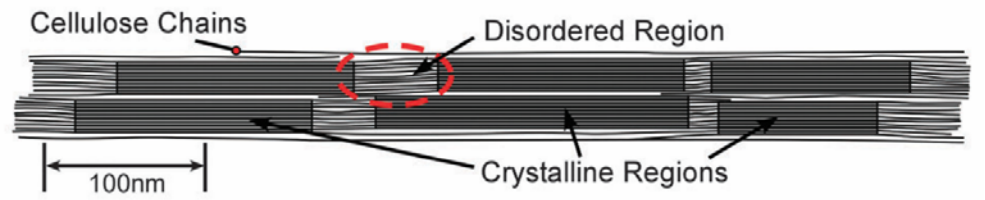

Figure 1.2 Crystalline and amorphous regions of an idealized cellulose microfibril [14].

Figure 1.3 (a) is the structure of biosynthetic cellulose I (native). This structure it has three H-bonds per glucosyl unit, that is two intramolecular H-bonds and one intermolecular H-bond to a neighboring cellulose molecule in the same sheet [16]. It was reported that van der Waals interactions in cellulose I is considered to be the main contribution to the stabilization of cellulose fibrils [17]. Cellulose I can be transformed into a non-natural cellulose II **(Figure 1.3 (b))** by swelling and dissolution/regeneration [18]. This structure is more thermodynamically stable than cellulose I. In the structure of cellulose II, the crystal symmetry is changed compared to cellulose I, and H-bonds between sheets occur [19].

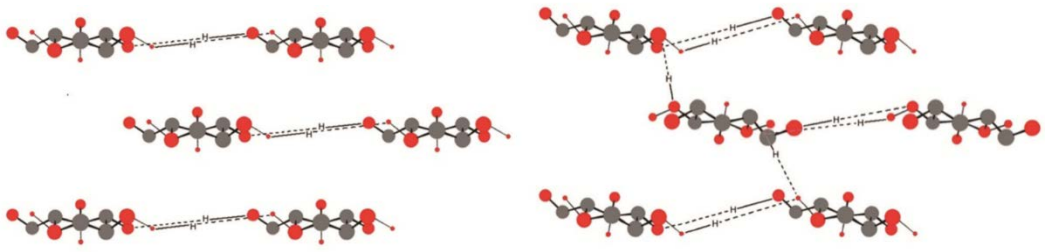

(a) **(b)**

Figure 1.3 (a) Structure of cellulose I [16]. **(b)** Structure of cellulose II [19].

1.3 Cellulose dissolution solvents

1.3.1 Traditional solvents

The first attempt to dissolve cellulose dates back to 1855. George Audemars dissolved the nitrated form of cellulose in a mixture of alcohol and ether, then mixed it with an ether solution of caoutchouc (natural rubber), and discovered that this solution could be drawn out into fine threads or filaments [20]. However, using this method to fabricate cellulose nitrate fibers had the very serious drawback in that they are very flammable.

Since then a series of cellulose dissolution solvents has been developed (**Figure 1.4**) [12], such as N-methylmorpholine oxide (NMMO) [21], N,N-

dimethylacetamide/lithium chloride (DMAc/LiCl) [22], N,N-dimethylformamide/nitrous tetroxide (DMF/N_2O_4) [23], molten salt hydrates ($LiClO_4·3H_2O$, $LiCH_3COO·2H_2O$, $LiCl/ZnCl_2/H_2O$, $NaSCN/KSCN/LiSCN·2H_2O$) [24,25], and aqueous NaOH or aqueous solutions of metal complexes (Cd-tren, Ni-tren and Cuoxam) [26]. Among the above mentioned solvents, NMMO is actually used to make cellulose fibers on an industrial level. In this process, cellulose is dissolved to form a solution named dope, and then the cellulose is regenerated in a water bath to produce a fiber [27]. However, there are some serious disadvantages in the NMMO process, especially its high dissolution temperature and thermally instability which means it has not yet replaced the viscose process to produce cellulose fiber. The other solvents mentioned above show some drawbacks to a different extent, such as high cost, high dissolution temperature, and volatility. Difficulty in solvent recovery and toxicity make them undesirable, and underlines the necessity to develop greener solvents and new technologies for cellulose dissolution [28,29].

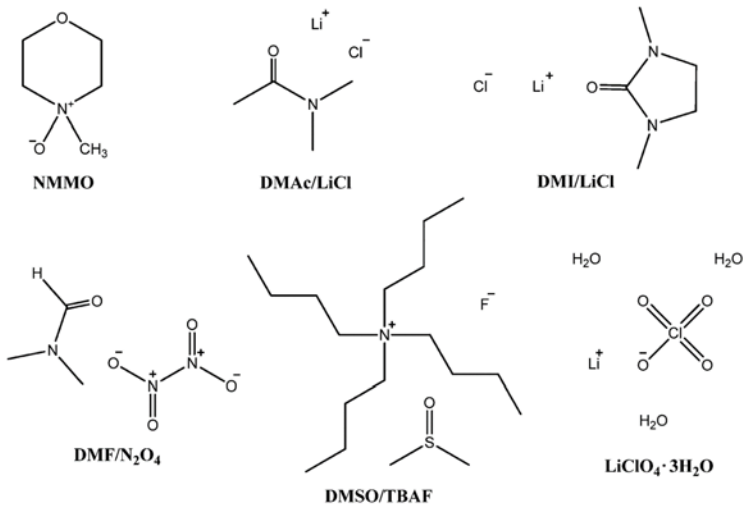

Figure 1.4 Structures of traditional solvents for cellulose dissolution [12].

1.3.2 Ionic liquids

In 1934, Graenacher discovered that benzylpyridinium chloride or N-ethylpyridinium chloride has the ability to dissolve cellulose [30]. This work has been described in hindsight in various ways such as ‘‘the first example of the cellulose

dissolution using ILs" [31], which is commonly defined as salts that melt below 100 ℃ [32].

In 2002, ILs were introduced as new green solvents for cellulose dissolution. It was reported that cellulose could be dissolved without derivatization in high concentrations using ILs, such as 1-butyl-3-methylimidazolium chloride (BmimCl) [33]. This attracted interest for a range of applications [34]. In recent years, more than 60 ILs have been investigated for their ability to dissolve cellulose [12]. The increasing interest in ILs as solvents is due to their remarkable properties such as immeasurably low vapor pressure, excellent chemical and thermal stability, electrical conductivity, nonflammability, etc. The most fascinating property of ILs is the structural diversity, as numerous possible cations and anions can be combined freely [35-37].

1.3.2.1 Cations of ionic liquids

In recent reports, the IL cations which were studied for cellulose dissolution were mainly based on imidazolium$^+$, pyridinium$^+$, pyrrolidinium$^+$, piperidinium$^+$ (**Figure 1.5**) [38]. Brandt et al. indicated that imidazolium-, and pyridinium-based ILs were considered to have high ability to dissolve cellulose [38]. They explained that aromatic rings are easily polarized and the interactions between the cations and anions of aromatic ILs are weak, which can decrease the electrostatic interaction. Zhao et al. illustrated that the heterocyclic structure and alkyl chain length of the cations have an important influence on the interactions of IL anions and cellulose. For imidazolium-based ILs, the shorter the alkyl chain is, the higher the solubility will be [39]. Erdmenger et al. have shown that the functional groups of IL cations has a significant influence on the cellulose solubility [40]. Pinkert et al. indicated that methylimidazolium and methylpyridinium structured with the groups of allyl-, ethyl-, butyl-, or hydroxyl- are the potential IL cations for cellulose dissolution [41]. However, [Me(OEt)$_3$-Bu-Im]OAc and [H(OEt)$_3$-Me-Im]OAc do not have the potential for dissolving cellulose because of the large size of the cations. And [H(OEt)$_3$-Me-Im]OAc easily forms H-bonds with its anion, which decreases the interaction with cellulose [42].

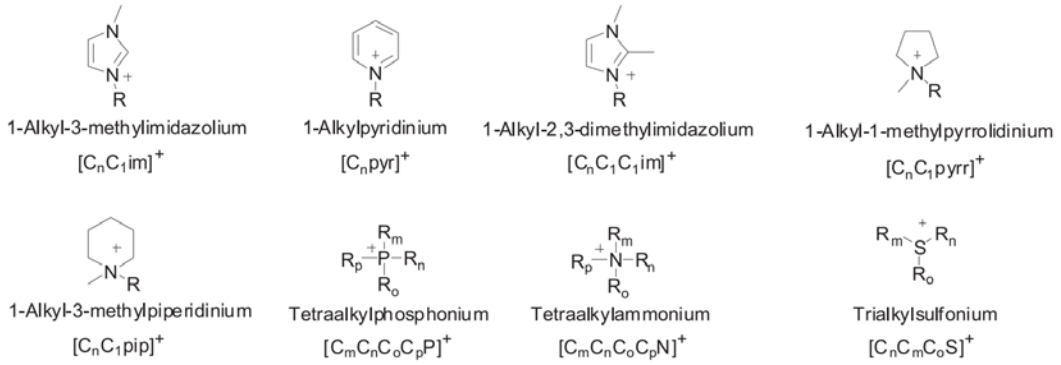

Figure 1.5 Structures of IL cations for cellulose dissolution [38].

1.3.2.2 Anions of ionic liquids

Table 1 lists the IL anions which were studied for cellulose dissolving. It has been shown that the anions most efficient for cellulose dissolving are chloride, acetate, formate, phosphate, sulphate, and sulfonate [43]. Some investigations claimed that the cellulose dissolution process is strongly anion dependent [44,45]. The IL anions, which are good H-bond acceptors are more effective in dissolving cellulose. Zavrel et al. explained that the big size and non-coordinating anions such as PF_6^-, BF_4^- and SCN^- are not conducive to dissolving cellulose [46]. The study also indicated that the higher the H-bond basicity and dipolarity of the anion, the greater is the ability of the IL to dissolve cellulose [12,43]. The suggested ILs anions for dissolving cellulose are:

1) $[(CH_3CH_2O)_2PO_2]^- \approx [OAc]^- > [HSCH_2COO]^- > [HCOO]^- > Cl^- > Br^- > [SCN]^-$ [47].

2) $[(C_5H_5)COO]^- > [H_2NCH_2COO]^- > [HOCH_2COO]^- > [CH_3CHOHCOO]^- > [DCA]^-$ or $[Nf_2T]^-$ [29].

Table 1 Structures of IL anions for cellulose dissolution

Name of anion	Acronym	Structure	Name of anion	Acronym	Structure
Acetate	Ac		Diethylphosphate	DEP	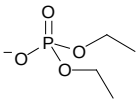
Bromide	Br		Formate	HCOO	
Tetrafluoroborate	BF_4		Hydrogensulfate	HSO_4	
Butylsulfate	$BuSO_4$	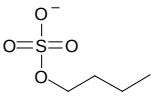	Methoxyethylsulfate	$MeOEtSO_4$	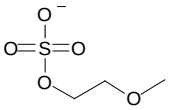
Benzoate	BEN	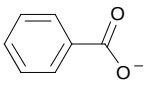	Methylsulfate	$MeSO_4$	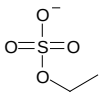
Chloride	Cl		Hexafluorophosphate	PF_6	
Dimethylphosphate	$DMPO_4$	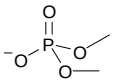	Bis(trifluoromethylsulfonyl)amide	Tf_2N	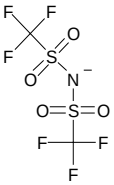

1.3.2.3 Mechanism of cellulose dissolution in ionic liquids

Although the mechanism of the dissolution of cellulose has not been fully determined, it is widely speculated that breaking up the intra- and intermolecular hydrogen bonds in cellulose is the key point in the dissolution process. Zhang et al. studied the dissolution mechanism of cellulose in AmimCl [48]. It was indicated that $Amim^+$ had a smaller ion size due to three carbon atoms and a double bond in AmimCl. Thus, small and strong polarizing cations, and large polarizable anions will have strong interactions with cellulose, which improves cellulose dissolution. **Figure 1.6** is the dissolution mechanism of cellulose in AmimCl explained by Zhang et al [48]. According to **Figure**

1.6, it can be found that the $Amim^+$ cations attached to the oxygen atom of cellulose hydroxyl groups, and the Cl^- anions associated with the cellulose hydroxyl proton, which helps disrupt hydrogen bonding in cellulose and results in the cellulose dissolution.

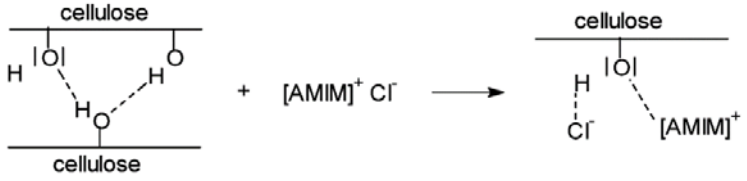

Figure 1.6 Dissolution mechanism of cellulose in AmimCl [48].

Based on the criterion of Zhang et al., Xu and her co-workers [49] described the dissolution mechanism of cellulose in EmimDMP (**Figure 1.7**). According to the assumption of Xu and her co-workers, the $Emim^+$ cations attach to cellulose hydroxyl oxygen and the DMP^- anions bonds with the cellulose hydroxyl proton, which disrupts the cellulose crystallinity.

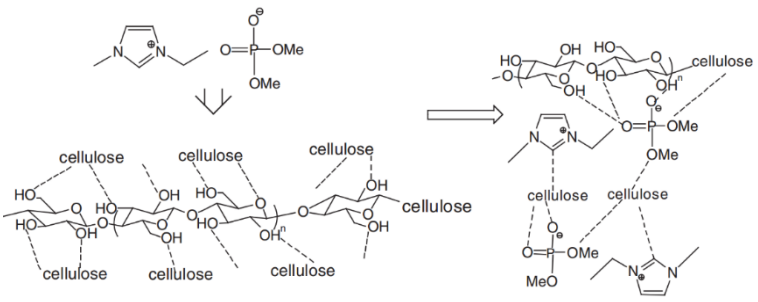

Figure 1.7 Dissolution mechanism of cellulose in EmimDMP [49].

Zhao et al. applied a molecular dynamics method to study the effects of IL structure on cellulose dissolution [39]. AmimCl and C_3mimCl were selected as the candidates to understand the effect of electron-withdrawing groups of the cations on the ability of ILs to dissolve cellulose. According to the spatial distribution functions calculated for AmimCl and C_3mimCl (**Figure 1.8**), it was found that some anions are distributed around the alkyl chain of $Amim^+$ rather than C_3mim^+, which indicates that allyl group can increase the electronegativity of the cation. Then, the interaction energies for

$Amim^+$ and C_3mim^+ together with cellulose were calculated by Zhao et al. The results show that the interaction energy between $Amim^+$ and cellulose (-659.3 kJ/mol) is stronger than the interaction energy between C_3mim^+ and cellulose (-480.8 kJ/mol). These two studies suggested that AmimCl is a better solvent for the dissolution of cellulose than C_3mimCl. Additionally, two configurations from the trajectory files of the interaction between AmimCl and cellulose were provided (**Figure 1.9**). The result illustrates that weak hydrogen bonds were formed between oxygen on the hydroxyl group of cellulose and hydrogen protons at C_8 and C_9 sites on the allyl chain of $[Amim]^+$ [39].

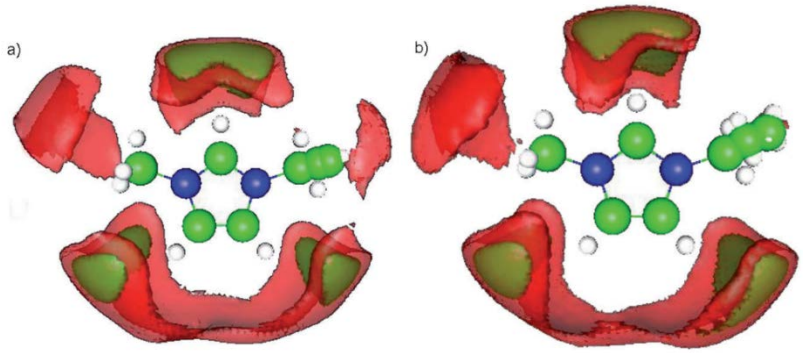

Figure 1.8 Spatial distribution functions for a) AmimCl and b) C_3mimCl [39].

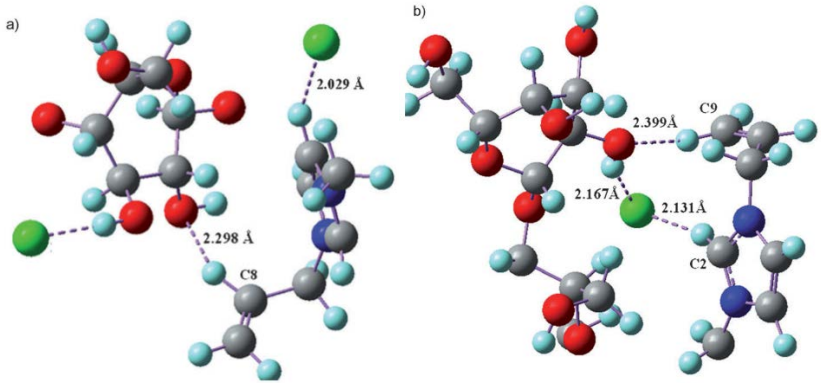

Figure 1.9 Two configurations from the trajectory files of the interaction between AmimCl and cellulose a) C_8H; b) C_9H [39].

Li et al studied the dissolving process of a cellulose bunch in the ILs EmimAc, EmimCl and BmimCl by the molecular dynamics method [44]. A 7×8 bunch (7 glucan chains, each with 8 residues) together with 1200 molecules of EmimAc, EmimCl and

BmimCl separately were used to study the H-bonds between cations/anions and the cellulose bunch. The results show that the number of H-bonds formed between cations and the cellulose bunch is $Emim^+$ (Ac^-, 24) > $Bmim^+$ (16) > $Emim^+$ (Cl^-, 12). And the number of H-bonds formed between anions and the cellulose bunch is Ac^- (152) > Cl^- ($Emim^+$, 110) > Cl^- ($Bmim^+$, 87). Compared with the number of H-bonds formed between cations or anions and the cellulose bunch, it can be found that the number of H-bonds between anions and cellulose bunch is larger than the numbers of cations and cellulose. This indicates that the interaction between the anions and cellulose is the main reason for dissolution, while cations may play a secondary role. The effects of the solvent structure on cellulose dissolution were also investigated by Li et al [44]. **Figure 1.10** displays the state of dissolving cellulose in EmimAc and EmimCl at 100 ns and **Figure 1.11** gives the final configuration of the 7×8 cellulose bunch in EmimCl (a) and BmimCl (b) at 3 μm by Li et al. According to **Figure 1.10** the H-bonds formed by Ac^- with cellulose can effectively loosen the neighboring connected cellulose chains. However, the Cl^- cannot separate cellulose chains at the calculation conditions of 100 ns, which indicates that Ac^- is more efficient than Cl^- for cellulose dissolving. **Figure 1.11** shows that the original cellulose structure is disorganized in EmimCl and BmmimCl but contacts between chains still exist, especially in BmimCl.

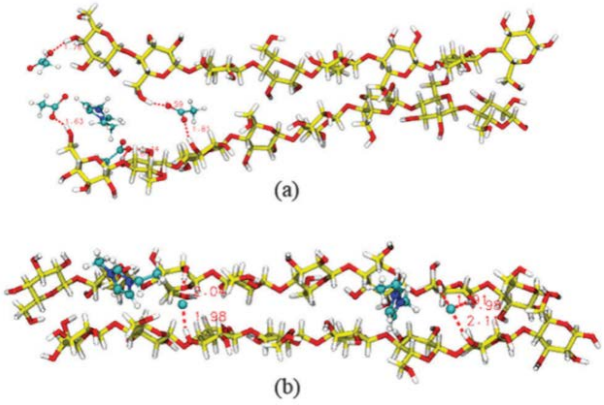

Figure 1.10 Dissolving state of cellulose in EmimAc (a) and EmimCl (b) at 100 ns [44].

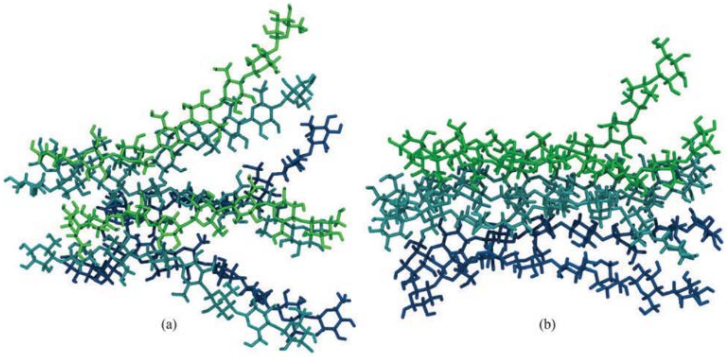

Figure 1.11 Configurations of the cellulose bunch in EmimCl (a) and BmimCl (b) at 3 μs [44].

1.4 COSMO-RS prediction

Due to the large number of ILs that can be synthesized from organic and inorganic cations and anions, it is an enormous challenge to screen the best ILs for dissolving cellulose. A rapid and a priori screening method to predict the cellulose solubility capacity for ILs is urgently needed. COSMO-RS (Conductor-like Screening Model for Real Solvents) [50] is such a tool. It is a quantum chemistry-based statistical thermodynamics model for the prediction of thermodynamic properties of fluids and liquid mixtures. The quantum chemical basis is a dielectric continuum model named COSMO (conductor-like screening model) [51]. It can be applied to process the screening charge density on the surface of molecules to calculate the chemical potential of each species in a solution. The resulting chemical potentials are the basis for other thermodynamic equilibrium property calculations such as activity coefficients, solubility, partition coefficients, vapor pressure and free energy of solvation. COSMO-RS also integrates dominant interactions of H-bonds (the most dominant interaction for ILs), misfits, and van der Waals forces in ILs systems to summarize multiple solvations [52]. It can also be used for performing mixture calculations at various temperatures. This is considered to possibly be the most accurate model for the prediction of the properties of ILs for the currently available tasks [53].

1.4.1 Theory of COSMO-RS

A brief description of the theory needed for understanding the COSMO-RS calculations of this project is given in this chapter. COSMO-RS treats a liquid as an ensemble of closely packed ideally screened molecules, and each piece of the molecular surface is in close contact with another one. It is assumed that each molecule is enclosed by a virtual conductor. In a contact area, the surface segments of both molecules have net screening charge densities of σ and σ'. The specific interaction energy (E_{misfit} or E_{MF}) per unit area arises from the "misfit" between σ and σ' and is calculated by equation 1.1 [54].

$$E_{misfit}(\sigma,\sigma') = a_{eff}e_{misfit}(\sigma,\sigma') = a_{eff}\frac{\alpha'}{2}(\sigma+\sigma')^2 \qquad (1.1)$$

a_{eff} is the effective contact area between two surface segments. a' is an adjustable parameter.

For strong polar compounds, H-bond interaction energy (E_{HB}) need to be considered and can also be described by the two adjacent σ and σ' (equation 1.2) [54].

$$E_{HB}(\sigma,\sigma') = a_{eff}c_{HB}(T)\times\min\{0;\min[0;\sigma_{donor}+\sigma_{HB}]\max[0;\sigma_{acceptor}-\sigma_{HB}]\} \qquad (1.2)$$

Where $\sigma_{acceptor}$=max[σ, σ'], σ_{donor}=min[σ, σ']. c_{HB} and σ_{HB} are adjustable parameters.

In addition to the interaction energy of E_{misfit} and E_{HB}, COSMO-RS also takes into account van der Waals (vdW) interactions between surface segments (equation 1.3) [54].

$$E_{vdW}(\sigma,\sigma') = a_{eff}(\tau_{vdW}+\tau'_{vdW}) \qquad (1.3)$$

Where τ_{vdW} and τ'_{vdW} are element specific adjustable parameters.

The total interaction energy per unit area can be written as equation 1.4 [54].

$$e(\sigma,\sigma') = (E_{vdW}(\sigma,\sigma')+E_{HB}(\sigma,\sigma')+E_{MF}(\sigma,\sigma'))/a_{eff} \qquad (1.4)$$

Using the $e(\sigma,\sigma')$ from equation (1.4), the chemical potential (also called σ-potential) of a surface segment with screening charge density σ in an ensemble described by normalized distribution function $p_s(\sigma)$ is given by equation 1.5 [54]. σ-potential is a

characteristic function of the liquid system, describing its affinity for the molecular surface of varying polarity σ.

$$\mu_s(\sigma) = -RT \times \ln[\int p_s(\sigma') \exp\left\{\frac{\mu_s(\sigma') - a_{eff}e(\sigma,\sigma')}{RT}\right\} d\sigma' \quad (1.5)$$

$p_s(\sigma)$ is a sum of the probability distributions of σ-profiles of the components i ($p_i(\sigma)$, to describe the composition of the surface segment ensemble with their mole fraction in the mixture x_i. The expressions for $p_i(\sigma)$ and $p_s(\sigma)$ are given in equations 1.6 and 1.7 [55]. In the COSMO-RS, the σ-profile histogram can be qualitatively divided into three main regions: the H-bond donor region ($\sigma < -0.0082$ e/Å^2), the H-bond acceptor region ($\sigma > +0.0082$ e/Å^2) and the nonpolar region ($-0.0082 < \sigma < +0.0082$ e/Å^2) [56].

$$p_i(\sigma) = \frac{A_i(\sigma)}{A_i} = \frac{n_i(\sigma)}{n_i} \quad (1.6)$$

Where $A_i(\sigma)$ is the sum of segment areas of screening charge densities σ. A_i is the surface area of compound i. $n_i(\sigma)$ is the sum segment number of screening charge densities σ. n_i is the sum segment number.

$$p_s(\sigma) = \frac{\sum x_i A_i p_i(\sigma)}{\sum x_i A_i} \quad (1.7)$$

Based on the chemical potential, the activity coefficient can be calculated as equation 1.8 [55].

$$\gamma_s^i = \exp(\frac{\mu_s^i - \mu_i^i}{RT}) \quad (1.8)$$

Where μ_s^i is the chemical potential of solvent S, and μ_i^i is the chemical potential of pure compound i.

1.4.2 Molecular description of ILs in COSMO-RS

Figure 1.12 describes the three possible representations of a 1:1 IL in COSMO-RS [55]. For the meta-file approach, the IL is treated as the sum of the σ-profiles, areas and volumes of the ions. It is different with the COSMO calculation. The ions in the COSMO calculation are treated separately in the quantum chemical. For the ion-pair approach, the ion-pair structure is optimized on the COSMO level. This usually requires a large set of conformations of the IL ions because of their weak coordination. For the

electroneutral mixtures, the molar fraction of the cations and anions of the ILs are treated as equal, i.e. $n_{cation}=n_{anion}=n_{IL}$ [57]. For a 1:1 IL+solute (cation+anion+solute), the mole fraction used in experiments depends on the binary system, whereas the mole fraction used in the COSMO-RS calculation depends on the ternary system. Therefore, a property such as the activity coefficient of a solute *X* in the ternary mixture (γ_X^{tern}) of COSMO-RS calculation has to be converted into binary definition (γ_X^{bin}). The relation for the conversion is $\gamma_X^{bin} = \gamma_X^{tern}(x_X^{tern} + x_{ion}^{tern})$, where x_X^{tern} is the mole fraction of solute, and x_{ion}^{tern} is the mole fraction of ion. According to this formula, the activity coefficient at infinite dilution of the solute X is $\gamma_X^{bin} = 0.5\gamma_X^{tern}$ $(x_X^{tern} \to 0, x_{ion}^{tern} \to 0.5)$ [55].

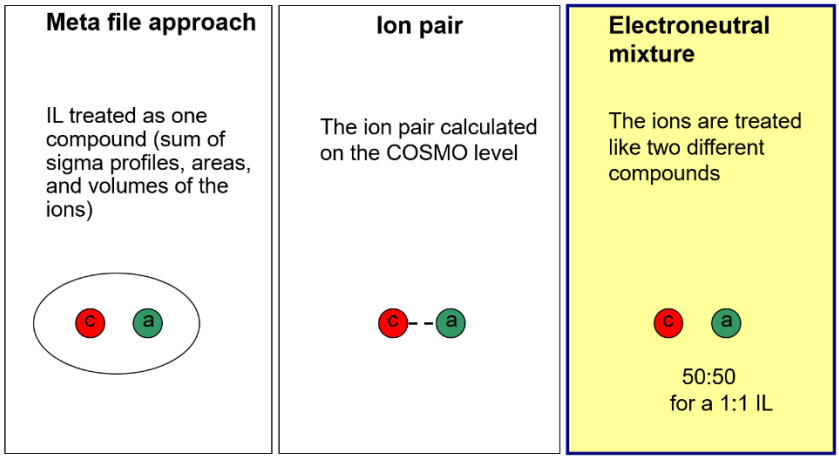

Figure 1.12 Three possible representations of a 1:1 IL in COSMORS [55].

1.4.3 Cellulose solubility prediction in ILs by COSMO-RS

Previous studies have demonstrated that COSMO-RS can successfully predict properties of ILs for cellulose solubility by activity coefficients, solubilities and excess enthalpies. Especially, activity coefficient calculations have been evidenced to be useful for predicting cellulose solubility in ILs [58]. Kahlen et al. applied a cellotriose COSMO file, and predicted the residual contributions to the activity coefficients of cellulose in 2272 different ILs at infinite dilution [59]. Then the prediction results were compared with the cellulose solubilities measured by Vitz et al [60]. The composition shows that these two results are in good agreement. Casas et al. used a glucose model

to represent cellulose and predicted the cellulose solubility by activity coefficient and excess enthalpy in different ILs. The result indicated that according to COSMO-RS IL anions play the main role in the cellulose dissolution process [45].

1.5 Conductive fiber

Conductive fibers have many possible applications. There are mainly two types of conductive fibers. One is carbon fiber, which had its earliest recorded in the 1860's and then in 1879 [61]. The carbon fibers produced today are mainly based on rayon, polyacrylonitrile (PAN) or pitch. It was favored in applications due to its superior tensile strength, good electro-conductivity and low specific weight, compared to traditional metal structural materials [62]. However, due to the complexity of the fabrication process (**Figure 1.13** [63]) it has unstable quality and a high price, which restricts its application and large-scale industrial manufacture. In recent years, another conductive fiber named carbon nano-fiber has attracted considerable attention due to its ability to conduct electric current, chemical and biochemical properties and the simplicity of its fabrication process.

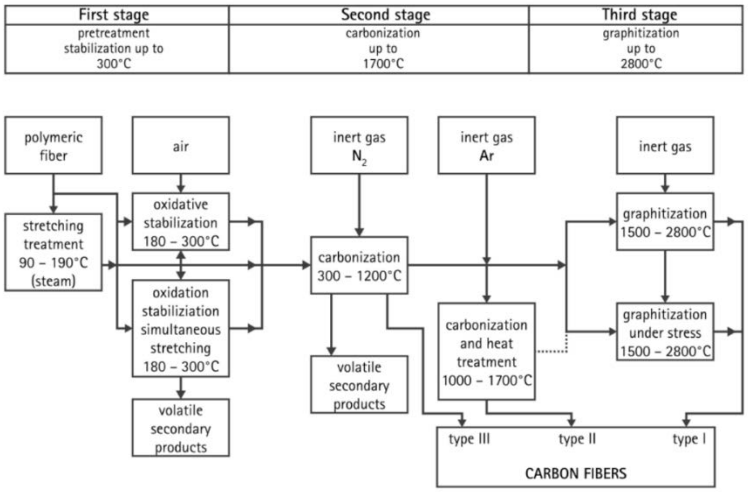

Figure 1.13 Carbon fiber fabrication process [63].

1.5.1 Carbon nano-fiber

It has been reported that carbon nanotubes (CNTs) are remarkable conductive

materials for producing conductive fiber [3]. They were first discovered in 1991[64], and come in two main types: single-walled CNTs (SWCNTs) and multiwalled CNTs (MWCNTs) (**Figure 1.14**) [65], with aspect ratios higher than 100 [66]. SWCNTs have a single cylindrical wall seamlessly wrapped by a single graphite sheet. MWCNTs are composed of multiple concentric cylinders like the rings of a tree trunk [5]. Some reports indicate that CNTs are very strong. The strength of CNTs can reach tens of gigapascal, and Young's modulus is in the range of terapascal [67]. Remarkably, the breaking strain is larger than 5% [68]. The electronic properties of MWNTs are little lower than those of perfect SWNTs because of the weak coupling between the cylinders. The thermal conductivity of an individual MWCNT at room temperature is larger than 3000 W/m·K, which is greater than that of a natural diamond and the basal plane of graphite (2000 W/m·K, respectively) [5]. The extraordinary properties of CNTs make them remarkable reinforcing fillers for high performance and multiple function polymer. In the earlier reports, the CNTs polymers mainly focuses on polypropylene–MWCNTs [69], polyethylene–MWCNTs [70], polyacrylonitrile–SWCNTs [71], polystyrene-block-poly(ethylene oxide)–SWCNTs and poly(methyl methacrylate)-block-poly(ethylene oxide)–SWCNTs [72], poly(p-phenylene benzobisoxazole)–SWCNTs [73], polyamide–MWCNTs [74], polycarbonate–MWCNTs [75], poly(vinyl alcohol)–SWCNTs [76] and polyamid–MWCNTs [77], etc. With the increasing requirement of biodegradable material, recent research has paid much attention to the natural CNT polymers [78,79].

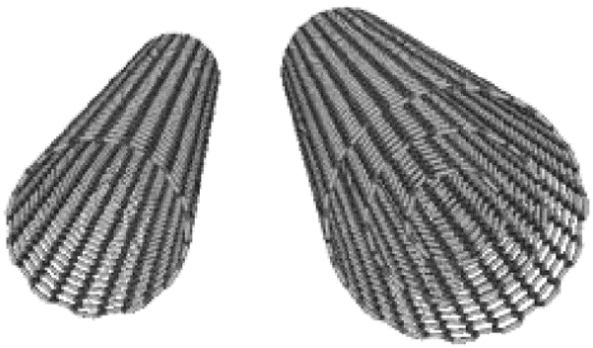

Figure 1.14 Structures of SWCNTs (left) and MWCNTs (right) [65].

1.5.2 Carbon nano-fiber fabrication method

1.5.2.1 Wet spinning

Wet spinning is a flexible method to prepare fiber. It has been applied for fabricating cellulose/CNTs fibers using ILs as solvents [3,9,67]. The research showed that stretching and spinning are the most effective approaches to increase the orientation of CNTs within a polymer matrix. The procedure of CNTs fiber manufacturing by wet spinning is shown in **Figure 1.15**. In this method, the CNTs conductive solution was first prepared in ILs before spinning and then placed in a syringe pump. In the spinning process, water is commonly used as an anti-solvent for the regeneration cellulose and for washing the fibers to remove the IL after spinning [80-82].

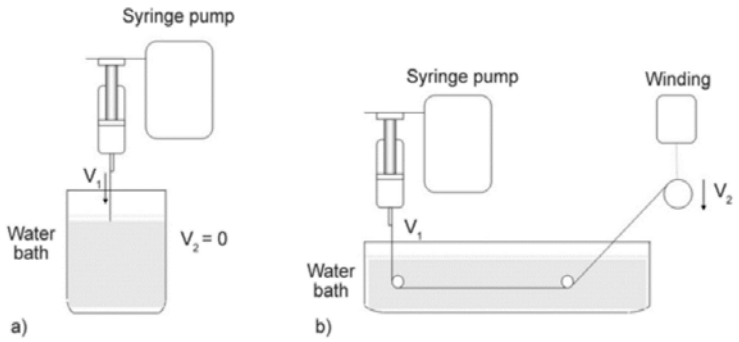

Figure 1.15 Wet spinning procedures to prepare the CNTs fibers (a) no winding. (b) with winding [9].

1.5.2.2 Electrospinning

Electrospinning is a unique spinning approach using electrostatic forces to produce fine fibers from polymer solutions (e.g. CNT-conductive solution) or melts. Using this method, the fibers were produced with a diameter from several micrometers down to tens of nanometers, and thus provide an ideal route to bridge the dimensional gap between the nano and macro scales [83,84]. The electrospinning system includes three major components, a high voltage power supply (several tens of kV), a spinneret, and a grounded collecting plate (**Figure 1.16**). In the electrospinning process, a polymer

solution or a melt held by its surface tension. An electric charge will appeared on the solution or melt surface during the electrospinning attribute to the electric supply. When the electrical forces overcome the surface tension forces, a charged jet of the solution is ejected from the end of the spinneret and then the fiber is left on the collector. Afterwards, the solvent is evaporated or washed away (e.g. ILs as a solvent) [83,85-87]. However, fiber prepared by the electrospinning method is not as strong as other fiber because of the lower chain orientation resulting from the low stretching forces [88].

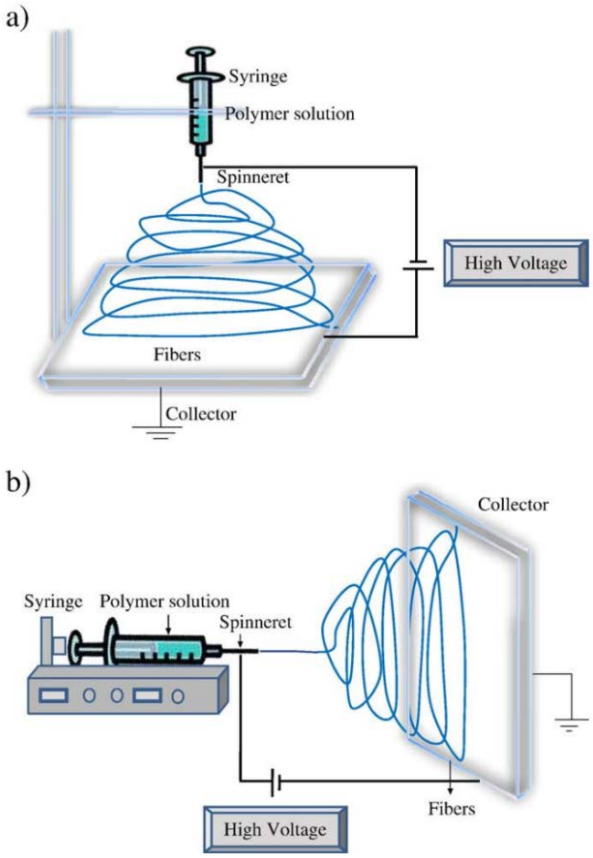

Figure 1.16 Electrospinning apparatus (a) typical vertical set up and (b) horizontal set up of electrospinning apparatus [83].

1.5.2.3 Dye-printing

Figure 1.17 is the schematic illustration of the dye-printing system of the CNTs-dyed yarns [89]. The dyeing bath mainly contains the dispersed CNTs and a certain amount of binder, called CNTs-based dyestuffs [90]. In the dye-printing process, initially the yarns are passed through a dye-bath containing the CNTs-based dyestuffs under the

temperature of 40 ℃. A microwave vibration system is used in the dye-bath to make each filament of the yarns dyed thoroughly by the CNTs-based dyestuffs. Then, the wet yarn is further dried at 170 ℃ to acquire the dry CNTs-dyed coating yarns. For this method, the adhesive force between the CNTs-dyed coating and the yarns is the challenge for the application of this CNTs-dyed conductive fiber.

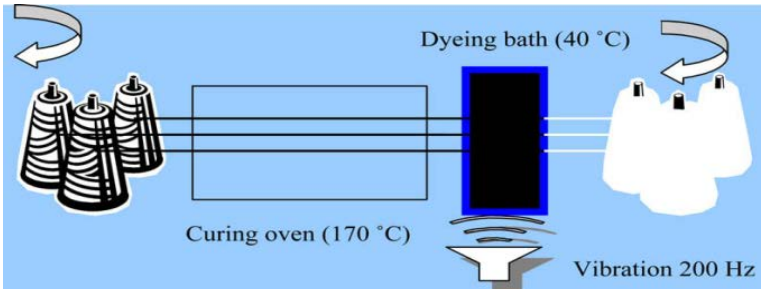

Figure 1.17 Dye-printing system of the CNTs-dyed yarns [89].

1.6 IL recycling

Although IL has many merits as the solvent, cost is still a key factor for the application of ILs in the industry. Therefore, recycling and reuse of ILs is crucial to achieving economical operation. Several IL recycling methods have been reported in the literature, such as membrane separation [91], evaporation [92], liquid-liquid extraction [93], centrifugal solvent-extraction [94], and Supercritical CO_2 extraction [95]. Lynam et al. [91] introduced the membrane separation for EmimAc+H_2O and EmimHCOO+H_2O system (Figure 1.18). In this research, ten times the original IL+H_2O solution were achieved (from 5–50% by mass). Membrane separation can be operated in the condition of low temperature and ambient pressure. However, this method usually has a low IL recovery when the IL mixtures reach a high viscosity [96]. Evaporation method can recycle the ILs from compounds with low boiling points. It is a direct and effective method for ILs recycling. But direct vacuum rotary evaporation is energy-consuming. In the liquid-liquid extraction process, traditional organic solvent is usually used to recycle ILs, which is against the green aspect of employing ILs. CO_2 is inexpensive, nonflammable, nontoxic and environmentally benign, making it a “green solvent”. The solute could then be separated from the CO_2 by simple depressurization.

Using this method, the final recovered product can be obtained without any ILs contamination [97].

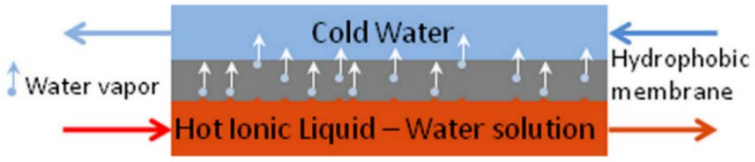

Figure 1.18 Diagram of membrane separation for IL+H_2O system

1.7 Mechanical properties improvement

Mechanical properties are an important parameter for the application of cellulose fiber. Some investigations have been reported on improving the fiber mechanical. It has been reported that the mechanical properties will be significantly improved by chemical or enzyme treatment. Mishra et al. studied the tensile strength of sisal using the chemical treatment method [98]. The result showed that the tensile strength will increase after 5% and 10% NaOH (dry fiber weight), cyanoethylation and acetylation treatment. Ten percent NaOH treatment gives the highest tensile strength in these three treatments.

Enzyme treatment might be an excellent alternative method compared with the traditional methods because of the efficiency and environmental impact. The addition of chelators has been evidenced to be an efficient method to improve the fiber tensile strength. Li et al. used Laccase and EDTMP to treat hemp fiber [99]. It was shown that the higher chelator concentration-treated hemp fiber composites had the highest tensile strength of 42 MPa, an increase of 19% compared to composites with untreated hemp fiber. Ming et al. treated the hemp fiber by 0.5% EDTA+0.2% endo-polygalacturonase+0.5% laccase [100]. It was found that the treated fibers had highest stiffness of 42 GPa and highest ultimate tensile strength of 326 MPa at a fiber volume content of 50%. Saleem et al. treated bast fibers with pectinase [101]. The result illustrated that tensile strength (43.7 vs. 47.6 MPa for control vs. pectinase incubation) and flexural strength (49.9 vs. 56.6 MPa) were increased when using fibers incubated in pectinase.

CHAPTER II–Predictive screening of ionic liquids for dissolving cellulose and experimental verification

In order to acquire the potential ILs from the numerous candidates for dissolving cellulose by a fast and a priori method, the first requirement of this thesis was to employ COSMO-RS to screen the potential IL for dissolving cellulose. Cellulose models and the ILs structures were first designed and the parameters of logarithmic activity coefficients, excess enthalpies, σ-potentials and σ-profiles determined using the model COSMO-RS for ILs and cellulose system. To verify the COSMO-RS prediction results, the experiment of cellulose solubility for seven potential ILs was studied.

2.1 Hypotheses

- Cellulose mode and the cation and anion structure of ILs both affect the COSMO-RS prediction results of cellulose solubility.
- The type of ILs of imidazolium-, pyridinium-, morpholinium- and pyrrolidinium- are the excellent ILs for dissolving cellulose.
- Ethyl, allyl, 2-hydroxylethyl, 2-methoxyethyl and acryloyloxypropyl are the functional groups of ILs for dissolving cellulose.

2.2 Related paper

This chapter was based on the following published paper.

Yan-Rong Liu, Kaj Thomsen, Yi Nie, Suo-Jiang Zhang and Anne S. Meyer

Predictive screening of ionic liquids for dissolving cellulose and experimental verification

Green Chemistry, 2016, 18, 624−625.

2.3 Significance of the study

Cellulose is widely used in industry, and this is attributed to its promising features of biocompatibility, biodegradability as well as thermal and chemical stability [10]. However, cellulose is insoluble in water and common organic solvents because of the highly ordered crystalline regions formed by the multiple H-bonds between cellulose molecules. Several traditional solvents such as NMMO, DMAc/LiCl, DMF/N_2O_4, etc. have been successfully applied in dissolving cellulose. Drawbacks of these solvents, including high dissolution temperature, volatility, difficulty in solvent recovery and toxicity, make them undesirable and underlines the necessity for developing greener solvents for cellulose dissolution [28,29]. ILs have been evidenced to be the green solvent for dissolving the cellulose in recent years. Numerous possible ILs composed of cations and anions make it time-consuming to acquire the potential ILs for dissolving cellulose. Therefore, it is necessary and important to use a rapid and a priori screening method to predict the cellulose solubility capacity for ILs.

2.4 Computational and experimental consideration

Three cellulose models were considered to present the cellulose in this study. They are glucose (Model 1), mid-monomer of cellotriose (Model 2), and mid-dimer of cellotetraose (Model 3) (**Figure 3.1**). These three models were designed because of the program package COSMOtherm, which usually uses one or several repeating units to model a polymer.

According to the previous work, imidazolium- and pyridinium-based ILs, which have the functional groups alkyl-, allyl-, hydroxyl-, ether- and ester-, are potential for dissolving cellulose [12]. Thus, the cations of methylimidazolium$^+$, pyridinium$^+$, ethylmorpholinium$^+$ and methylpyrrolidinium$^+$ with functional groups of ethyl, allyl, 2-hydroxylethyl, 2-methoxyethyl or acryloyloxypropyl were combined with 21 anions resulting in the 357 ILs studied in this work.

The structures of 21 anions in this study come from COSMO-RS database. The three

cellulose models and the cation structures, which do not include in the COSMO-RS database, were first optimized by the quantum chemical Gaussian09 package at the B3LYP/6-31++G (d, p) level. Then the COSMO files of the optimized structures were opened by Gaussian03, and COSMO continuum solution models were calculated using the BVP86/TZVP/DGA1 level theory. Finally, the logarithmic activity coefficients, excess enthalpies, σ-potentials and σ-profiles were determined using the model COSMO-RS to evaluate the solubility of cellulose in ILs. When conducting calculations in the COSMO-RS program, the molar fractions of the cations and anions of the ILs were treated as equal, i.e. $n_{cation} = n_{anion} = n_{IL}$ [57].

In order to verify the COSMO-RS prediction results, Microcrystalline cellulose (MCC) was selected to dissolve in seven high solubility ILs from the COSMO-RS calculation to determine the cellulose solubility and compared with the prediction results. The dissolving temperature in the experiment is 90 ℃, which is the same temperature with the COSMO-RS prediction.

2.5 Highlights

The cations of methylimidazolium$^+$, pyridinium$^+$, ethylmorpholinium$^+$ and methylpyrrolidinium$^+$ structured with functional groups including ethyl, allyl, 2-hydroxylethyl, 2-methoxyethyl and acryloyloxypropyl, combined with anions Ac^-, Dec^-, $HCOO^-$, Cl^-, BEN^-, $DMPO_4^-$, DEP^-, DBP^- and Br^- were predicted to be the best for dissolving cellulose according to the logarithmic activity coefficient prediction results (**Figure 2.1**). Excess enthalpy calculations indicated that H-bond interactions between cellulose (i.e. the three cellulose models) and the 7 studied ILs are key factors for the solubility of cellulose, and the anions play a crucial role in the cellulose dissolution process (**Figure 2.2** and **2.3**). The experimental results illustrated that the logarithmic activity coefficient prediction has a good agreement with it and found that the mid-monomer part of cellotriose model represents cellulose better than the glucose model and mid-dimer part of the cellotetraose model. In a word, the prediction of logarithmic activity coefficients of cellulose in ILs by COSMO-RS can, therefore, be

considered an effective parameter to evaluate the dissolution power of the ILs, and COSMO-RS is an efficient model to predict cellulose solubility.

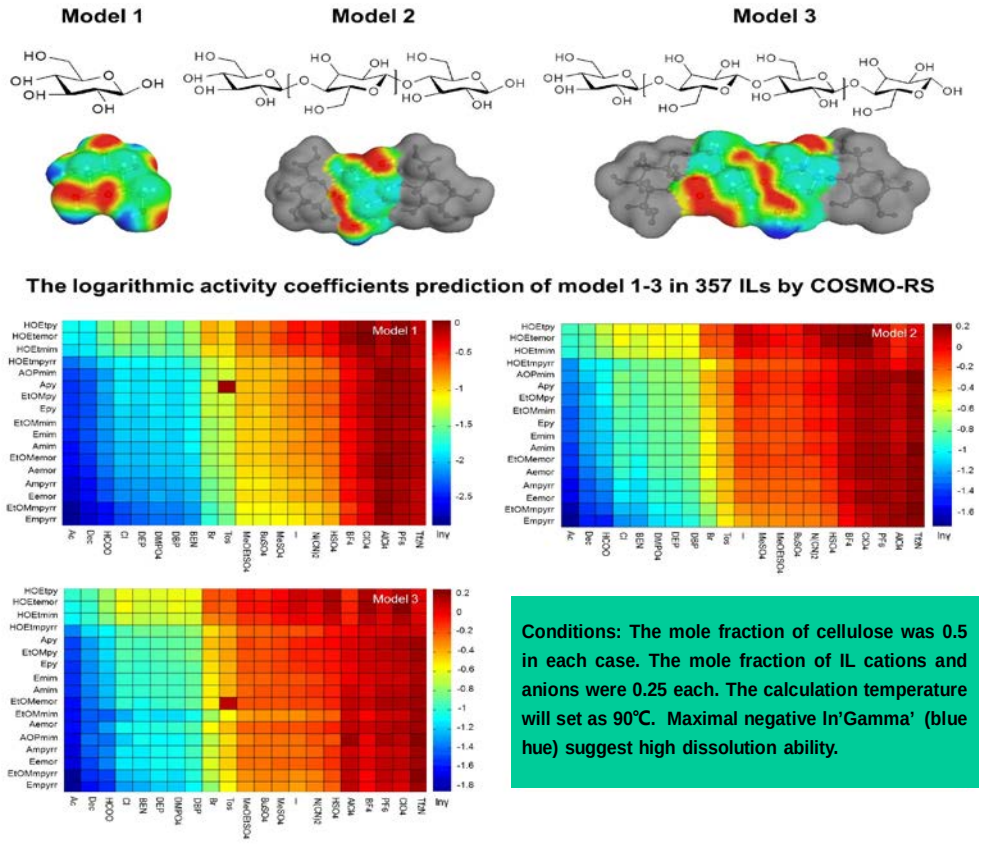

Figure 2.1 Designed cellulose models 1–3 and the logarithmic activity coefficient prediction results of models 1–3 in 357 ILs by COSMO-RS

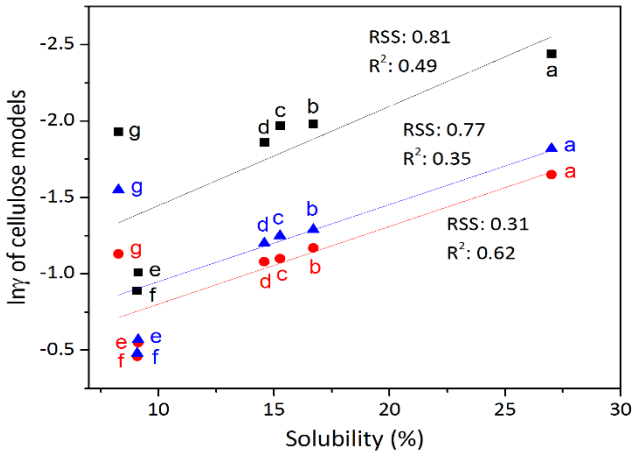

Figure 2.2 Experimental values of MCC solubilities in seven ILs plotted against lnγ: Model 1 (Black square), Model 2 (Red circle) and Model 3 (Blue triangle). a: EmimAc,

b: AmimCl, c: EmimDep, d: ApyCl, e: HOEtmimBr, f: HOEtpyBr, g: EtOMmimCl

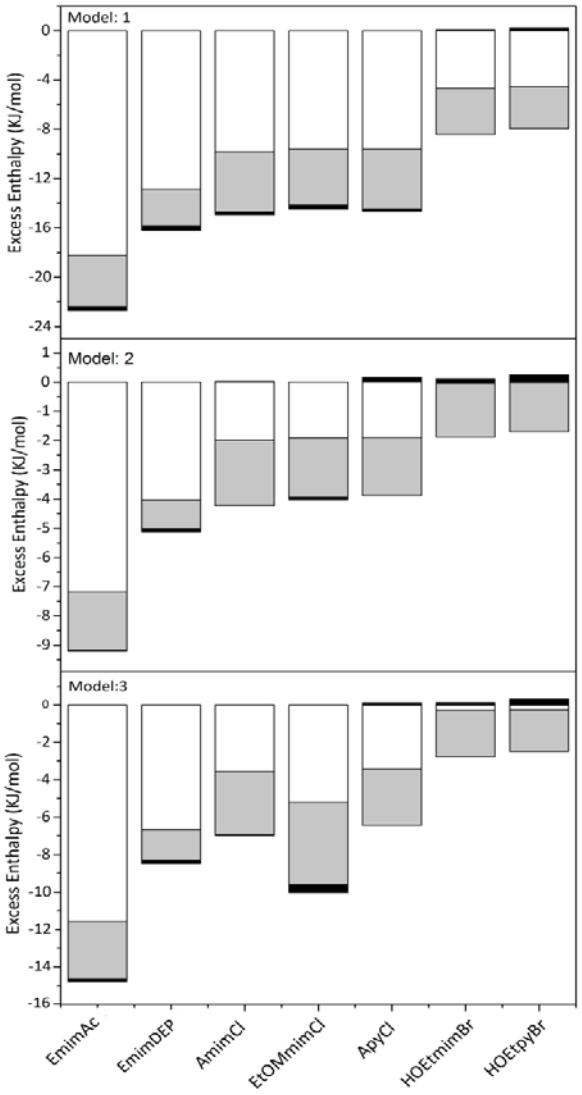

Figure 2.3 Excess enthalpies between the three cellulose models and seven ILs, H-bond (white histogram), misfit (grey histogram) and van der Waals force (black histogram)

CHAPTER III–Freezing point determination of water−ionic liquid mixtures

In the cellulose regeneration process, water is commonly used as an antisolvent for the coagulation of cellulose. In this process, ILs will mix together with water to form ILs aqueous solution. Considering the high cost of using the ILs for cellulose products, recovery and reuse of ILs are crucial. The purpose of this chapter is to measure the freezing point of the ILs aqueous solution to determine if freeze crystallization could be a feasible method for IL recovery.

3.1 Hypotheses

- ILs can dissociate in water, and the ILs aqueous solution will form pure ice when the temperature is decreased like the inorganic salt.
- Freeze crystallization could be a feasible method for IL recovery from IL+H_2O mixtures.
- The cations and anions of the ILs both affect the freezing point values.
- COSMO-RS can be used to predict the freezing point of ILs aqueous solution.

3.2 Related paper

Yanrong Liu, Anne S. Meyer, Yi Nie, Suojiang Zhang, Yongsheng Zhao, Philip L. Fosbøl, Kaj Thomsen

Freezing point determination of water-ionic liquid mixtures

Journal of Chemical & Engineering Data, 2017, 62, 2374−2383.

3.3 Significance of the study

In the recycling of an organic solvent, it has been indicated that eutectic freeze crystallization was technically and economically feasible in cases where high product quality was required. Energy costs can be reduced by about 70% for certain systems by

the freeze crystallization method compared to three-stage evaporative crystallization. However, this method is hardly reported for ILs recycling. Thus, the freezing point measurement can help to know the properties of the ILs aqueous solution and the recycling scope of different ILs aqueous solutions.

3.4 Experimental and computational consideration

Six imidazolium-based ILs of EmimAc, EmimDep, AmimCl, HOEtpyBr, HOEtmimBr, and EtOMmimCl were selected in this study which has evidenced that these ILs have high cellulose solubility. These ionic liquids were selected as three principles. The same cations with different anions, same function group, same anions but different cation types; same cation type, same anions but different function groups. Based on this classification, the effect of the cations and anions on the interactions of ILs and water will be acquired. These ionic liquids were mixed with different molarity and mole fraction of water, and then the freezing points were measured using a modified Beckmann apparatus with automatic data logging. The refrigerants are ethanol in the freezing point depression process. When the freezing point cannot be required under the cool of the ethanol, liquid nitrogen will serve as the refrigerant.

To verify that the hypothesis of IL has the similar property as the inorganic salt, the freezing points of $MgSO_4$ and $MgCl_2$ solutions were compared with the studied ILs aqueous solutions under the scale of mole solutes per kg water. Then the whole scope freezing point of the selected ILs in a mole fraction of water was measured to study which phase will be formed (e.g. ice or solid IL or IL·$n$$H_2O$).

According to the introduction that COSMO-RS is a fast and a priori method to predict the thermodynamic parameters, water activity and excess enthalpy of the ILs+H_2O system were calculated by COSMO-RS. Because water activity is an important parameter, if water activity is high, less amount of energy will be consumed during the freezing process, which is conducive to IL recovery. Another calculation software of COSMO-SAC introduced in-water activity prediction to study the prediction accuracy of these two software programs. To verify the prediction results, the measurement

freezing points were converted into water activity and compared with the prediction results.

3.5 Highlights

The comparison of freezing points' results of $MgCl_2$ [102, 103] and $MgSO_4$ [104, 105] solutions and the ILs+H_2O mixtures indicated that the freezing point curves of the six studied IL solutions were basically in the middle between the freezing point curves of $MgSO_4$ solutions and $MgCl_2$ solutions in the concentration range from 0 to 1 mol solutes/kg water (**Figure 3.1**). This result agreed with the hypotheses that IL has properties similar to those of inorganic salts in depressing the freezing point of water. The freezing point results of the studied ILs as a function of mole fraction of water showed that ice starts forming when the solutions are cooled to their freezing points (**Figure 3.2**). A change in slope of the freezing point curve indicates a change in solid phase. The solid phases at high IL concentrations are expected to be pure, solid ILs or hydrates of the form IL·$n$$H_2O$. And the study also displayed that the ice phase scope according to the freezing point measurement results were possible for recycling ILs from H_2O. **Figure 3.2** indicates that HOEtpyBr+H_2O and HOEtmimBr+H_2O systems formed simple eutectic systems and the freezing points were higher than the other four ILs' aqueous solutions. This result indicated that these two Bromide ILs were more easily recovered from H_2O than the other four ILs.

The freezing point measurement results of **Figure 3.2** evidenced that both cation and anion of ILs affect the interaction between ILs and water which confirms the hypotheses. However, the excess enthalpy prediction results by COSMO-RS showed that the anion is the key factor for the interaction of IL and water, and the H-bonds formed by IL anions are the dominant type of interaction between ILs with water (**Figure 3.3**). The freezing point results' plot against excess enthalpy has a good agreement (**Figure 3.4**), which demonstrates that the hypotheses of COSMO-RS can be used to predict the freezing point of ILs aqueous solution.

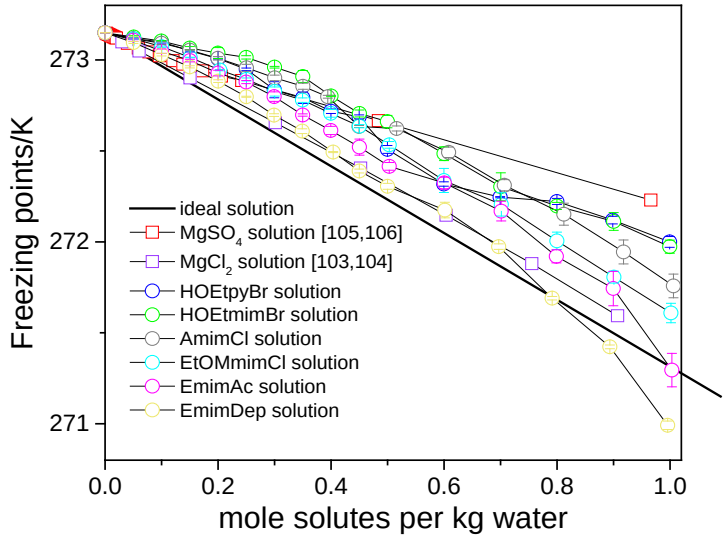

Figure 3.1 Freezing points of the studied IL solutions and of salt solutions compared at low concentrations

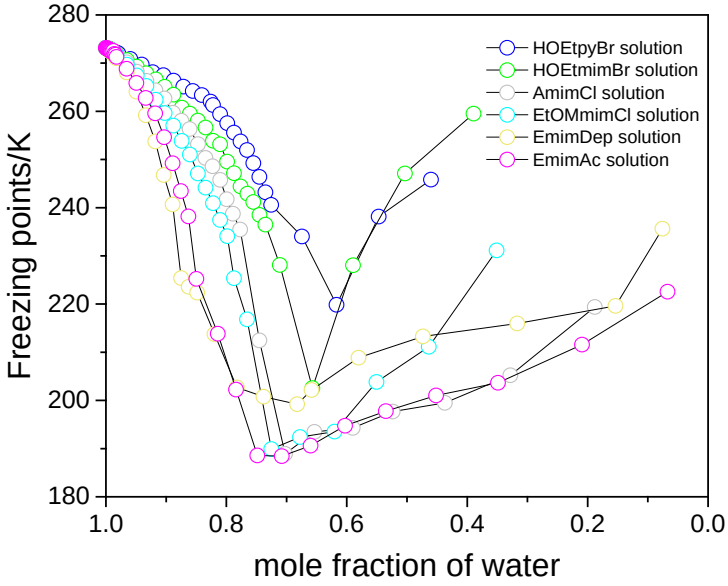

Figure 3.2 Measured freezing points of six IL solutions as a function of mole fraction of water

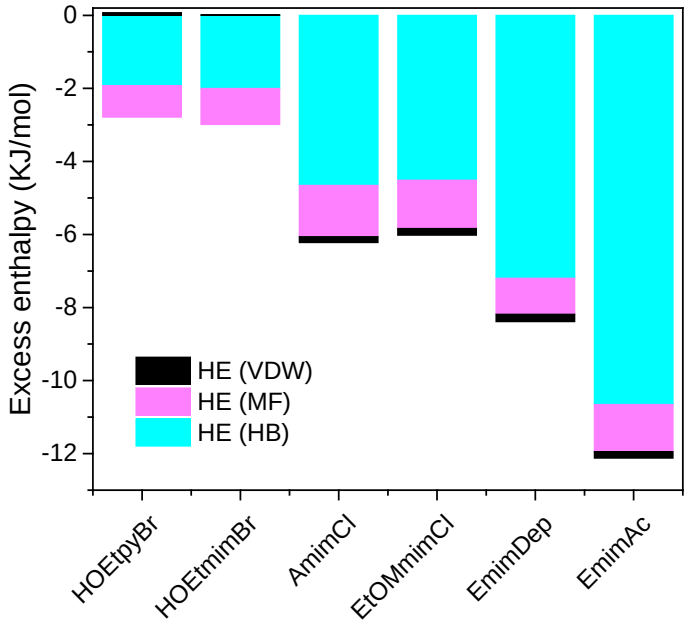

Figure 3.3 Contribution to the excess enthalpy of ILs+H_2O systems at 298.15 K predicted by COSMO-RS at x_{H2O}=0.65

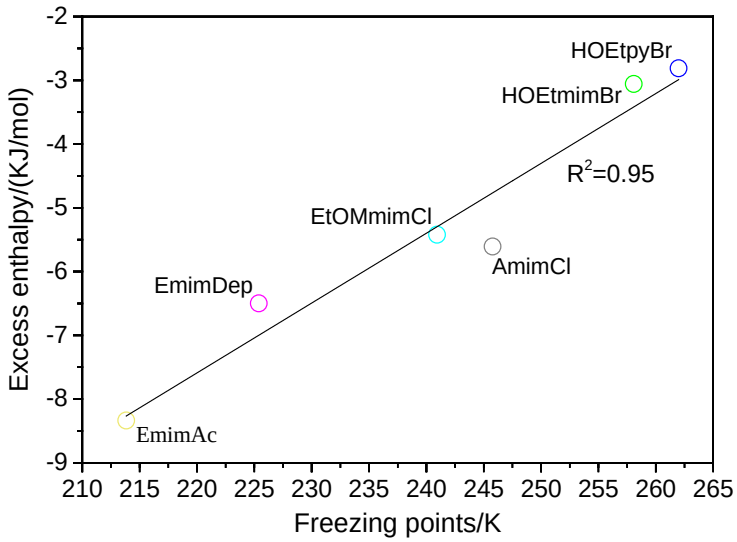

Figure 3.4 Freezing point values of six IL solutions plotted against excess enthalpy predicted by COSMO-RS at a water mole fraction of approximately 0.85

CHAPTER IV–Low energy recycling of ionic liquids via freeze crystallization during cellulose spinning

As described in chapter III, freeze crystallization is a feasible method for IL recovery from IL+H_2O mixtures. This chapter introduces ILs recycling using freezing point values acquired in chapter III after cellulose spinning and predicting the energy in the recycling process.

4.1 Hypotheses

- EmimDep and EmimAc are still acceptable solvents for cellulose when mixed with certain amounts of water.
- Using freeze crystallization method to recycle ILs from water will save more energy than the evaporation method.
- Using ILs as a solvent for the cellulose spinning process will save more energy than traditional solvent when recycling them from water.

4.2 Related paper

Yanrong Liu, Anne S. Meyer, Yi Nie, Suojiang Zhang, Kaj Thomsen

Low energy recycling of ionic liquids via freeze crystallization during cellulose spinning

Green Chemistry, 2017, DOI: 10.1039/C7GC02880F.

4.3 Significance of the study

Several IL recycling methods have been reported in the literature, including membrane separation, evaporation, liquid-liquid extraction, centrifugal solvent-extraction, and Supercritical CO_2 extraction. The disadvantage of these recycling

methods is their unsuitability for industrial implementation. For example, membrane separation usually results in low IL recovery due to the high viscosity of IL mixtures [96]. Evaporation is obviously energy consuming with a large energy requirement. Liquid–liquid extraction by use of conventional organic solvents has also been suggested for recycling of ILs, but the use of organic solvents is not compatible with the "green" aspect of employing ILs [96]. The cost is still a key inhibitory factor for ILs application in the cellulose fiber industry. Therefore, it is urgent and necessary to develop methods for IL recycling including feasible recovery of ILs from IL+H_2O systems in cellulose spinning processes.

4.4 Experimental and computational consideration

To acquire the optimal initial water content for recycling process after the cellulose spinning, two kinds of ILs of EmimAc and EmimDep which have high cellulose solubility were selected as the solvent for cellulose spinning and recycling. These two ILs were mixed with different mass percentages of water as the dissolving solvents based on the hypotheses that EmimDep and EmimAc are still an acceptable solvent for cellulose when mixed with certain amounts of water. Under this method, we hypothesize that it will save energy in the recycling process. The cellulose-dissolving temperature was fixed at 90 ℃ according to the previous study.

During the cellulose spinning process, water was selected as the regeneration solvent instead of an organic solvent to avoid environmental pollution. Then, the cellulose fiber was washed two times to remove the EmimAc and EmimDep after the regeneration [81]. In order to determine the recycling yield, the concentrations of EmimAc and EmimDep were determined by the measurement of electrical conductivity. In chapter III, the ice scopes of studied IL+H_2O mixtures have been determined by the freezing point measurements. Thus, the EmimAc and EmimDep aqueous solutions were first separated by freeze crystallization method to the maximum concentration of the ice stage, then the rest of the water was evaporated because of the high viscosity of the remain EmimAc and EmimDep aqueous solutions. The water in the wet fiber was also

removed using the evaporation method.

For the energy requirement prediction, specific enthalpy of water (liquid and vapor) was calculated using the NIST/ASME steam properties program. Considering that the heat capacity of liquid water cannot easily be measured below 273.15 K, the heat capacity of liquid water in the freezing step was set as the approximate value of 4.2 kJ/(kg·K). The water enthalpy in the freezing step was calculated from a reference temperature of 273.16 K to the experimental temperature (the triple point temperature of water) by equation 3. Based on the study, the heat capacity of ice was cited from Arshad et al. [106] which corresponds to 2.76 kJ/(kg·K). The value used for the heat of fusion of ice in this study was 333.55 kJ/kg [107]. The specific enthalpy of ice was calculated from equation (4). T_{ref} in equation 4 is the reference temperature for water enthalpy, 273.16 K.

The heat capacities of EmimAc (298.15 K to 393.22 K) [108,109] and EmimDep (298 K to 343 K) [110] were cited from the published values. These values can also be obtained from the Ionic Liquids Database-IL Thermo (V2.0) [111]. These values were assumed to be an almost linear function of temperature up to 393.15 K for EmimDep. The heat capacity of MCC was cited from the published work of Blokhin et al. [112]. The enthalpies of ILs and MCC were calculated according to the following equations of 1, 2 and 3.

$$a = \frac{C_{p,T_2} - C_{p,T_1}}{T_2 - T_1} \quad (1)$$

$$C_p = C_{p,298.15K} + a(T - 298.15) \quad (2)$$

$$H = \int_{T_{ref}}^{T} C_p dT \quad (3)$$

$$H_{ice} = \int_{T_{ref}}^{T} 2.76\, dT - 333.55 = 2.76\left(T - T_{ref}\right) - 333.55 \quad (4)$$

4.5 Highlights

Table 4.1 MCC solubility in total mixtures at 363.15 K.

EmimAc (1)+H_2O (2)+MCC (3)		EmimDep (1)+H_2O (2)+MCC (3)	
w_2	w_3	w_2	w_3
0.005	0.27[37]	0.0019	0.15 [37]
0.025	0.23	0.025	0.11
0.05	0.16	0.04	0.08
0.075	0.15	0.045	0.003
0.10	0.14		
0.125	0.12		
0.13	0.004		

w_2: weight fraction of H_2O in solvent. w_3: weight fraction of MCC in total mixture. The standard uncertainty of the weight fraction is 0.001.

Table 4.2 Energy requirements for recycling EmimAc and EmimDep using a freeze crystallization+evaporation process and a process in which all water is removed by evaporation.

Freeze crystallization + evaporation	Vacuum drying (MJ)	Freezing (MJ)	Evaporation (MJ)	Total (MJ)	Energy consumption per kg cellulose (MJ)
EmimAc	123	354*	141	618	45.4
EmimDep	124	316*	105	545	62.6
Evaporation	**Vacuum drying (MJ)**	**Freezing (MJ)**	**Evaporation (MJ)**	**Total (MJ)**	**Energy consumption per kg cellulose (MJ)**
EmimAc	123	–	787	910	66.9
EmimDep	124	–	745	869	99.9

*The freezing process is assumed to have an efficiency of 60 % while the vacuum drying and the evaporation processes are assumed to have efficiencies of 100%.
The total energy requirement for recycling EmimAc corresponds to producing 13.6 kg cellulose fiber. The total energy requirement for recycling EmimDep corresponds to producing 8.7 kg cellulose fiber.

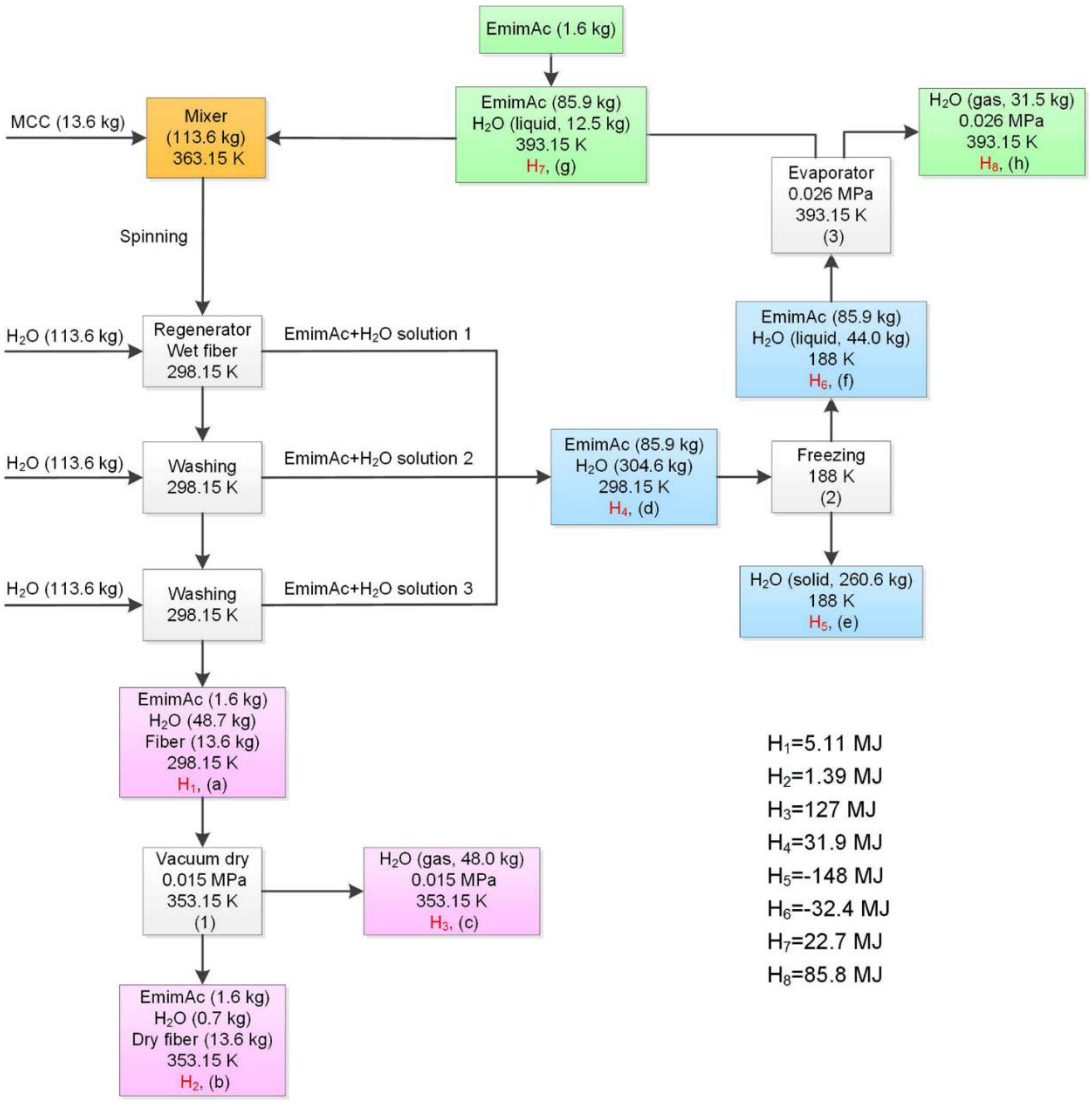

Figure 4.1 EmimAc recycling by freeze crystallization+evaporation method in a cellulose spinning process. H1–H8 are the enthalpies of the mixtures described in box (a) to box (h).

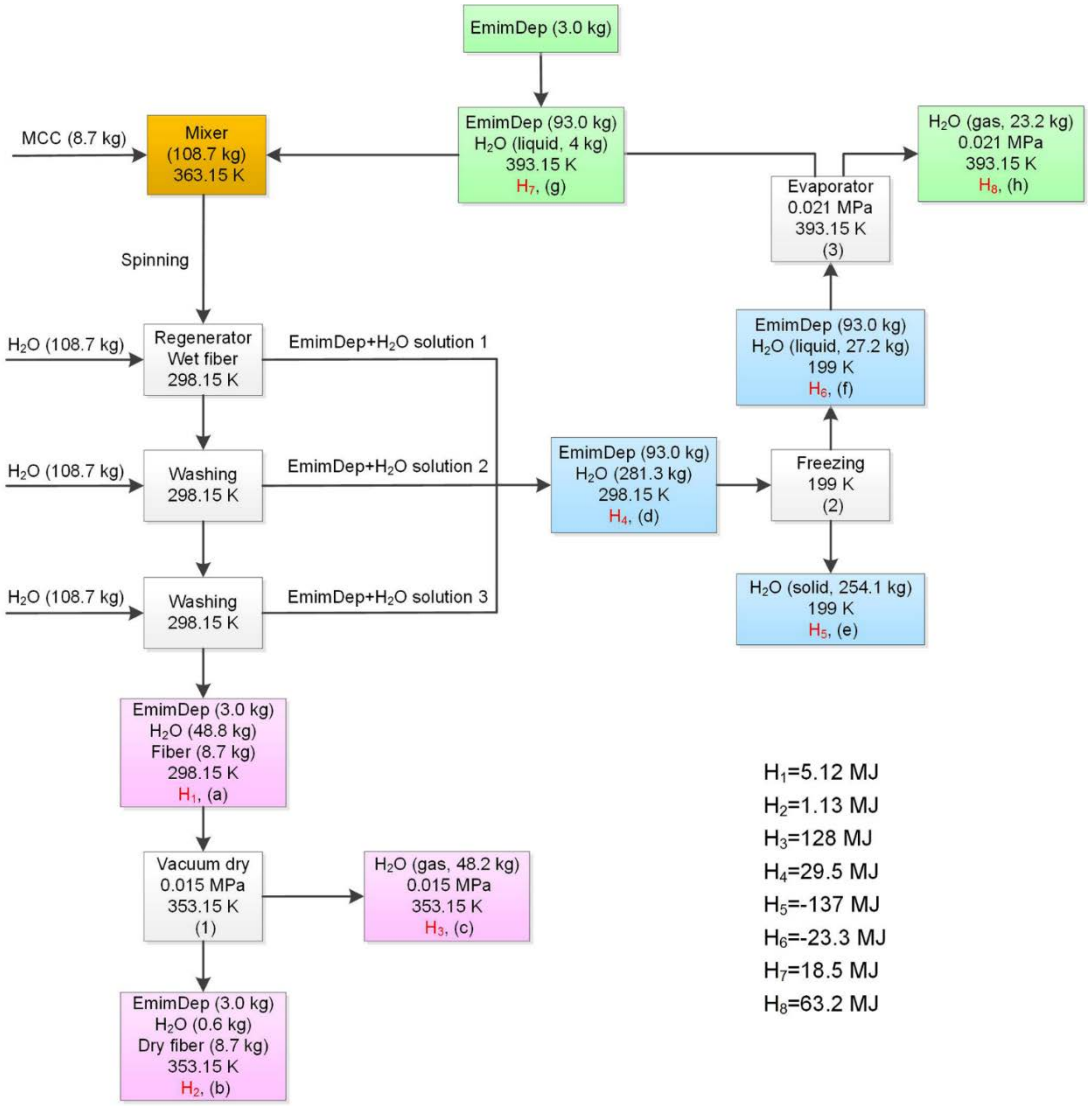

Figure 4.2 EimmDep recycling by freeze crystallization+evaporation method in a cellulose spinning process. H1–H8 are the enthalpies of the mixtures described in box (a) to box (h).

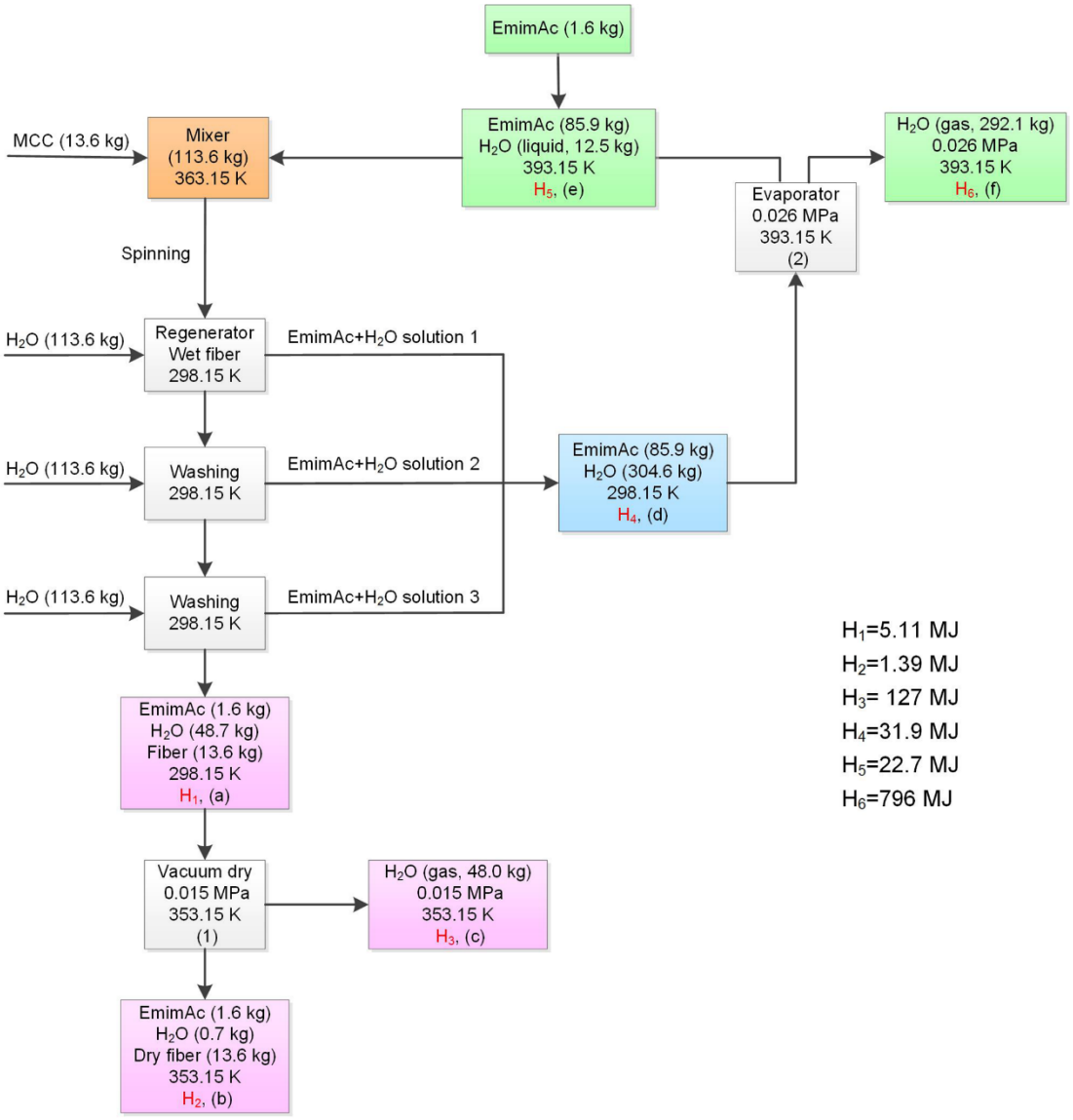

Figure 4.3 EmimAc recycling by evaporation method in a cellulose spinning process. H1-H8 are the enthalpies of the mixtures described in each box (a) to box (h).

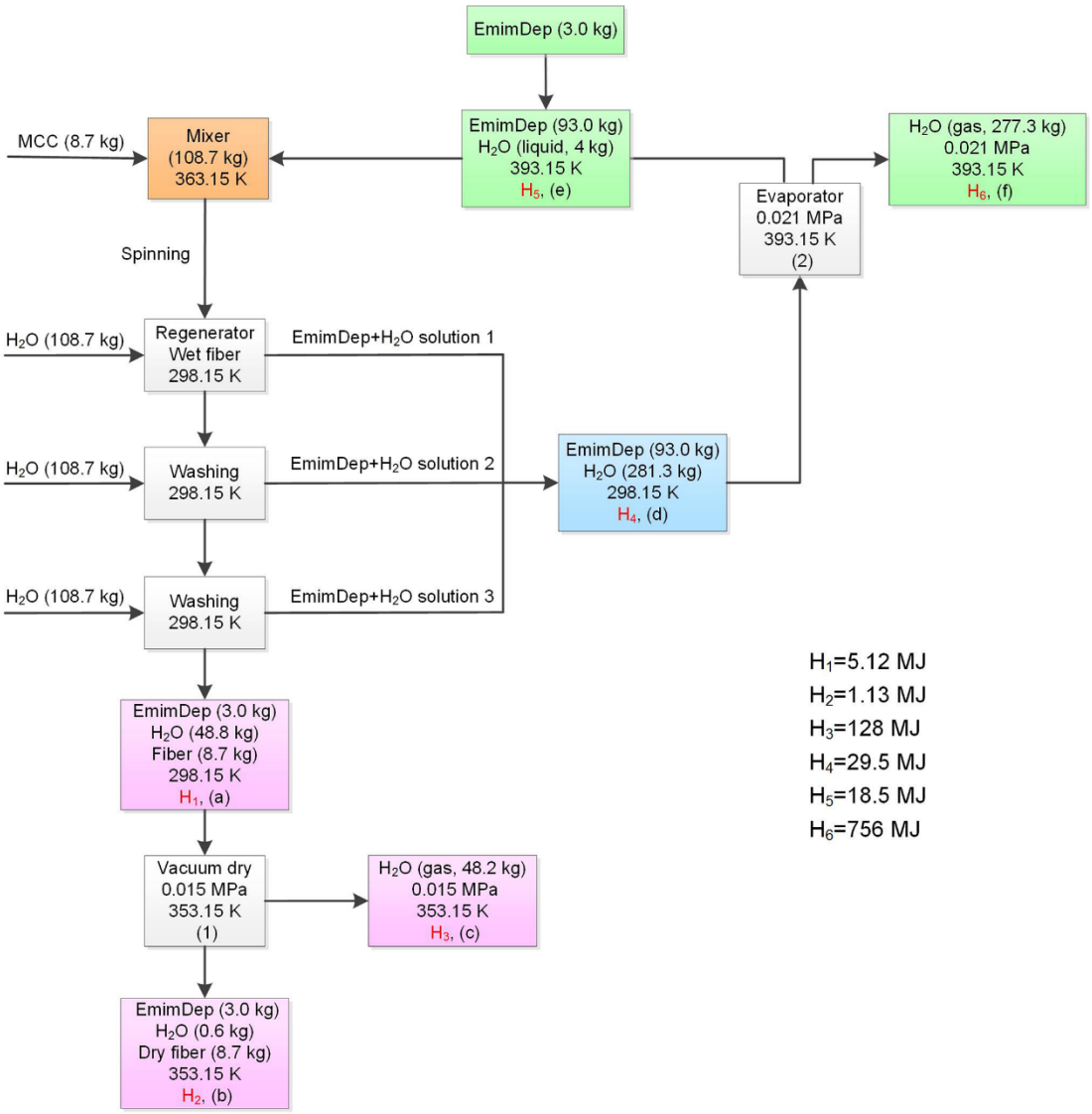

Figure 4.4 EmimDep recycling by evaporation method in a cellulose spinning process. H1-H8 are the enthalpies of the mixtures described in each box (a) to box (h).

CHAPTER V–Wet-spinning conductive cellulose fiber base on ionic liquids as solvent and enzymatic modification

The cellulose-CNTs fiber preparation by wet spinning was studied in this chapter. The spinning extrusion flow, spinneret diameters and mass ratios of MWCNTs with respect to cellulose were investigated to understand these effects on the cellulose-CNTs fiber. Phenol and enzyme (Laccase) were used to treat the wet spinning fiber after removing ILs in order to improve the tensile strength of the fiber.

5.1 Hypotheses

- The spinning extrusion flow and spinneret diameters affect the properties of the cellulose-CNTs fiber.
- The increase of CNTs amount in this study will decrease the tensile strength of the fiber.
- Enzymatic modification for the surface of the cellulose-CNTs fiber will increase the tensile strength of the fiber.

5.2 Related paper

Yanrong Liu, Yi Nie, Kaj Thomsen, Suojiang Zhang, Anne S. Meyer

Wet-spinning conductive cellulose fiber based on ionic liquids as solvent and enzymatic modification

Yet to be submitted.

5.3 Significance of the study

Electrically conductive polymer fiber has many desirable applications in electrochemical and biomedical fields, such as electronic devices, capacitor electrode,

neural probes, biosensors and bio-actuators, and shielding materials. According to the previous study, cellulose combined with CNTs can offer a good biocompatibility, electrical conductivity, and the ability to be easily spun to fiber. However, it is difficult to make the cellulose-conductive fiber have both the excellent conductivity and the high tensile strength. In order to promote the application of the cellulose-conductive fiber, it is important to design a method to fabricate excellent conductivity and improve the tensile strength cellulose-conductive fiber.

5.4 Experimental consideration

There are three selected materials in this study: cellulose, MWCNTs and EmimDep. Cellulose-based composites are of great importance because of the low cost of cellulose and its biodegradability. MWCNTs were selected as the conductive material because of their cost advantage compared to single-walled carbon nanotubes (SWCNTs). EmimDep is the solvent for dissolving cellulose and dispersing MWCNTs. This solvent has been verified to be a potential solvent to disperse MWCNTs in our previous study [37] and a super solvent to dissolve cellulose to acquire high modulus regenerated cellulose fiber by spinning [79]. It is reported that spinning parameters affect the conductivity and tensile strength of the fiber. It has been found that if the winding speed is increased the fiber electrical conductivity will decrease [9]. Thus, the spinning parameters in this study are based on spinning extrusion flow (0.01, 0.1, 0.4, 0.8, and 1.0 mL/min) and spinneret diameters (0.46 mm and 0.98 mm) with no winding. When the MWCNTs amount is less than or equal to cellulose amount, the fiber conductivity is unsatisfactory; thus, the MWCNTs amount in this study was selected as 2:1, 3:1, 4:1 and 5:1 with respect to the cellulose amount. The increase of the MWCNTs will decrease the tensile strength of the fiber, according to the investigation of Ming et al. that using enzyme to treat the fiber will increase the fiber tensile strength. Therefore, 10% phenol and 0.5% Laccase solution was used to treat the fiber after removing the EmimDep. In order to verify if the EmimDep remaining in the fiber affected the enzyme activity, ABTS (0.5 mM) was applied to study the enzyme activity using deionized

water and fiber washing water (5 times, including the regeneration step) to prepare the solution.

5.5 Highlights

The fiber electrical conductivity increases with the increasing of the mass ratio of MWCNTs. The largest electrical conductivity acquired is 760 S/m at the spinning extrusion flow of 1 mL/min, spinneret diameter of 0.46 mm and 5:1 of MWCNTs with respect to cellulose (**Figure 5.1**). The best surface area at this study was approximately 188 m^2/g at the ratio of 5:1 of MWCNTs with respect to cellulose which is better than the investigated work of Neimark et al. [113], and the fiber surface area is increased with the increasing of MWCNTs amount (**Figure 5.2**). TGA and surface area results evidenced that the fiber more stable at the spinneret diameter of 0.46 mm than 0.98 mm (**Figure 5.3**). SEM result illustrated that a pore structure could be observed in the fiber surface and alignment MWCNTs in the fiber will decrease the fiber electrical conductivity (**Figure 5.4**). The remaining EmimDep hardly affects the enzyme activity after 5 times washing of the fiber because of the similar slop of **Figure 5.5**. The results illustrated that the tensile strength was decreased with the increasing of MWCNTs on the fiber. And after the phenol and Laccase (Myceliophthora thermophila) were treated, the fiber tensile strength was increased. This result was particularly significant for the 1 wt% cellulose fiber (Figure **5.6**).

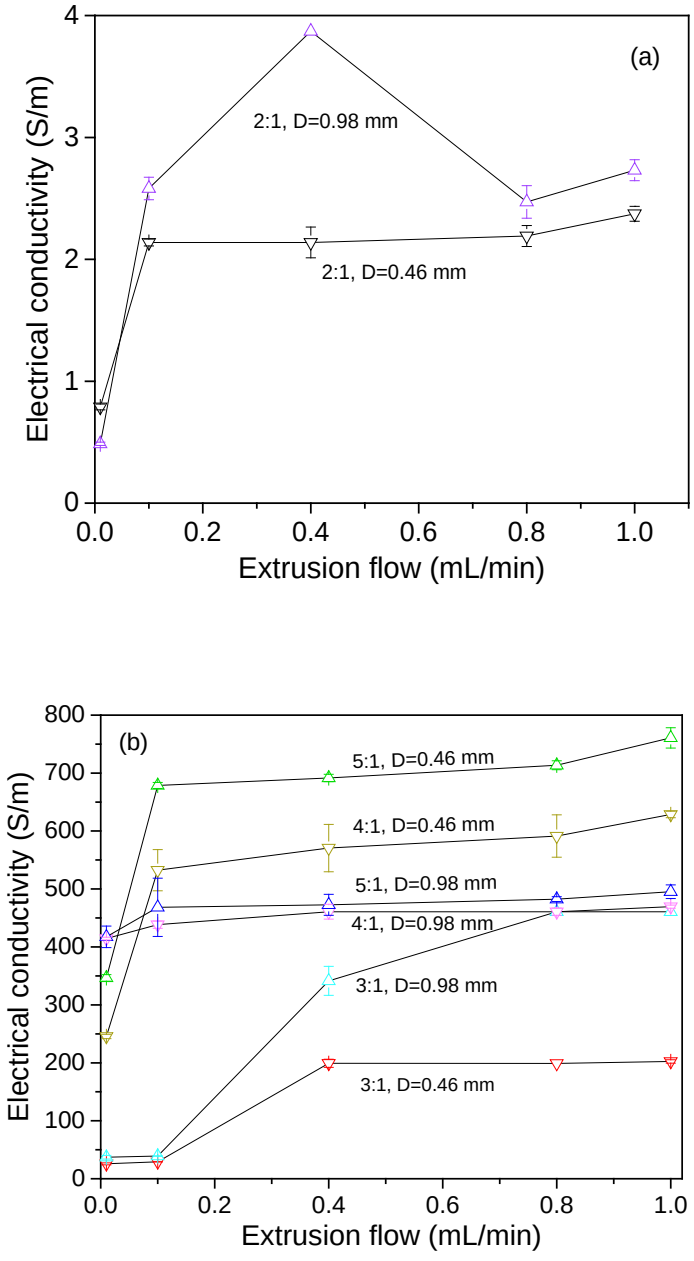

Figure 5.1 Electrical conductivities of MWCNT-cellulose fibers at different amounts of MWCNTs, spinneret diameter and extrusion flow. (a) Electrical conductivities at the mass ratio of MWCNTs with respect to cellulose of 2:1. (b) Electrical conductivities at the mass ratios of MWCNTs with respect to cellulose of 3:1, 4:1 and 5:1.

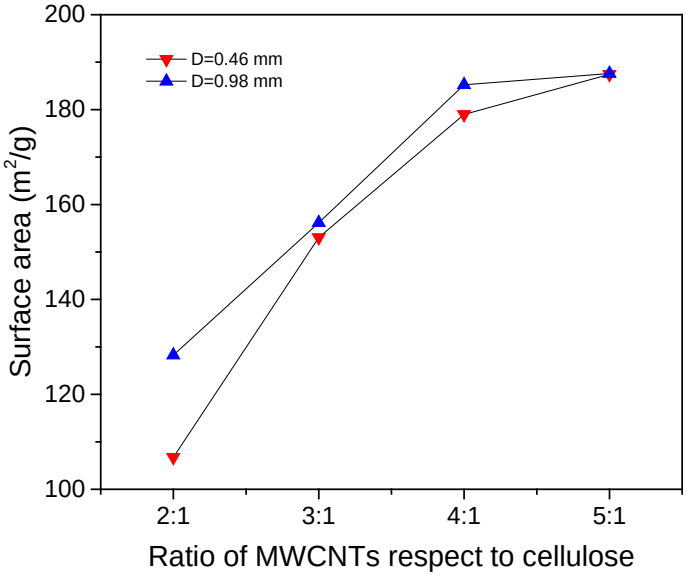

Figure 5.2 Surface area of MWCNTs-cellulose fibers at different extrusion flow of 1 mL/min and spinneret needle diameters of 0.46 mm and 0.98 mm. 2:1, 3:1, 4:1 and 5:1 are the mass ratios of MWCNTs with respect to cellulose.

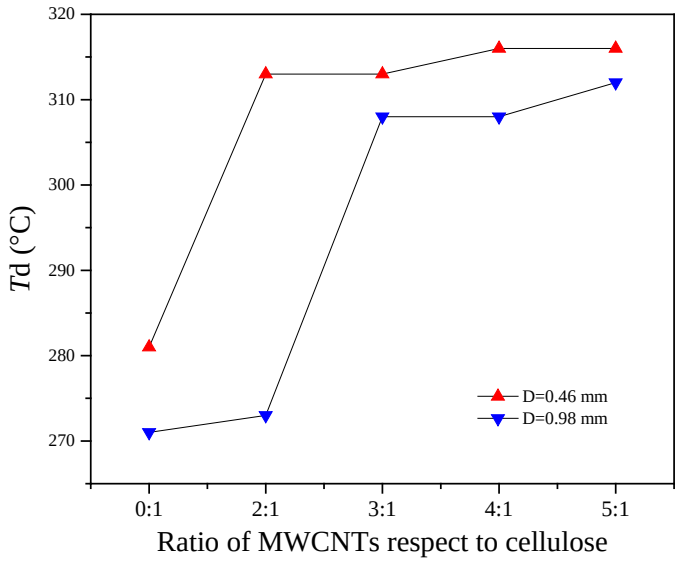

Figure 5.3 Decomposition temperature of cellulose and MWCNTs-cellulose fibers. Extrusion flow of the TGA study is 1 mL/min. 0:1 is the 1 wt% cellulose solution. 2:1, 3:1, 4:1 and 5:1 are the ratios of MWCNTs respect to cellulose.

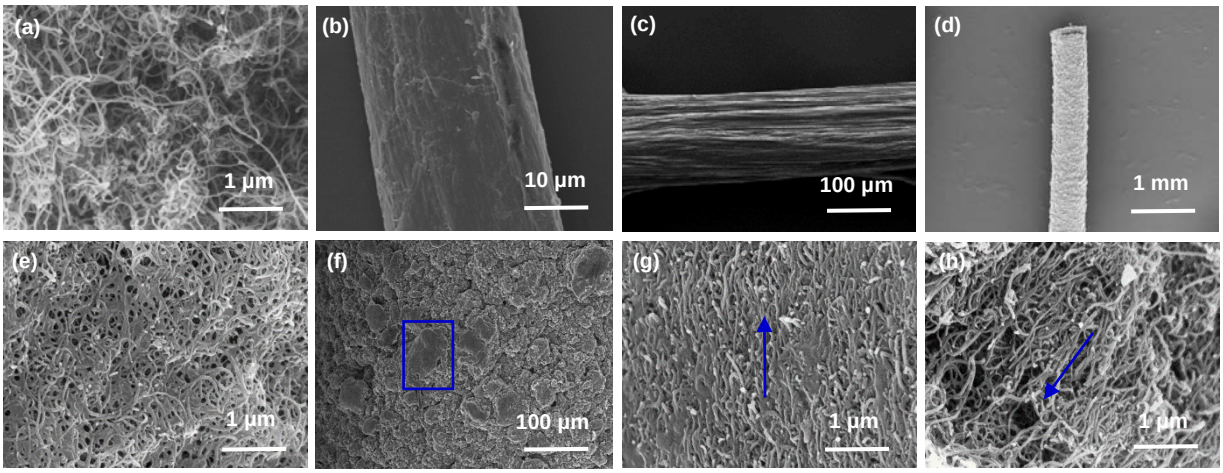

Figure 5.4 SEM of original material and spinning fiber. (a) Original MWCNTs. (b) Original cotton pulp. (c) 1 wt% cellulose fiber. Extrusion flow is 1 mL/min, diameter is 0.46 mm. (d) 5:1 MWCNTs-cellulose fiber (low magnification). Extrusion flow is 1 mL/min, spinneret diameter is 0.46 mm. (e) Morphology of 5:1 MWCNT-cellulose fiber. Extrusion flow is 1 mL/min, diameter is 0.46 mm. (f), (g) and (h) Morphology of 5:1 MWCNTs-cellulose fiber. Extrusion flow is 0.01 mL/min, spinneret diameter is 0.46 mm.

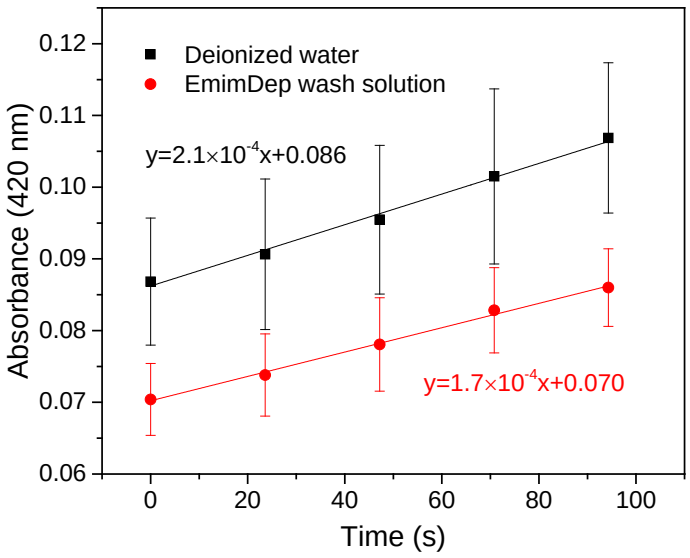

Figure 5.5 Absorbance plotted against time of two reaction solution of ABTS with enzyme prepared in deionized water and EmimDep wash solution

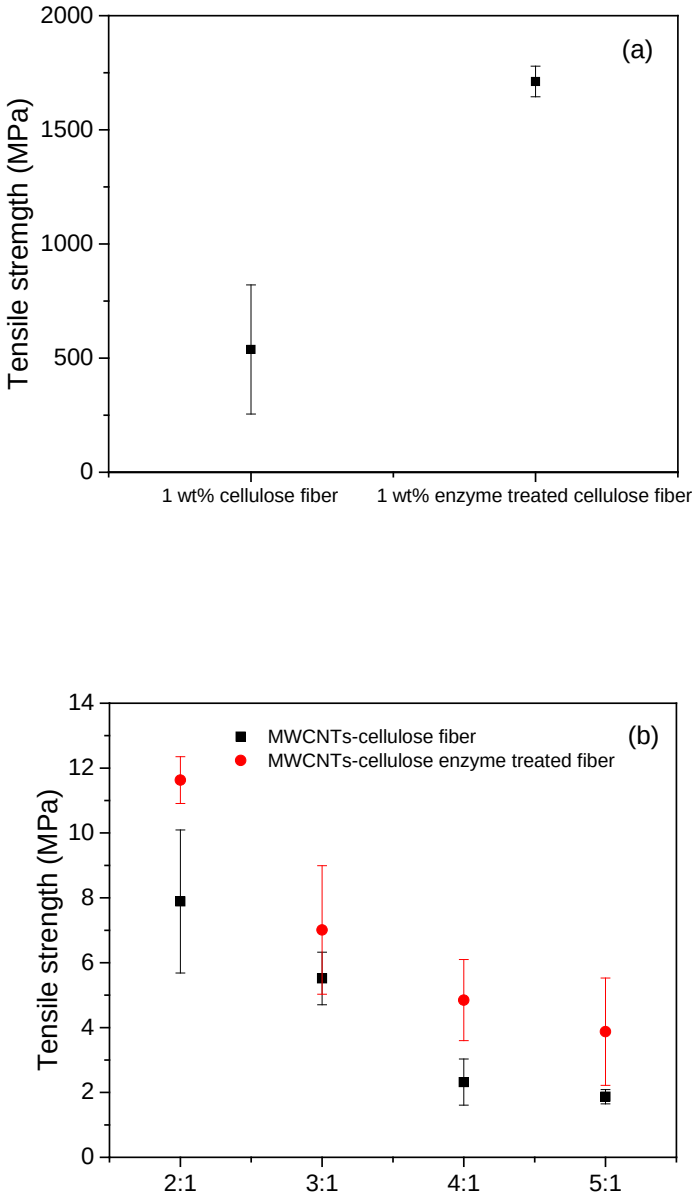

Figure 5.6 Tensile strength of cellulose and MWCNTs-cellulose fiber. (a) 1 wt% cellulose fiber and 1 wt% enzyme treated cellulose fiber. (b) MWCNT-cellulose fiber and MWCNT-cellulose enzyme treated fiber.

CHAPTER VI–Conclusions and future perspectives

6.1 Conclusion

The overall aim of this Ph.D. study was to fabricate cellulose-CNTs fiber by wet spinning, which has excellent conductivity and high tensile strength. In this process, a prerequisite for the Ph.D. study was using COSMO-RS to predicate the potential ILs for dissolving cellulose and selecting one also that can be used for dispersing CNTs. In addition, a new method of freeze crystallization for recycling ILs from ILs+H_2O mixtures was studied. In this method, freezing points of ILs+H_2O solutions were first measured, and then the energy requirement in the cellulose spinning process for ILs recycling from H_2O using the measured freezing point values was predicted.

The cellulose models and the functional ILs were designed and optimized, and then the logarithmic activity coefficients, excess enthalpies, σ-potentials and σ-profiles by COSMO-RS for ILs and cellulose system were calculated. The objective of this study was to find the potential ILs for dissolving cellulose from 375 ILs, the better model to represent cellulose, the key factor of IL for dissolving cellulose, and doing the cellulose solubility experiment to verify the prediction results (paper I). The initial hypothesis for this study that COSMO-RS is a fast and efficient tool for screening the potential ILs of dissolving cellulose, and the type of ILs of imidazolium-, pyridinium-, morpholinium- and pyrrolidinium- were the excellent ILs for dissolving cellulose. The result of this study confirmed this initial hypothesis. COSMO-RS prediction and the cellulose solubility experimental results showed that the mid-monomer part of the cellotriose model was found to be closer to the experimental results than a neat glucose model and the model of the mid-dimer part of cellotetraose. And the logarithmic activity coefficients predicted by COSMO-RS can be used to represent the cellulose solubility for IL and the cellulose system. The excess enthalpy prediction results show that the anions play an important role for the cellulose dissolving process and the higher energy values of H-bonds qualitatively of ILs and cellulose system reflect the higher solubility

of cellulose in ILs. Importantly, the study confirms the hypothesis that the cations of methylimidazolium$^+$, pyridinium$^+$, ethylmorpholinium$^+$ and methylpyrrolidinium$^+$ structured with functional groups, including ethyl, allyl, 2-hydroxylethyl, 2-methoxyethyl and acryloyloxypropyl, combined with anions Ac^-, Dec^-, $HCOO^-$, Cl^-, BEN^-, $DMPO_4^-$, DEP^-, DBP^- and Br^-, were predicted to be the best for dissolving cellulose.

To investigate the IL recycling after cellulose spinning, a new recycling method of freeze crystallization was introduced in this Ph.D. study based on our hypothesis that that freeze crystallization could be a feasible method for IL recovery from IL+H_2O mixtures because of the lower energy cost of freezing water rather than evaporating (paper II and III). According to paper I, six imidazolium-based ILs which have higher cellulose solubility were selected to measure the freezing points of these ILs aqueous solutions. The freezing point results indicated that the studied ILs exhibited features similar to those of inorganic salts in depressing the freezing point of water. Ice starts forming when the IL aqueous solutions are cooled to their freezing points. Then a change in slope of the freezing point curve indicates a solid phase change, such as solid ILs or hydrates of the form IL·$n$$H_2O$. In the scope of ice, it can separate the IL from H_2O which confirms the hypotheses. The freezing point measurement results also indicate that cations and anions both affect the freezing points of the ILs aqueous solutions. The COSMO-RS prediction results show that H-bonds formed by IL anions are the dominant type of interaction between ILs and water.

On the basis of freezing point measurement values, the energy requirement in the ILs recycling process after cellulose spinning was investigated (paper III). Two ILs of EimAc and EmimDep were selected for this study. The results reveal that using the method of freeze crystallization+evaporation, compared with the evaporation method, to recover the IL from water not only saves energy in itself but also ensures that less H_2O is evaporated compared with the traditional solvent of NMMO. These results further confirm our previous hypotheses that using the freeze crystallization method to recycle ILs will save more energy than the evaporation method.

The effect of spinning parameters and the amount of MWCNTs in the fiber were investigated. The extrusion flow and spinneret diameter both affect the conductivity of the cellulose-CNTs fiber. The fiber conductivity first increases and then has a relatively small variation. The spinneret diameter result illustrated that the diameter at 0.98 mm has a larger effect than 0.46 mm with the increase of extrusion flow at mass ratios of 2:1 and 3:1. When the mass ratios increased to 4:1 and 5:1, the smaller diameter makes a higher electrical conductivity. The conductivity of cellulose-CNTs fiber increased with the increasing amount of CNTs. However, the tensile strength decreased with the increasing amount of CNTs. These results confirm our hypotheses. Finally, the effect of enzymatic modification on the treatment of the fiber surface was studied. The treatment solution includes phenol and Laccase. The result shows that the fiber tensile strength will be increased after the phenol and enzyme solution treatment, especially as a significant increase for the studied cellulose fiber.

6.2 Future perspectives

As we have shown in this study, the prepared cellulose-CNTs fiber has a great potential for application in the electrochemical and biomedical fields. A series of fiber properties have been investigated in this work, including ILs recycling. However, the practical applications of the cellulose-CNTs fiber and the ILs recycling in the cellulose fabrication process have not yet been studied. Therefore, there is still a lot of work that can be done to accelerate the application of cellulose-CNTs conductive fiber.

In the previous study, several kinds of ILs have been applied to spin cellulose fiber using water as coagulation solvent. However, recycling of ILs from IL+H_2O mixtures after the fiber spinning was investigated in none of these studies. Since the freeze crystallization method can save energy in ILs recycling from water, design and establish the ILs recycling process by the freeze crystallization method and extend it into industrial scale, it is important to expand the application of ILs as the solvent for dissolving cellulose or some other polymer.

As has been shown in this study, the cellulose-CNTs fiber has an excellent

conductivity of 760 S/m and a large surface area of 188 m^2/g. However, the future application of this fiber was not investigated in this study. In the investigation of Neimark et al. [113], they prepared the SWCNTs fiber with the surface area of 160 m^2/g and employed this fiber for N_2 and hexadecane wetting liquid absorption successfully. Thus, this technique could be applied in this cellulose-CNTs fiber, and it can be assumed that the absorption will be a significant amount. Another application for this fiber might be as electrically conductive wire and electric heating [2]. The CNTs can launch far infrared ray at the wavelengths of 3–15 μm [114]. This wavelength is a health scope for plants and human body among other things, which makes the studied fiber have a potential application in electric heating and body health care.

CHAPTER−References

[1] R. Janmanee, S. Chuekachang, S. Sriwichai, A. Baba, S. Phanichphant, Functional conducting polymers in the application of spr biosensors, J Nanotechnol 2012 (2012) 1-7.

[2] T.-W. Lee, M. Han, S.-E. Lee, Y.G. Jeong, Electrically conductive and strong cellulose-based composite fibers reinforced with multiwalled carbon nanotube containing multiple hydrogen bonding moiety, Compos Sci Technol 123 (2016) 57-64.

[3] L. Härdelin, B. Hagström, Wet spun fibers from solutions of cellulose in an ionic liquid with suspended carbon nanoparticles, J Appl Polym Sci 132 (2015) 41417-414113.

[4] F. Alimohammadi, M.P. Gashti, A. Shamei, A novel method for coating of carbon nanotube on cellulose fiber using 1,2,3,4-butanetetracarboxylic acid as a cross-linking agent, Prog Org Coat, 74 (2012) 470-478.

[5] R.H. Baughman, A.A. Zakhidov, W.A. de Heer, Carbon nanotubes--the route toward applications, Science 297 (2002) 787-792.

[6] F. Alimohammadi, M. Parvinzadeh Gashti, A. Shamei, Functional cellulose fibers via polycarboxylic acid/carbon nanotube composite coating, J Coat Technol Res 10 (2012) 123-132.

[7] A.-S. Michardière, C. Mateo-Mateo, A. Derré, M.A. Correa-Duarte, N. Mano, P. Poulin, Carbon Nanotube Microfiber Actuators with Reduced Strength Relaxation, J Phys Chem C 120 (2016) 6851-6858.

[8] S.S. Rahatekar, A. Rasheed, R. Jain, M. Zammarano, K.K. Koziol, A.H. Windle, J.W. Gilman, S. Kumar, Solution spinning of cellulose carbon nanotube composites using room temperature ionic liquids, Polymer 50 (2009) 4577-4583.

[9] C. Zhu, J. Chen, K.K. Koziol, J.W. Gilman, P.C. Trulove, S.S. Rahatekar, Effect of fibre spinning conditions on the electrical properties of cellulose and carbon nanotube composite fibres spun using ionic liquid as a benign solvent, Express Polym Lett 8 (2014) 154-163.

[10] C. Tsioptsias, A. Stefopoulos, I. Kokkinomalis, L. Papadopoulou, C. Panayiotou, Development of micro- and nano-porous composite materials by processing cellulose with ionic liquids and supercritical CO_2, Green Chem 10 (2008) 965.

[11] A.H. Conner, in Handbook of Size Exclusion Chromatography, Chromatographic Science Series, Marcel Dekker, New York, (1995).

[12] H. Wang, G. Gurau, R.D. Rogers, Ionic liquid processing of cellulose, Chem Soc Rev, 41 (2012)

1519-1537.

[13] D. M. Updegraff, Semimicro determination of cellulose in biological materials, Anal Biochem 32 (1969) 420-424.

[14] R.J. Moon, A. Martini, J. Nairn, J. Simonsen, J. Youngblood, Cellulose nanomaterials review: structure, properties and nanocomposites, Chem Soc Rev 40 (2011) 3941-3994.

[15] H. Ohno, Y. Fukaya, Task Specific Ionic Liquids for Cellulose Technology, Chem Lett 38 (2009) 2-7.

[16] X.H. Qian, S.Y. Ding, M.R. Nimlos, D.K. Johnson, M.E. Himmel, Atomic and electronic structures of molecular crystalline cellulose I beta: A first-principles investigation, Macromolecules 38 (2005) 10580-10589.

[17] Y. Nishiyama, P. Langan, H. Chanzy, Crystal structure and hydrogen-bonding system in cellulose from synchrotron X-ray and neutron fiber diffraction, J Am Chem Soc 124 (2002) 9074-9082.

[18] M.V. Elizabeth Dinand, Henri Chanzy and Laurent Heux,, Mercerization of primary wall cellulose and its implication for the conversion of cellulose I→cellulose II, Cellulose 9 (2002) 7–18.

[19] F.J. Kolpak, J. Blackwell, Determination of the structure of cellulose II, Macromolecules 9 (1976) 273–278.

[20] A. George, Obtaining and treating vegetable fibres, British patents, 285 (1885).

[21] H.P. Fink, P. Weigel, H.J. Purz, J. Ganster, Structure formation of regenerated cellulose materials from NMMO-solutions, Prog Polym Sci 26 (2001) 1473-1524.

[22] C.L. Mccormick, T.R. Dawsey, Preparation of cellulose derivatives via ring-opening reactions with cyclic reagents in lithium-chloride N,N-Dimethylacetamide, Macromolecules 23 (1990) 3606-3610.

[23] R.B. Hammer, A.F. Turbak, Abstracts of Papers of the American Chemical Society, 173 (1977) 8.

[24] S. Fischer, W. Voigt, K. Fischer, The behaviour of cellulose in hydrated melts of the composition $LiX \cdot n\ H_2O$ ($X=I^-$, NO_3^-, CH_3COO^-, ClO_4^-), Cellulose 6 (1999) 213-219.

[25] S. Fischer, H. Leipner, K. Thummler, E. Brendler, J. Peters, Inorganic molten salts as solvents for cellulose, Cellulose 10 (2003) 227-236.

[26] K. Saalwachter, W. Burchard, P. Klufers, G. Kettenbach, P. Mayer, D. Klemm, S. Dugarmaa,

Cellulose solutions in water containing metal complexes, Macromolecules 33 (2000) 4094-4107.

[27] T. Rosenau, A. Potthast, H. Sixta, P. Kosma, The chemistry of side reactions and byproduct formation in the system NMMO/cellulose (Lyocell process), Prog Polym Sci 26 (2001) 1763-1837.

[28] Y. Zhao, X. Liu, J. Wang, S. Zhang, Insight into the cosolvent effect of cellulose dissolution in imidazolium-based ionic liquid systems, J Phys Chem B 117 (2013) 9042-9049.

[29] A. Xu, J. Wang, H. Wang, Effects of anionic structure and lithium salts addition on the dissolution of cellulose in 1-butyl-3-methylimidazolium-based ionic liquid solvent systems, Green Chem 12 (2010) 268-275.

[30] C. Graenacher, Cellulose solution, US Patent, (1934).

[31] S. Zhu, Y. Wu, Q. Chen, Z. Yu, C. Wang, S. Jin, Y. Ding, G. Wu, Dissolution of cellulose with ionic liquids and its application: a mini-review, Green Chem 8 (2006) 325-327.

[32] R.D. Rogers, K.R. Seddon, Ionic liquid: industrical applications to green chemistry, Am Chem Soc Washington D. C, (2002).

[33] R.P. Swatloski, S.K. Spear, J.D. Holbrey, R.D. Rogers, Dissolution of cellulose with ionic liquids, J Am Chem Soc 124 (2002) 4974-4975.

[34] X. Li, N. Li, J. Xu, X. Duan, Y. Sun, Q. Zhao, Cellulose fibers from cellulose/1-ethyl-3-methylimidazolium acetate solution by wet spinning with increasing spinning speeds, J Appl Polym Sci 131 (2014) 742−751.

[35] J. Palomar, J.S. Torrecilla, V.R. Ferro, F. Rodriguez, Development of an a priori ionic liquid design tool. 2. ionic liquid selection through the prediction of COSMO-RS molecular descriptor by inverse neural network, Ind Eng Chem Res 48 (2009) 2257-2265.

[36] M. Kosmulski, J. Gustafsson, J.B. Rosenholm, Thermal stability of low temperature ionic liquids revisited, Thermochim Acta 412 (2004) 47-53.

[37] Y.-R. Liu, K. Thomsen, Y. Nie, S.-J. Zhang, A.S. Meyer, Predictive screening of ionic liquids for dissolving cellulose and experimental verification, Green Chem 18 (2016) 6246-6254.

[38] A. Brandt, J. Gräsvik, J.P. Hallett, T. Welton, Deconstruction of lignocellulosic biomass with ionic liquids, Green Chem 15 (2013) 550.

[39] Y. Zhao, X. Liu, J. Wang, S. Zhang, Effects of cationic structure on cellulose dissolution in ionic liquids: a molecular dynamics study, Chemphyschem 13 (2012) 3126-3133.

[40] T. Erdmenger, C. Haensch, R. Hoogenboom, U.S. Schubert, Homogeneous tritylation of cellulose in 1-butyl-3-methylimidazolium chloride, Macromol Biosci 7 (2007) 440-445.

[41] A. Pinkert, K.N. Marsh, S.S. Pang, M.P. Staiger, Ionic liquids and their interaction with cellulose, Chem Rev 109 (2009) 6712-6728.

[42] H. Zhao, G.A. Baker, Z. Song, O. Olubajo, T. Crittle, D. Peters, Designing enzyme-compatible ionic liquids that can dissolve carbohydrates, Green Chem 10 (2008) 696.

[43] P. Mäki-Arvela, I. Anugwom, P. Virtanen, R. Sjöholm, J.P. Mikkola, Dissolution of lignocellulosic materials and its constituents using ionic liquids—A review, Ind Crop Prod 32 (2010) 175-201.

[44] Y. Li, X. Liu, S. Zhang, Y. Yao, X. Yao, J. Xu, X. Lu, Dissolving process of a cellulose bunch in ionic liquids: a molecular dynamics study, Phys Chem Chem Phys 17 (2015) 17894-17905.

[45] A. Casas, J. Palomar, M.V. Alonso, M. Oliet, S. Omar, F. Rodriguez, Comparison of lignin and cellulose solubilities in ionic liquids by COSMO-RS analysis and experimental validation, Ind Crop Prod 37 (2012) 155-163.

[46] M. Zavrel, D. Bross, M. Funke, J. Buchs, A.C. Spiess, High-throughput screening for ionic liquids dissolving (ligno-)cellulose, Bioresour Technol 100 (2009) 2580-2587.

[47] N. Sun, H. Rodriguez, M. Rahman, R.D. Rogers, Where are ionic liquid strategies most suited in the pursuit of chemicals and energy from lignocellulosic biomass?, Chem Commun 47 (2011) 1405-1421.

[48] H. Zhang, J. Wu, J. Zhang, J.S. He, 1-Allyl-3-methylimidazolium chloride room temperature ionic liquid: A new and powerful nonderivatizing solvent for cellulose, Macromolecules 38 (2005) 8272-8277.

[49] J.L. Xu, X.Q. Yao, J.Y. Xin, X.M. Lu, S.J. Zhang, An effective two-step ionic liquids method for cornstalk pretreatment, J Chem Technol Biot, 90 (2015) 2057-2065.

[50] A. Klamt, Conductor-like screening model for real solvents: a new approach to the quantitative calculation of solvation phenomena, J Phys Chem 99 (1995) 2224-2235.

[51] A. Klamt, G. Schuurmann, Cosmo: a new approach to dielectric screening in solvents with explicit expressions for the screening energy and its gradient, J Chem Soc Perk T 2, (1993) 799-805.

[52] Z. Guo, B.-M. Lue, K. Thomasen, A.S. Meyer, X. Xu, Predictions of flavonoid solubility in ionic liquids by COSMO-RS: experimental verification, structural elucidation, and solvation characterization, Green Chem 9 (2007) 1362-1373.

[53] A. Klamt, The COSMO and COSMO-RS solvation models, Adv Rev 2011, 1, 699–709.

[54] F. Eckert, Klamt A, COSMO therm Users Manual, Version C3.0 Release 14.01, Leverkusen,

Germany: COSMOlogic GmbH & Co KG, (2014).

[55] M. Diedenhofen, A. Klamt, COSMO-RS as a tool for property prediction of IL mixtures-A review, Fluid Phase Equilibr, 294 (2010) 31-38.

[56] M. Gonzalez-Miquel, M. Massel, A. DeSilva, J. Palomar, F. Rodriguez, J.F. Brennecke, Excess enthalpy of monoethanolamine + ionic liquid mixtures: how good are COSMO-RS predictions?, J Phys Chem B 118 (2014) 11512-11522.

[57] A. Casas, S. Omar, J. Palomar, M. Oliet, M.V. Alonso, F. Rodriguez, Relation between differential solubility of cellulose and lignin in ionic liquids and activity coefficients, RSC Adv 3 (2013) 3453-3460.

[58] C. Loschen, A. Klamt, Prediction of solubilities and partition coefficients in polymers using COSMO-RS, Ind Eng Chem Res 53 (2014) 11478-11487.

[59] J. Kahlen, K. Masuch, K. Leonhard, Modelling cellulose solubilities in ionic liquids using COSMO-RS, Green Chem 12 (2010) 2172-2181.

[60] J. Vitz, T. Erdmenger, C. Haensch, U.S. Schubert, Extended dissolution studies of cellulose in imidazolium based ionic liquids, Green Chem 11 (2009) 417-424.

[61] Y. Deng, Carbon fiber electronic interconnects, PhD Dissertation (2007).

[62] H.O. Pierson, Handbook of Carbon, graphite, diamond and fullerenes-properties, processing and applications, William Andrew Publishing/Noyes (1993).

[63] Carbon fibers, https://en.wikipedia.org/wiki/Carbon_fibers (accessed October, 2017).

[64] S. Iijima, Helical microtubules of graphitic carbon, Nature 354 (1991) 56-58.

[65] M. Scarselli, P. Castrucci, M. De Crescenzi, Electronic and optoelectronic nano-devices based on carbon nanotubes, J Phys Condens Matter 24 (2012) 313202.

[66] S. Subramoney, Novel nanocarbons - Structure, properties, and potential applications, Adv Mater 10 (1998) 1157-1171.

[67] H. Zhang, Z.G. Wang, Z.N. Zhang, J. Wu, J. Zhang, J.S. He, Regenerated-cellulose/multiwalled-carbon-nanotube composite fibers with enhanced mechanical properties prepared with the ionic liquid 1-allyl-3-methylimidazolium chloride, Adv Mater 19 (2007) 698-704.

[68] J.P. Salvetat, J.M. Bonard, N.H. Thomson, A.J. Kulik, L. Forro, W. Benoit, L. Zuppiroli, Mechanical properties of carbon nanotubes, Appl Phys A-Mater 69 (1999) 255-260.

[69] X.W. Jiang, Y.Z. Bin, N. Kikyotani, M. Matsuo, Thermal, electrical and mechanical properties of ultra-high molecular weight polypropylene and carbon filler composites, Polym J 38 (2006) 419-

431.

[70] T. McNally, P. Pötschke, P. Halley, M. Murphy, D. Martin, S.E.J. Bell, G.P. Brennan, D. Bein, P. Lemoine, J.P. Quinn, Polyethylene multiwalled carbon nanotube composites, Polymer 46 (2005) 8222-8232.

[71] S.H. Kim, B.G. Min, S.C. Lee, S.B. Park, T.D. Lee, M. Park, S. Kumar, Morphology and properties of polyacrylonitrile/single wall carbon nanotube composite films, Fiber Polym 5 (2004) 198-203.

[72] I. Cotiuga, F. Picchioni, U.S. Agarwal, D. Wouters, J. Loos, P.J. Lemstra, Block-copolymer-assisted solubilization of carbon nanotubes and exfoliation monitoring through viscosity, Macromol Rapid Comm 27 (2006) 1073-1078.

[73] S. Kumar, T.D. Dang, F.E. Arnold, A.R. Bhattacharyya, B.G. Min, X.F. Zhang, R.A. Vaia, C. Park, W.W. Adams, R.H. Hauge, R.E. Smalley, S. Ramesh, P.A. Willis, Synthesis, structure, and properties of PBO/SWNT composites, Macromolecules 35 (2002) 9039-9043.

[74] J.K.W. Sandler, S. Pegel, M. Cadek, F. Gojny, M. van Es, J. Lohmar, W.J. Blau, K. Schulte, A.H. Windle, M.S.P. Shaffer, A comparative study of melt spun polyamide-12 fibres reinforced with carbon nanotubes and nanofibres, Polymer 45 (2004) 2001-2015.

[75] P.A. Brühwiler, M. Barbezat, A. Necola, D.J. Kohls, O. Bunk, D.W. Schaefer, P. Pötschke, Comparison of quasistatic to impact mechanical properties of multiwall carbon nanotube/polycarbonate composites, J Mater Res 25 (2011) 1118-1130.

[76] B.G. Min, H.G. Chae, M.L. Minus, S. Kumar, Polymer/carbon nanotube composite fibers-An overview, Functional Composites of Carbon Nanotubes and Applications, (2009) 43–73.

[77] A.V. Eletskii, A.A. Knizhnik, B.V. Potapkin, J.M. Kenny, Electrical characteristics of carbon nanotube-doped composites, Phys-Usp 58 (2015) 209-251.

[78] A. Takegawa, M.-a. Murakami, Y. Kaneko, J.-i. Kadokawa, Preparation of chitin/cellulose composite gels and films with ionic liquids, Carbohyd Polym 79 (2010) 85-90.

[79] W. Wang, Y. Nie, Y. Liu, L. Bai, J. Gao, S. Zhang, Preparation of cellulose/multi-walled carbon nanotube composite membranes with enhanced conductive property regulated by ionic liquids, Fiber Polym 18 (2017) 1780-1789.

[80] J.H. Hong, M.K. Ku, Y. Ahn, H.J. Kim, H. Kim, Air-gap spinning of cellulose/ionic liquid solution and its characterization, Fiber Polym 14 (2014) 2015-2019.

[81] L. Sun, J.Y. Chen, W. Jiang, V. Lynch, Crystalline characteristics of cellulose fiber and film regenerated from ionic liquid solution, Carbohydr Polym 118 (2015) 150-155.

[82] Z. Luo, A. Wang, C. Wang, W. Qin, N. Zhao, H. Song, J. Gao, Liquid crystalline phase behavior and fiber spinning of cellulose/ionic liquid/halloysite nanotubes dispersions, J Mater Chem A, 2 (2014) 7327.

[83] N. Bhardwaj, S.C. Kundu, Electrospinning: a fascinating fiber fabrication technique, Biotechnol Adv 28 (2010) 325-347.

[84] D. Liang, B.S. Hsiao, B. Chu, Functional electrospun nanofibrous scaffolds for biomedical applications, Adv Drug Deliv Rev 59 (2007) 1392-1412.

[85] A.L. Yarin, S. Koombhongse, D.H. Reneker, Bending instability in electrospinning of nanofibers, J Appl Phys 89 (2001) 3018-3026.

[86] E. Adomaviciute, R. Milasius, The influence of applied voltage on poly(vinyl alcohol) (PVA) nanofibre diameter, Fibres Text East Eur 15 (2007) 69-72.

[87] P. Lu, Y.L. Hsieh, Multiwalled carbon nanotube (MWCNT) reinforced cellulose fibers by electrospinning, ACS Appl Mater Interfaces 2 (2010) 2413-2420.

[88] H.Q. Hou, J.J. Ge, J. Zeng, Q. Li, D.H. Reneker, A. Greiner, S.Z.D. Cheng, Electrospun polyacrylonitrile nanofibers containing a high concentration of well-aligned multiwall carbon nanotubes, Chem Mater 17 (2005) 967-973.

[89] B. Fugetsu, E. Akiba, M. Hachiya, M. Endo, The production of soft, durable, and electrically conductive polyester multifilament yarns by dye-printing them with carbon nanotubes, Carbon 47 (2009) 527-530.

[90] J. He, H. Yu, B. Fugetsu, S. Tanaka, L. Sun, Electrochemical removal of bisphenol A using a CNT-covered polyester yarn electrode, Sep Purif Technol 110 (2013) 81-85.

[91] J.G. Lynam, G.I. Chow, C.J. Coronella, S.R. Hiibel, Ionic liquid and water separation by membrane distillation, Chem Eng J 288 (2016) 557-561.

[92] X. Liu, Y. Nie, X. Meng, Z. Zhang, X. Zhang, S. Zhang, DBN-based ionic liquids with high capability for the dissolution of wool keratin, RSC Adv 7 (2017) 1981-1988.

[93] T. Fukuyama, M. Shinmen, S. Nishitani, M. Sato, I. Ryu, A copper-free Sonogashira coupling reaction in ionic liquids and its application to a microflow system for efficient catalyst recycling, Org Lett 4 (2002) 1691-1694.

[94] J.F. Birdwell, J. McFarlane, R.D. Hunt, H. Luo, D.W. DePaoli, D.L. Schuh, S. Dai, Separation of ionic liquid dispersions in centrifugal solvent extraction contactors, Sep Sci Technol 41 (2006) 2205-2223.

[95] L.A. Blanchard, J.F. Brennecke, Recovery of organic products from ionic liquids using supercritical carbon dioxide, Ind Eng Chem Res 40 (2001) 287-292.

[96] B. Wu, W. Liu, Y. Zhang, H. Wang, Do we understand the recyclability of ionic liquids?, Chem-Eur J 15 (2009) 1804-1810.

[97] L.A. Blanchard, D. Hancu, E.J. Beckman, J.F. Brennecke, Green processing using ionic liquids and CO_2, Nature 399 (1999) 28-29.

[98] S. Mishra, A.K. Mohanty, L.T. Drzal, M. Misra, S. Parija, S.K. Nayak, S.S. Tripathy, Studies on mechanical performance of biofibre/glass reinforced polyester hybrid composites, Compos Sci Technol 63 (2003) 1377-1385.

[99] Y. Li, K.L. Pickering, Hemp fibre reinforced composites using chelator and enzyme treatments, Compos Sci Technol 68 (2008) 3293-3298.

[100] M. Liu, A. Baum, J. Odermatt, J. Berger, L. Yu, B. Zeuner, A. Thygesen, J. Holck, A.S. Meyer, Oxidation of lignin in hemp fibres by laccase: Effects on mechanical properties of hemp fibres and unidirectional fibre/epoxy composites, Compos Part A-Appl S 95 (2017) 377-387.

[101] Z. Saleem, H. Rennebaum, F. Pudel, E. Grimm, Treating bast fibres with pectinase improves mechanical characteristics of reinforced thermoplastic composites, Compos Sci Technol 68 (2008) 471-476.

[102] E.H. Loomis, On the freezing-points of dilute aqueous solutions, Phys Rev 3 (1896) 270-292.

[103] W.H. Rodebush, The freezing points of concentrated solutions and the free energy of solution of salts, J Am Chem Soc 40 (1918) 1204-1213.

[104] H.C. Jones, F.H. Getman, Über das vorhandensein von hydraten in konzentrierten wässerigen lösungen, Z Phys Chem 49 (1904) 385-455.

[105] H.C. Jones, Über die bestimmung des gefrierpunktes sehr verdünnter salzlösungen, Z Phys Chem 11 (1893) 529-551.

[106] M.W. Arshad, P.L. Fosbøl, N. von Solms, K. Thomsen, Freezing point depressions of phase change CO_2 solvents, J Chem Eng Data 58 (2013) 1918-1926.

[107] Enthalpy of fusion. https://en.wikipedia.org/wiki/Enthalpy_of_fusion. (accessed August 2017).

[108] M.G. Freire, A.R.R. Teles, M.A.A. Rocha, B. Schröder, C.M.S.S. Neves, P.J. Carvalho, D.V. Evtuguin, L.M.N.B.F. Santos, J.A.P. Coutinho, Thermophysical characterization of ionic liquids able to dissolve biomass, J Chem Eng Data 56 (2011) 4813–4822.

[109] C. Su, X.Y. Liu, C.Y. Zhu, M.G. He, Isobaric molar heat capacities of 1-ethyl-3-methylimidazolium acetate and 1-hexyl-3-methylimidazolium acetate up to 16 MPa, Fluid Phase Equilib 427 (2016) 187–193.

[110] C.M. Tenney, M. Massel, J.M. Mayes, M. Sen, J.F. Brennecke, E.J. Maginn, A computational and experimental study of the heat transfer properties of nine different ionic liquids, J Chem Eng Data 59 (2014) 391–399.

[111] IL Thermo: Ionic Liquids Database. http://ilthermo.boulder.nist.gov/. (accessed December 2017).

[112] A.V. Blokhin, O.V. Voitkevich, G.J. Kabo, Y.U. Paulechka, M.V. Shishonok, A.G. Kabo, V.V. Simirsky, Thermodynamic properties of plant biomass components. heat capacity, combustion energy, and gasification equilibria of cellulose, J Chem Eng Data 56 (2011) 3523–3531.

[113] A.V. Neimark, S. Ruetsch, K.G. Kornev, P.I. Ravikovitch, Hierarchical pore structure and wetting properties of single-wall carbon nanotube fibers, Nano Lett 3 (2003) 419-423.

[114] S.J. Zhang, Y.R. Liu, Y. Nie, K.L. Zhang, Research and application of ionic liquid-carbon nano far-infrared radiation heating material, CN106183320 A (2016).

Paper I

Yan-Rong Liu, Kaj Thomsen, Yi Nie, Suo-Jiang Zhang and Anne S. Meyer

Predictive screening of ionic liquids for dissolving cellulose and experimental verification

Green Chemistry, 2016, 18, 624−625.

Volume 18 | Number 23 | 7 December 2016 | Pages 6147–6398

Green Chemistry

Cutting-edge research for a greener sustainable future

www.rsc.org/greenchem

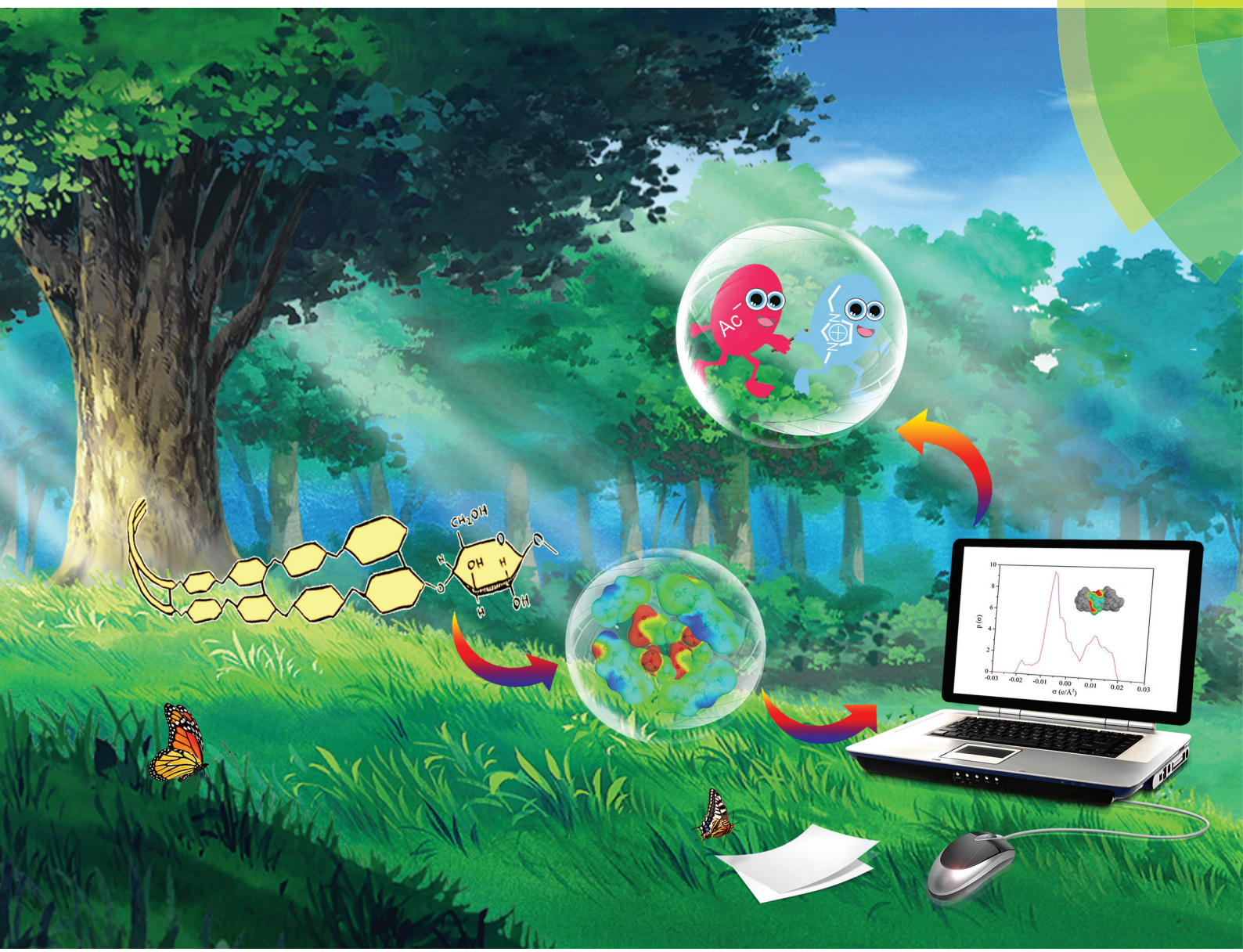

ISSN 1463-9262

ROYAL SOCIETY OF CHEMISTRY

PAPER

Suo-Jiang Zhang, Anne S. Meyer *et al.*

Predictive screening of ionic liquids for dissolving cellulose and experimental verification

175 YEARS

Green Chemistry

PAPER

Cite this: *Green Chem.*, 2016, **18**, 6246

Predictive screening of ionic liquids for dissolving cellulose and experimental verification†

Yan-Rong Liu,[a,b,c] Kaj Thomsen,[b] Yi Nie,[c] Suo-Jiang Zhang*[c] and Anne S. Meyer*[a]

Received 4th July 2016,
Accepted 5th September 2016

DOI: 10.1039/c6gc01827k

www.rsc.org/greenchem

In this work, 357 ionic liquids (ILs) formed from 17 cations and 21 anions were selected for evaluation of their ability to dissolve cellulose by COSMO-RS. In order to evaluate the predictive model and method, experimental measurements of the solubility of microcrystalline cellulose (MCC) in 7 of these ILs were also conducted. Predicted results from logarithmic activity coefficients were generally in good agreement with the experimental results. Three different models were used for describing cellulose, and the mid-monomer part of the cellotriose model was found to be closer to the experimental results than a neat glucose model and the model of the mid-dimer part of cellotetraose. Excess enthalpy calculations indicated that hydrogen-bond (H-bond) interactions between cellulose (*i.e.* the three cellulose models) and the 7 studied ILs are key factors for the solubility of cellulose, and the anions play a crucial role in the cellulose dissolution process. Importantly, the cations of methylimidazolium$^+$, pyridinium$^+$, ethylmorpholinium$^+$ and methylpyrrolidinium$^+$ structured with functional groups including ethyl, allyl, 2-hydroxylethyl, 2-methoxyethyl and acryloyloxypropyl, combined with anions Ac^-, Dec^-, $HCOO^-$, Cl^-, BEN^-, $DMPO_4^-$, DEP^-, DBP^- and Br^- were predicted to be the best for dissolving cellulose.

1. Introduction

Cellulose is widely used in paper products, textiles, plastics, coatings, composites, laminates, optical film, pharmaceuticals and other applications. The numerous applications of cellulose is attributed to its promising features, such as biocompatibility, biodegradability, thermal and chemical stability.[1,2] Cellulose is a linear polymer consisting of several hundred to over ten thousand β-(1 → 4)-linked glucose repeating units, together with numerous intermolecular and intramolecular H-bonds.[3,4] The multiple H-bonds between cellulose molecules form highly ordered crystalline regions which makes cellulose insoluble in water and common organic solvents.[5] Some traditional solvent systems have been investigated for cellulose dissolution processes, for example, *N*-methylmorpholine oxide (NMMO),[6] *N*,*N*-dimethylacetamide/lithium chloride (DMAc/LiCl),[7] *N*,*N*-dimethylformamide/nitrous tetroxide (DMF/N_2O_4),[8] molten salt hydrates ($LiClO_4{\cdot}3H_2O$, $LiCH_3COO{\cdot}2H_2O$, $LiCl/ZnCl_2/H_2O$, $NaSCN/KSCN/LiSCN{\cdot}2H_2O$),[9,10] and aqueous NaOH or aqueous solutions of metal complexes (Cd-tren, Ni-tren and Cuoxam).[11] However, drawbacks of these processes including high cost, high dissolution temperature, volatility, difficulty in solvent recovery and toxicity make them undesirable, and underlines the necessity for developing greener solvents for cellulose dissolution.[12,13] Ionic liquids (ILs) can be considered green solvents.[14–17] In the recent years, more than 60 ILs have been investigated for their ability to dissolve cellulose.[3] The increasing interest in ILs as solvents is due to their remarkable properties such as immeasurably low vapour pressure, excellent chemical and thermal stability, electrical conductivity, and non-flammability. The most fascinating property of ILs is the structural diversity, as numerous possible cations and anions can be combined freely.[3,18,19]

It is reported that the best cations for dissolving cellulose are mainly derivatives of imidazolium and pyridinium,[3] and that the most efficient anions are chloride, acetate, formate, phosphate, sulphate, and sulfonate.[20] Some researchers claim that the cellulose dissolution process is strongly anion-dependent,[3,21,22] whereas others claim that not only the properties of anions or cations, but also their combination, make ILs efficient for dissolving cellulose.[23] Erdmenger[24] and Zhao[25] indicated that cations can influence the dissolution of cellulose. Increasing the alkyl chain length of the cation decreases

[a]*Center for Bioprocess Engineering, Department of Chemical and Biochemical Engineering, Technical University of Denmark, Søltofts Plads 227, 2800 Lyngby, Denmark. E-mail: am@kt.dtu.dk*
[b]*Center for Energy Resources Engineering (CERE), Department of Chemical and Biochemical Engineering, Technical University of Denmark, Søltofts Plads 229, 2800 Lyngby, Denmark. E-mail: kth@kt.dtu.dk*
[c]*Beijing Key Laboratory of Ionic Liquids Clean Process, Key Laboratory of Green Process and Engineering, State Key Laboratory of Multiphase Complex Systems, Institute of Process Engineering, Chinese Academy of Sciences, P.O. Box 353 Beijing, 100190, China. E-mail: sjzhang@ipe.ac.cn*

†Electronic supplementary information (ESI) available: General synthesis processes and the properties of the ILs studied in this work. See DOI: 10.1039/c6gc01827k

the ability of the IL to dissolve cellulose. By adjusting the functional groups on the cations of ILs, more efficient and functionalized ILs for dissolving cellulose can be obtained. Feng *et al.*[26] concluded that AmimCl with a double bond is more effective in dissolving cellulose than BmimCl. Luo *et al.*[27] synthesized 1-(2-hydroxyethyl)-3-methyl imidazolium chloride (HOEtmimCl) and found that ILs containing hydroxyl groups on the imidazole cation are excellent solvents for dissolving cellulose due to the H-bonds formation with cellulose. The solubility of microcrystalline cellulose (MCC) in HOEtmimCl can reach 5%–7% at 70 °C. However, cellulose has a low solubility in $[H(OEt)_3mim]Ac$ because the flexibility of $[H(OEt)_3mim]Ac$ allows it to form H-bonds with its anions, which decreases the cellulose solubility.[28]

Numerous possible ILs composed of cations and anions can be synthesized. The functional groups of the cations can be modified to affect the capacity of ILs to dissolve cellulose. It is nevertheless a challenge to identify the best ILs for dissolving cellulose. A rapid and *a priori* screening method to predict the cellulose solubility capacity for ILs is needed in chemical engineering research and industry. COSMO-RS (Conductor-like Screening Model for Real Solvents), integrates dominant interactions of H-bonds, misfits, and van der Waals forces in IL systems to summarize multiple solvation.[29] COSMO-RS can be used for performing mixture calculations at various temperatures, which renders it considered by many to be the most accurate model for the prediction and development of ILs for specific tasks currently available.[30]

Previous publications have demonstrated that COSMO-RS can successfully predict properties of ILs in the field of biomass dissolution, such as activity coefficients,[31] solubilities[32–34] and excess enthalpies.[35] Activity coefficient calculations have been shown to be useful for predicting cellulose solubility in ILs.[36] Kahlen *et al.*[37] found that the anion played an important role in dissolving cellulose according to COSMO-RS calculations. Casas *et al.*[22] studied the solubility of cellulose and lignin in different ILs using activity coefficient and excess enthalpy calculations from COSMO-RS. They reported activity coefficients and excess enthalpies with similar tendencies, and demonstrated that the exothermal behaviour and low activity coefficients of cellulose and lignin in ILs was related to higher solubilities.[22] On the basis of that work, Casas *et al.*[35] subsequently designed 3 × 3 cellulose model structures consisting of nine "differently cut" monomers, M1 to M9, to be used by COSMO-RS to represent cellulose. Based on the calculated activity coefficients, excess enthalpies and the experimental results for 12 ILs, the M4 model was finally selected as the best cellulose model.[35]

The aims of this work were to use COSMO-RS to screen potential ILs for their ability to dissolve cellulose and to select the best cellulose model from three cellulose models considered. These three cellulose models investigated included a glucose model (Model 1), a mid-monomer part of a cellotriose model (Model 2), and a mid-dimer part of a cellotetraose model (Model 3). The ILs tested in this work mainly focused on 17 cations based on methylimidazolium$^+$, pyridinium$^+$, ethylmorpholinium$^+$ and methylpyrrolidinium$^+$ structures with ethyl, allyl, 2-hydroxyethyl, 2-methoxyethyl and acryloyloxypropyl functional groups. The 17 cations were combined with 21 different anions. The solubility of MCC in seven different ILs was measured experimentally to verify the predictions of the logarithmic activity coefficients and excess enthalpies of the three cellulose models in the ILs. The best cellulose model was then identified by comparing the predictions with the experimental results.

2. Computational details and calculation sets of cellulose models and ionic liquids

2.1 COSMO-RS computation details

The COSMO-RS calculations were carried out using several procedures. First, the quantum chemical Gaussian09 package was used to optimize the structure of the studied compounds at the B3LYP/6-31++G (d, p) level. Second, the COSMO files of the optimized structures were opened by Gaussian03 and COSMO continuum solution models were calculated using the BVP86/TZVP/DGA1 level theory. Third, the logarithmic activity coefficients, excess enthalpies, σ-potentials and σ-profiles were determined using the model COSMO-RS (implementation: COSMOtherm version C3.0 release 14.01, applied with parameterization BP_TZVP_C30_1401, COSMOlogic, Leverkusen, Germany). The calculation temperature for COSMO-RS was set to 90 °C, the same temperature as used for the experimental determination of cellulose solubility.

When conducting calculations in the COSMO-RS program, the molar fractions of the cations and anions of the ILs were treated as equal, *i.e.* $n_{cation} = n_{anion} = n_{IL}$.[35] The logarithmic activity coefficients and excess enthalpies for solutions of cellulose in ILs were also investigated by COSMO-RS. In these two calculations, the molar fraction of cellulose was set as 0.5, the molar fraction of the IL cations was set as 0.25, and the molar fraction of the IL anions was set as 0.25. The activity coefficients and the excess enthalpies were calculated according to the COSMO-RS theory. The activity coefficient calculation equation has been described previously by Diedenhofen and Klamt,[31] and the excess enthalpy equation has been described by Gonzalez-Miquel *et al.*[38]

2.2 Cellulose models

The program package COSMOtherm has several methods to model a polymer. Usually, only one or several repeating units are selected for the calculation. Then, the end group of the polymer is deactivated using a function of COSMO-RS called "weight string", which allows for selectively switching on/off certain atoms within a COSMOfile.[36] Using this function, with the weight string code for off being "0" and for on being "1", the weight string sequences for each atom in the mid-monomer part of a cellotriose model and the mid-dimer part of a cellotetraose model were obtained (Fig. 1). For this con-

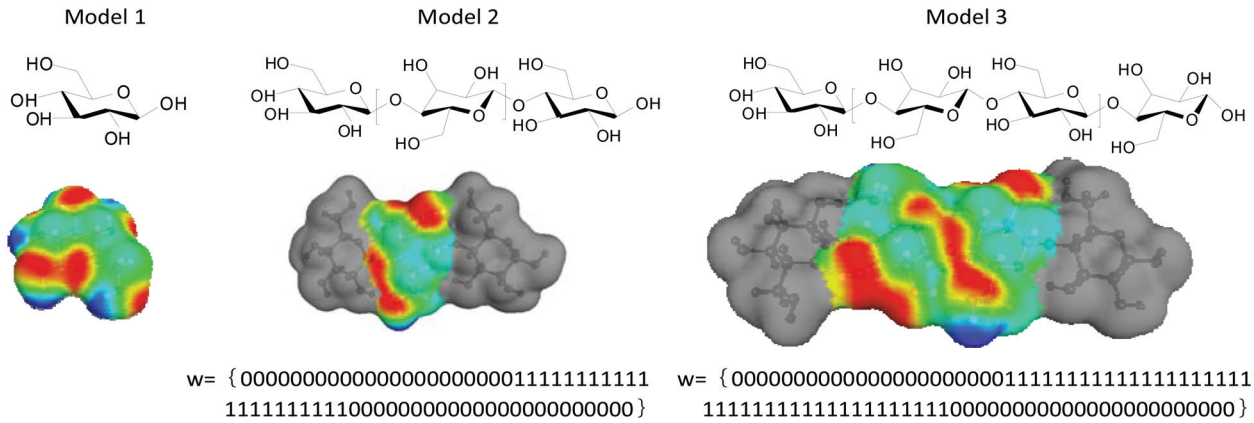

Fig. 1 COSMO-RS charge surfaces of three cellulose representation models: Model 1: glucose; Model 2: mid-monomer of cellotriose; Model 3: mid-dimer of cellotetraose. Red zones indicate a positive surface charge, yellow and green zones indicate almost neutral charges, navy blue designate negative surface charge. The code-sequences inside the brackets correspond to the weight string codes for each model: "0" indicates that the atom was deactivated (switched "off") and "1" indicates that the atom was activated (switched "on") in the COSMO-RS calculation.

figuration, the total free energy of each model was calculated as the sum of its DFT/COSMO energy in the conductor reference state and its individual pseudo chemical potential, obtained from the COSMO-RS model.[37] In this case, three representations were selected for cellulose, and these structures were obtained according to the procedures described in section 2.1–2.2. The resulting chemical structures and charge surface regions are displayed in Fig. 1.

2.3 Structure of cations and anions

The structure of cations and anions employed in this work can be seen in Tables 1 and 2 respectively. The COSMOfiles for the cations no. 1–5, 10–13, and 14–17 in Table 1 and all the COSMOfiles for the anions in Table 2 come from the COSMO-RS database. The COSMOfiles for the cations no. 6–9 in Table 1 were calculated based on the procedures outlined in 2.1.

According to the work of Wang *et al.*[3] imidazolium-based and pyridinium-based ILs which have the functional groups alkyl-, allyl-, hydroxyl-, ether- and ester- are potential for dissolving cellulose. Morpholinium-based and pyrrolidinium-based ILs with these function groups were considered based on the works of Raut *et al.*[39] and Zavrel *et al.*[40] The cations of methylimidazolium$^+$, pyridinium$^+$, ethylmorpholinium$^+$ and methylpyrrolidinium$^+$ with functional groups of ethyl, allyl, 2-hydroxylethyl, 2-methoxyethyl or acryloyloxypropyl were combined with 21 anions resulting in the 357 ILs studied in this work.

Table 1 Cations studied in this work

No.	Name of cation	Acronym	Structure
1–5	1-*R*-3-Methylimidazolium	[Emim, Amim, HOEtmim, EtOMmim, AOPmim] R = ethyl, allyl, 2-hydroxylethyl, 2-methoxyethyl, acryloyloxypropyl	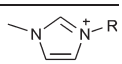
6–9	*N*-*R*-Pyridinium	[Epy, Apy, HOEtpy, EtOMpy] R = ethyl, allyl, 2-hydroxylethyl, 2-methoxyethyl	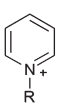
10–13	4-*R*-4-Ethylmorpholinium	[Eemor, Aemor, HOEtemor, EtOMemor] R = ethyl, allyl, 2-hydroxylethyl, 2-methoxyethyl	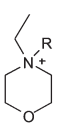
14–17	1-*R*-1-Methylpyrrolidinium	[Empyrr, Ampyrr, HOEtmpyrr, EtOMmpyrr] R = ethyl, allyl, 2-hydroxylethyl, 2-methoxyethyl	

3. Results and discussion

3.1 σ-Potential of three cellulose models

In COSMO-RS, σ-potential is a measure of the affinity of the system to a surface of polarity σ. The σ-potential can be divided into three main regions: the H-bond donor region ($\sigma < -0.0082$ e Å^{-2}), the H-bond acceptor region ($\sigma > +0.0082$ e Å^{-2}), and the non-polar region ($-0.0082 < \sigma < +0.0082$ e Å^{-2}).[38] Fig. 2 shows that the σ-potential values of Model 1 are more negative than those of Model 2 and Model 3 in the H-bond acceptor region, which means that Model 1 gives more affinity for H-bond acceptor surfaces than the other two models.

3.2 Logarithmic activity coefficient prediction by COSMO-RS

The predicted logarithmic activity coefficients ($\ln\gamma$) of the three cellulose models in each of the 357 ILs are depicted in Fig. 3–5. The cations and anions are listed according to their cellulose dissolution ability. The ILs with high cellulose dissolution capacities according to the predicted logarithmic activity coefficients are located to the left, while the ILs with lower cellulose dissolution capacities are located to the right.

Table 2 Anions studied in this work

No.	Name of anion	Acronym	Structure	No.	Name of anion	Acronym	Structure
1	Acetate	Ac		12	Formate	HCOO	
2	Tetrachloroaluminate	$AlCl_4$		13	Hydrogensulfate	HSO_4	
3	Bromide	Br	Br^-	14	Iodide	I	I^-
4	Tetrafluoroborate	BF_4		15	Methoxyethylsulfate	$MeOEtSO_4$	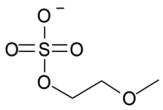
5	Butylsulfate	$BuSO_4$	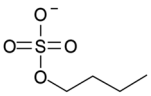	16	Methylsulfate	$MeSO_4$	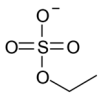
6	Benzoate	BEN	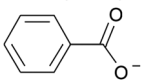	17	Dicyanamide	$N(CN)_2$	
7	Chloride	Cl	Cl^-	18	Hexafluorophosphate	PF_6	
8	Perchlorate	ClO_4		19	Bis(trifluoromethylsulfonyl)amide	Tf_2N	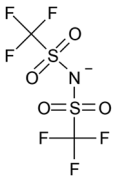
9	Dimethylphosphate	$DMPO_4$	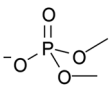	20	Toluene-4-sulfonate	Tos	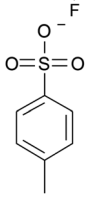
10	Diethylphosphate	DEP	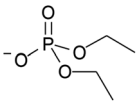	21	Decanoate	Dec	
11	Dibutylphosphate	DBP	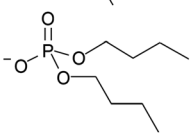				

The logarithmic activity coefficients of these three cellulose models in different ILs varied significantly with the use of different anions (Fig. 3–5), suggesting that the cellulose dissolution capacity is mostly determined by the anion while the cation only has a moderate effect on the dissolution process. In particular, the methylpyrrolidinium-based ILs have a remarkably high predicted logarithmic activity coefficient, which may be due to its ability to form H-bonds with cellulose. The anions Ac^-, Dec^-, $HCOO^-$, Cl^-, DEP^-, $DMPO_4^-$, DBP^-, BEN^- and Br^- were predicted to be best anions for dissolving cellulose. Our results are in agreement with the findings of Kahlen *et al.*[37] and Casas *et al.*[22] Kahlen *et al.*[37] gave an explanation for this phenomenon: the energy of the H-bonds of cellulose is up to 25 kJ mol^{-1},[41] thus the interactions between cellulose and solvent need to go beyond this energy in order to result in cellulose dissolution. This requires that either the cation or the anion of the IL is highly polar and the combination of the anion and cation is only slightly polar. Tabulated values of the predicted logarithmic activity coefficients for cellulose in ILs can be found in the ESI.†

3.3 Experimental solubility in seven ILs

In Fig. 3–5, the ILs are sorted according to their ability to dissolve cellulose. The best IL for cellulose dissolution appears in

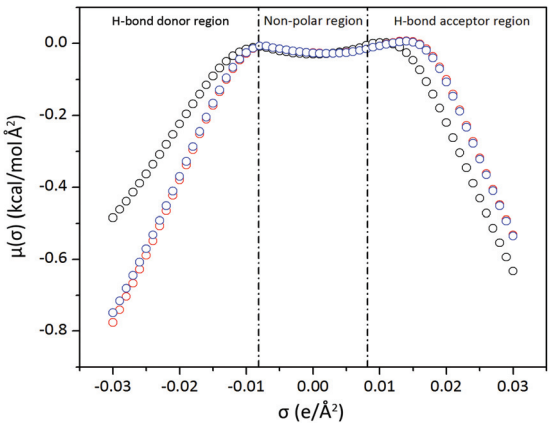

Fig. 2 σ-Potentials of Model 1 (black circle), Model 2 (blue circle) and Model 3 (red circle) predicted by COSMO-RS.

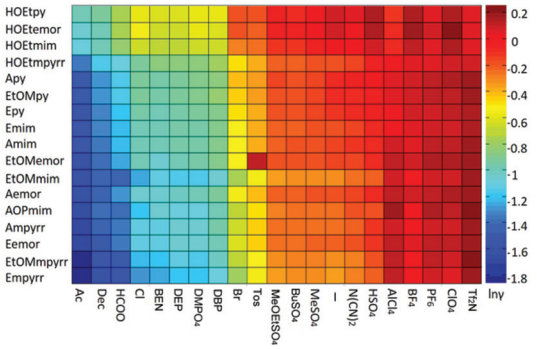

Fig. 5 The logarithmic activity coefficients prediction of model 3 in 357 ILs. Conditions: the mole fraction of cellulose model 3 was 0.5, the mole fraction of IL cations and anion was 0.25 each. The calculation temperature was 90 °C.

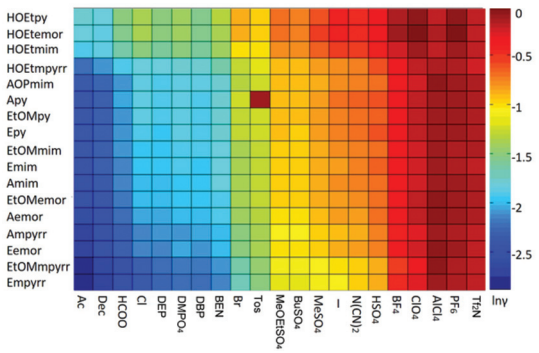

Fig. 3 The logarithmic activity coefficients prediction of model 1 in 357 ILs. Conditions: the mole fraction of cellulose model 1 was 0.5, the mole fraction of IL cations and anions was 0.25 each. The calculation temperature was 90 °C.

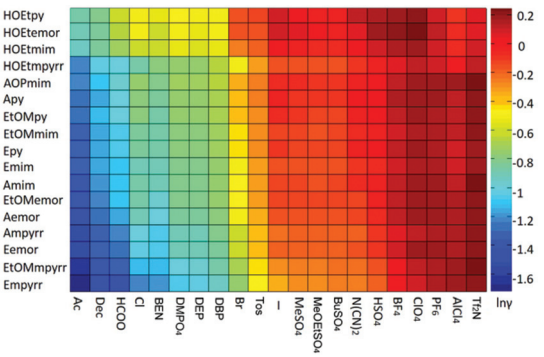

Fig. 4 The logarithmic activity coefficients prediction of model 2 in 357 ILs. Conditions: the mole fraction of cellulose model 2 was 0.5, the mole fraction of IL cations and anions was 0.25 each. The calculation temperature was 90 °C.

the lower left corner of each of the three charts. It should be noted that the cations appear in almost the same order in Fig. 3 and 4. In Fig. 5, the order of the cations is slightly different. However, the order of the anions is almost identical in each of the figures. In order to validate the COSMO-RS prediction results and obtain the best model to represent cellulose, the solubility of cellulose in seven ILs was measured at 90 °C. These seven ILs were chosen mainly because they contain the functional groups ethyl, allyl, 2-hydroxylethyl, or 2-methoxyethyl with methylimidazolium$^+$ and pyridinium$^+$ as the cations (section 2.3). Ac^-, Cl^-, DEP^-, Br^- were selected as the anions because the prediction of logarithmic activity coefficients showed that these anions are efficient for cellulose dissolution (Fig. 3–5). EmimAc has previously been identified as having superior properties for cellulose dissolution.[35] In addition, three types of comparisons for cellulose dissolution capacity can be distinguished among the seven ILs chosen: 1. EmimAc and EmimDEP have the same imidazolium cation but different anions, 2. AmimCl and EtOMmimCl have the same anion but different imidazolium cations, and 3. The sets of AmimCl/ApyCl and HOEtmimBr/HOEtpyBr have the same anions but different kinds of cations (one is an imidazolium cation, the other is a pyridinium cation). Table 3 shows that except for [EtOMmim]Cl, the ILs have dissolution trends identical to the logarithmic activity coefficient trends. Predictive quantitative modelling by COSMO-RS calculations can thus be used to qualitatively assess and notably rank the ability of different ILs to dissolve cellulose. Casas *et al.*[35] (using a selected monomeric structure (M4) inside a 3 × 3 cellulose macrostructure as cellulose model) and Kahlen *et al.*[37] (using the mid-monomer glucose unit of cellotriose as a cellulose model) have previously predicted the abilities of different ILs to dissolve cellulose, but some of their predictions turned out not to be consistent with the experimental results. Kahlen *et al.*[37] explained the reason for divergence between prediction and experimental results as being due to that water might be hindering the interaction between IL and cellulose.

In this work, HOEtmimBr and HOEtpyBr turned out to have a higher water content than the rest of ILs (shown in the ESI†), which might explain the deviation between the predicted and the experimental result (point e, f being off the

Table 3 Experimental solubility of MCC in seven ILs and COSMO-RS prediction results for the three cellulose models

No.	ILs	Solubility (wt%)	Solubility (g mol^{-1} IL)	ln γ prediction results by COSMO-RS		
				Model 1	Model 2	Model 3
a	EmimAc	27	46	−2.44	−1.65	−1.82
b	AmimCl	<17	<26	−1.98	−1.17	−1.29
c	EmimDEP	15	40	−1.97	−1.10	−1.25
d	ApyCl	15	23	−1.86	−1.08	−1.20
e	HOEtmimBr	9.1	19	−1.01	−0.55	−0.57
f	HOEtpyBr	9.1	18	−0.89	−0.46	−0.48
g	EtOMmimCl	8.3	15	−1.93	−1.13	−1.55

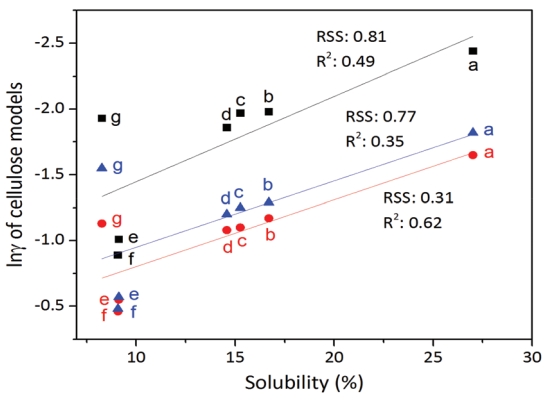

Fig. 6 Experimental values of MCC solubilities in seven ILs plotted against ln γ: Model 1 (■), Model 2 (●) and Model 3 (▲).

linear correlation in Fig. 6). Casas *et al.*[35] studied the cellulose dissolving property of EtOEmimCl which contains the ether functional group by predicting the activity coefficient in COSMO-RS. Casas *et al.*[35] reported the activity coefficient (γ) of EtOEmimCl to be 0.61 and that of HOEtmimBr to be 1.32 meaning that EtOEmimCl was predicted to have a better cellulose dissolving capacity than HOEtmimBr (as they concluded cellulose to be soluble when $\gamma < 0.85$ in their selected model for cellulose). In the present work we also consistently found that the predicted logarithmic activity coefficient, ln γ, of EtOMmimCl was lower than that of HOEtmimBr (Table 3), which was in agreement with the prediction tendency of Casas *et al.*[35] However, the experimental result slightly contrasted the prediction result between EtOMmimCl and HOEtmimBr, and showed that EtOMmimCl fitted poorly to the fitting line (Table 3 and Fig. 6), but it needs to be added that both solvents had low cellulose dissolution capacity with <10 wt% cellulose solubility.

Kahlen *et al.*[37] reported contradictions between predictions and experimental results for BmimCl and BmimAc. The prediction result from COSMO-RS documented that BmimAc had a better cellulose dissolving capacity than BmimCl, but, according to the experimental result reported by Vitz *et al.*[42] the cellulose solubility of BmimCl is 20%, and that of BmimAc is 12%. Kahlen *et al.*[37] explained that the ability of Chloride to form hydrogen bonds is not yet totally clear and difficult to model properly in COSMO-RS, which may explain why experimental results and prediction data for ILs with chloride anion do not always agree. Fig. 6 indicates that the residual sum of squares (RSS) of Model 2 is smaller and R square (R^2) is larger than the other two models. Hence, the prediction results of Model 2 were best correlated with the experimental solubility results. According to the predicted logarithmic activity coefficients of these three models, the logarithmic activity coefficients of Model 1 were significantly lower than the logarithmic activity coefficients of the other two cellulose models. This might be explained by the Model 1 being too simple to represent cellulose.[35]

3.4 Excess enthalpy prediction by COSMO-RS

The excess enthalpies from the intermolecular interactions (H-bonds, misfits and van der Waals forces) between the cellulose models and seven ILs were calculated by COSMO-RS (Fig. 7). The histogram in Fig. 7 illustrates that the H-bond interactions between the three cellulose models and the cations and anions of ILs have a high influence on the solubility of cellulose in the IL, followed by misfit and van der Waals force interactions. ILs with the same cations and different anions, such as EmimAc and EmimDEP, exhibit excess enthalpies that are very different. However, when the ILs have the same anion and different cations, the excess enthalpies have similar values. This is valid for the two bromides and the chloride in Fig. 7 (Model 1 and Model 2), which indicates that the anions play a crucial role in the dissolution process. These two results are in agreement with the study of Casas *et al.*[35] Casas *et al.*[22] indicated that H-bond energy values predicted by COSMO-RS reflects the affinity of ILs and cellulose, that is higher energy values of H-bonds qualitatively reflect higher solubility of cellulose in ILs. The molecular dynamics simulation works of Huo *et al.*[43] elucidated that the anions interact much more strongly with the cellulose surface than the cations. In their paper, they show that the main driving force for the cellulose dissolution is the H-bonds formed between anions of ILs and hydroxyl groups of cellulose, and this is supported here by the excess enthalpy result. It is observably in Fig. 7 that the excess enthalpy of EtOMmimCl in Model 3 is more negative than the excess enthalpy of EmimDEP and AmimCl. This is in disagreement with the experimentally

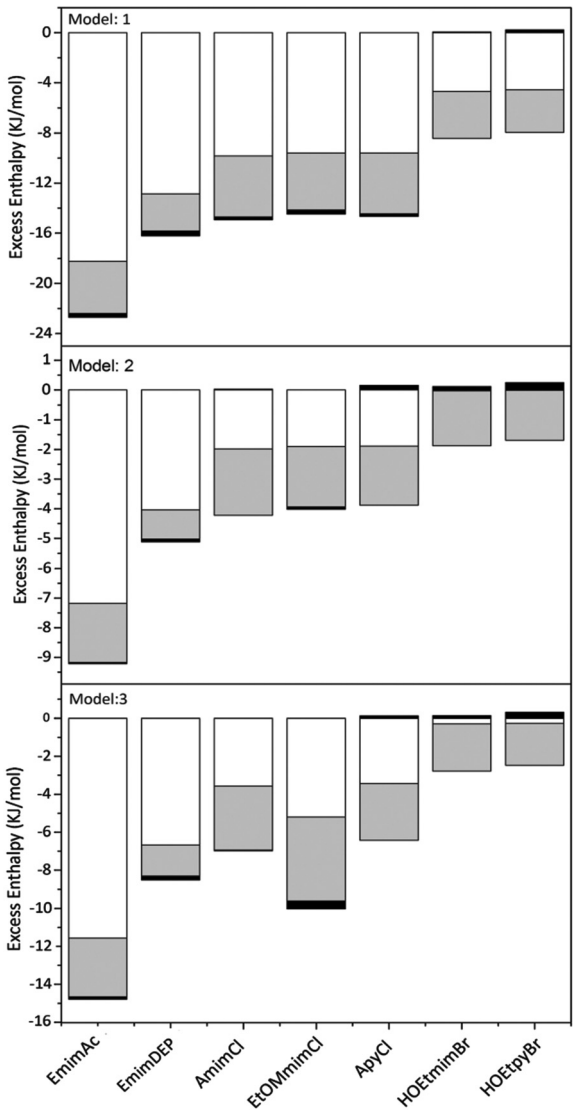

Fig. 7 Excess enthalpies between the three cellulose models and seven ILs, H-bond (white histogram), misfit (grey histogram) and van der Waals force (black histogram).

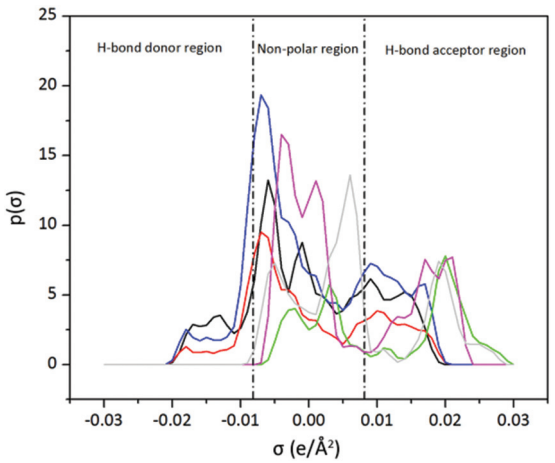

Fig. 8 σ-Profiles of Model 1 (black line), Model 2 (red line), Model 3 (blue line) and anions Ac^- (green line), DEP^- (pink line) and BEN^- (grey line).

determined solubility of cellulose in EtOMmimCl, thus Model 3 is not a good model to represent cellulose.

3.5 σ-Profiles prediction by COSMO-RS

The logarithmic activity coefficient and excess enthalpy prediction results illustrated that the cellulose dissolution process is strongly anion-dependent. Additionally, the σ-profiles between three cellulose models and the anions of Ac^-, DEP^- and BEN^- shown in Fig. 8 further describe the possible interactions of the three models and the anions. The σ-profiles of the candidates show that Ac^- and the three cellulose models are almost complementary, while DEP^- is not as complementary result within the nonpolar region. This means that with the same cations, the presence of the Ac^- renders the IL a better cellulose solvent than DEP^-. This is in agreement with the experimental results, which showed that EmimAc is better than EmimDEP for dissolving cellulose. So, the σ-profile result can be used to describe the anions dissolution capacity when combined with the same cations. σ-Profiles have also has been studied by Gonzalez-Miquel *et al.*[38] who used this method to successfully identify the better cations for ILs. Comparing the orders of the anions in the $\ln\gamma$ predictions of the Model 1 and Model 2 in Fig. 3 and 4 (blue colour region), it can be seen that the order of DEP^- and BEN^- is different for Model 1 and 2. According to Fig. 8, the σ-profile of BEN^- has a more complementary region around the peak of +0.006 e $Å^{-2}$ and +0.019 e $Å^{-2}$ than DEP^-. Therefore, BEN^- should be more to the left than DEP^- in the logarithmic activity coefficient figures. Model 2 predicts this better than Model 1. Overall, according to the prediction and experimental results, Model 2, the mid-monomer part of cellotriose model, is better than the glucose model (Model 1) and the mid-dimer cellotetraose model (Model 2).

4. Experimental

4.1 Chemical reagents

Seven different ILs were synthesized and used for the experimental validation of the cellulose solubility results obtained from COSMO-RS. The initial synthetic materials included: 1-methylimidazole (CP, Sinopharm Chemical Reagent Co., Ltd), pyridine (≥99.5%, Xilong Chemical Co., Ltd), *N*-ethylmorpholine (99%, aladdin), allyl chloride (≥97.0%, Sinopharm Chemical Reagent Co., Ltd), 2-bromoethanol (97%, (Beijing) J&K Scientific Ltd), 2-chloroethyl methyl ether (98%, aladdin), triethyl phosphate (CP, Sinopharm Chemical Reagent Co., Ltd), ether absolute (99%, Tianjin jingdongtianzheng precision chemical reagent factory), ethyl acetate (≥99.5%, Xilong Chemical Co., Ltd). Only 1-ethyl-3-methylimidazolium (99%) was purchased from Shanghai Cheng Jie Chemical Co. Ltd. The other six ILs were synthesized in the

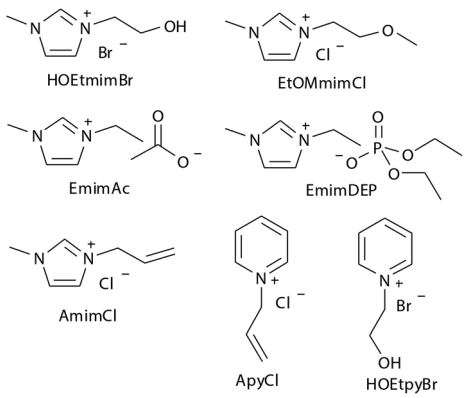

Scheme 1 The structures of the ILs synthesized and studied experimentally in this work.

lab. Microcrystalline cellulose was selected as the cellulose material (Column Chromatography, Sinopharm Chemical Reagent Co., Ltd) for the solubility analysis.

4.2 Nuclear magnetic resonance (NMR) and dissolution of MCC in ionic liquids

The structures of the seven ILs which were studied in this work can be seen in Scheme 1. The ILs were dried at 80 °C under vacuum for 48 hours after purification. The water content of each of the synthesized ILs was determined by Karl Fischer titration using a C20 Coulometric KF Titrator (Mettler Toledo Intl., Shanghai, China). Each of IL's water content was measured three times and the average value was used. The structures of these ILs were confirmed by ^{1}H NMR and ^{13}C NMR spectroscopy using a Bruker 600 spectrometer. The purities of the six synthesized ILs are HOEtmimBr (98.67 wt%), EtOMmimCl (99.31 wt%), EmimDEP (99.62 wt%), AmimCl (98.53 wt%), ApyCl (99.78 wt%), HOEtpyBr (98.33 wt%). The MCC was dried at 80 °C under vacuum for 48 h before use. MCC was added stepwise to a weighed amount of each of the seven ILs separately in a thermostatic oil bath at 90 °C. In the process of dissolution, an OLYMPUS BX 51 optical microscope was used to check the solubility of the MCC in these seven ILs. The limit of solubility was determined by gradually adding MCC until MCC could be observed under the optical microscope without dissolving after 12 hours.[35,44,45] The synthesis procedures and the properties of six synthesized ILs are shown in the ESI.†

5. Conclusion

COSMO-RS was used to screen potential ILs for their ability to dissolve cellulose. Three cellulose representation models were tested in COSMO-RS. It was found that the mid-monomer part of cellotriose model is better to represent cellulose than the glucose model and mid-dimer part of cellotetraose model. The experimental solubilities of MCC in the ILs followed the trend prediction from the logarithmic activity coefficient values, except in the case of [EtOMmim]Cl. The prediction of logarithmic activity coefficients of cellulose in ILs by COSMO-RS can therefore be considered an effective parameter to evaluate the dissolution power of the ILs. From the prediction results of the three cellulose models, it can be concluded that Ac^{-}, Dec^{-}, $HCOO^{-}$, Cl^{-}, BEN^{-}, $DMPO_4^{-}$, DEP^{-}, DBP^{-} and $Br^{-}$with various cations studied in this work are promising for cellulose dissolution. Cations with ethyl, allyl, 2-hydroxylethyl, 2-methoxyethyl and acryloyloxypropyl functional groups exhibited particularly good properties for cellulose dissolution. The excess enthalpy calculations indicated that the main forces in the cellulose dissolution in ILs are H-bonds, while the contribution of misfit forces and van der Waals forces are secondary. The dissolution process is largely anion-dependent. Although there are divergences between the calculated and the experimental results, the main dissolution trend can be obtained from COSMO-RS predictions. The prediction of the capacity of ILs to dissolve cellulose may be further optimized by advancing the cellulose models even beyond the mid-monomer part of cellotriose and the mid-dimer part of cellotetraose cellulose models used here to obtain even more precise predictions that are in accord with experimental results. Further work may moreover encompass predictions considering the degree of cellulose crystallinity in different types of cellulose raw materials.

Acknowledgements

We sincerely thank Dr Xiaochun Zhang, Dr Feng Huo and Dr Yongsheng Zhao for many helpful suggestions in the COSMO-RS calculation, and Wenjun Wang for helping with synthesis of ILs. This work was supported by the Department of Chemical and Biochemical Engineering, Technical University of Denmark and the National Natural Science Foundation of China (Grant No. 91434203 and 21576262), International S&T Cooperation Program of China (2014DFA61670) and CAS/SAFEA International Partnership Program for Creative Research Teams (20140491518).

References

1 C. Tsioptsias, A. Stefopoulos, I. Kokkinomalis, L. Papadopoulou and C. Panayiotou, *Green Chem.*, 2008, **10**, 965–971.
2 K. J. Edgar, C. M. Buchanan, J. S. Debenham, P. A. Rundquist, B. D. Seiler, M. C. Shelton and D. Tindall, *Prog. Polym. Sci.*, 2001, **26**, 1605–1688.
3 H. Wang, G. Gurau and R. D. Rogers, *Chem. Soc. Rev.*, 2012, **41**, 1519–1537.
4 D. M. Updegraff, *Anal. Biochem.*, 1969, **32**, 420–424.
5 H. Ohno and Y. Fukaya, *Chem. Lett.*, 2009, **38**, 2–7.
6 H.-P. Fink, P. Weigel, H. J. Purz and J. Ganster, *Prog. Polym. Sci.*, 2001, **26**, 1473–1524.
7 C. L. McCormick and T. R. Dawsey, *Macromolecules*, 1990, **23**, 3606–3610.

8 R. B. Hammer and A. F. Turbak, *Abstracts of Papers of the American Chemical Society*, 1977, vol. 173, p. 8.
9 S. Fischer, W. Voigt and K. Fischer, *Cellulose*, 1999, **6**, 213–219.
10 S. Fischer, H. Leipner, K. Thümmler, E. Brendler and J. Peters, *Cellulose*, 2003, **10**, 227–236.
11 K. Saalwächter, W. Burchard, P. Klüfers, G. Kettenbach, P. Mayer, D. Klemm and S. Dugarmaa, *Macromolecules*, 2000, **33**, 4094–4107.
12 Y. L. Zhao, X. M. Liu, J. J. Wang and S. J. Zhang, *J. Phys. Chem. B*, 2013, **117**, 9042–9049.
13 A. R. Xu, J. J. Wang and H. Y. Wang, *Green Chem.*, 2010, **12**, 268–275.
14 S. D. Zhu, Y. X. Wu, Q. M. Chen, Z. N. Yu, C. W. Wang, S. W. Jin, Y. G. Ding and G. Wu, *Green Chem.*, 2006, **8**, 325–327.
15 R. P. Swatloski, S. K. Spear, J. D. Holbrey and R. D. Rogers, *J. Am. Chem. Soc.*, 2002, **124**, 4974–4975.
16 N. Sun, M. Rahman, Y. Qin, M. L. Maxim, H. Rodríguez and R. D. Rogers, *Green Chem.*, 2009, **11**, 646–655.
17 M. Zavrel, D. Bross, M. Funke, J. Büchs and A. C. Spiess, *Bioresour. Technol.*, 2009, **100**, 2580–2587.
18 J. Palomar, J. S. Torrecilla, V. Ferro and F. Rodríguez, *Eng. Chem. Res.*, 2009, **48**, 2257–2265.
19 M. Kosmulski, J. Gustafsson and J. B. Rosenholm, *Thermochim. Acta*, 2004, **412**, 47–53.
20 P. Mäki-Arvel, I. Anugwom, P. Virtanen, R. Sjöholm and J. P. Mikkola, *Ind. Crops Prod.*, 2010, **32**, 175–201.
21 Y. Li, X. M. Liu, S. J. Zhang, Y. Y. Yao, X. Q. Yao, J. L. Xu and X. M. Lu, *Phys. Chem. Chem. Phys.*, 2015, **17**, 17894–17905.
22 A. Casas, J. Palomar, M. V. Alonso, M. Oliet, S. Omar and F. Rodriguez, *Ind. Crops Prod.*, 2012, **37**, 155–163.
23 I. Kilpeläinen, H. B. Xie, A. King, M. Granstrom, S. Heikkinen and D. S. Argyropoulos, *J. Agric. Food Chem.*, 2007, **55**, 9142–9148.
24 T. Erdmenger, C. Haensch, R. Hoogenboom and U. S. Schubert, *Macromol. Biosci.*, 2007, **7**, 440–445.
25 Y. L. Zhao, X. M. Liu, J. J. Wang and S. J. Zhang, *ChemPhysChem*, 2012, **13**, 3126–3133.
26 L. Feng and Z. L. Chen, *J. Mol. Liq.*, 2008, **142**, 1–5.
27 H. M. Luo, C. R. Zhou and Y. Q. Li, *Polym. Mater. Sci. Eng.*, 2005, **21**, 233–235.
28 H. Zhao, G. A. Baker, Z. Y. Song, O. Olubajo, T. Crittle and D. Peters, *Green Chem.*, 2008, **10**, 696–705.
29 Z. Guo, B.-M. Lue, K. Thomsen, A. S. Meyer and X. Xu, *Green Chem.*, 2007, **9**, 1362–1373.
30 A. Klamt, *Advanced Review*, 2011, **1**, 699–709.
31 M. Diedenhofen and A. Klamt, *Fluid Phase Equilib.*, 2010, **294**, 31–38.
32 A. Navas, J. Ortega, R. Vreekamp and E. Marrero, *Ind. Eng. Chem. Res.*, 2009, **48**, 2678–2690.
33 J. Palomar, M. Gonzalez-Miquel, A. Polo and F. Rodriguez, *Ind. Eng. Chem. Res.*, 2011, **50**, 3452–3463.
34 M. Gonzalez-Miquel, J. Palomar, S. Omar and F. Rodriguez, *Ind. Eng. Chem. Res.*, 2011, **50**, 5739–5748.
35 A. Casas, S. Omar, J. Palomar, M. Oliet, M. V. Alonsoa and F. Rodrigueza, *RSC Adv.*, 2013, **3**, 3453–3460.
36 C. Loschen and A. Klamt, *Ind. Eng. Chem. Res.*, 2014, **53**, 11478–11487.
37 J. Kahlen, K. Masuch and K. Leonhard, *Green Chem.*, 2010, **12**, 2172–2181.
38 M. Gonzalez-Miquel, M. Massel, A. DeSilva, J. Palomar, F. Rodriguez and J. F. Brennecke, *J. Phys. Chem. B*, 2014, **118**, 11512–11522.
39 D. G. Raut, O. Sundman, W. Q. Su, P. Virtanen, Y. Sugano, K. Kordas and J. Mikkola, *Carbohydr. Polym.*, 2015, **130**, 18–25.
40 M. Zavrel, D. Bross, M. Funke, J. Büchs and A. C. Spiess, *Bioresour. Technol.*, 2009, **100**, 2580–2587.
41 A. M. Bochek, *Russ. J. Appl. Chem.*, 2003, **76**, 1711–1719.
42 J. Vitz, T. Erdmenger, C. Haensch and U. S. Schubert, *Green Chem.*, 2009, **11**, 417–424.
43 F. Huo, Z. P. Liu and W. C. Wang, *J. Phys. Chem. B*, 2013, **117**, 11780–11792.
44 L. Liu, M. T. Ju, W. Z. Li and Q. D. Hou, *Carbohydr. Polym.*, 2013, **98**, 412–420.
45 S. Agarwal, A. M. Hossain, Y. Choi, M. Cheong, H. G. Jang and J. S. Lee, *Bull. Korean Chem. Soc.*, 2013, 3771–3775.

Paper II

Yanrong Liu, Anne S. Meyer, Yi Nie, Suojiang Zhang, Yongsheng Zhao, Philip L. Fosbøl, Kaj Thomsen

Freezing point determination of water-ionic liquid mixtures

Journal of Chemical & Engineering Data, 2017, 62, 2374−2383.

Journal of chemical & engineering data

Article

pubs.acs.org/jced

Freezing Point Determination of Water−Ionic Liquid Mixtures

Yanrong Liu,[†,‡,§] Anne S. Meyer,[†] Yi Nie,[§] Suojiang Zhang,[§] Yongsheng Zhao,[§] Philip L. Fosbøl,[‡] and Kaj Thomsen*[,‡]

[†]Center for Bioprocess Engineering, Department of Chemical and Biochemical Engineering, Technical University of Denmark, Søltofts Plads 227, 2800, Lyngby, Denmark

[‡]Center for Energy Resources Engineering (CERE), Department of Chemical and Biochemical Engineering, Technical University of Denmark, Søltofts Plads 229, 2800, Lyngby, Denmark

[§]Beijing Key Laboratory of Ionic Liquids Clean Process, Key Laboratory of Green Process and Engineering, State Key Laboratory of Multiphase Complex Systems, Institute of Process Engineering, Chinese Academy of Sciences, P.O. Box 353, Beijing, 100190, China

Supporting Information

ABSTRACT: Freezing points of aqueous solutions of HOEtpyBr, HOEtmimBr, AmimCl, EtOMmimCl, EmimDep, and EmimAc were measured using a modified Beckmann apparatus with automatic data logging. The ionic liquids (ILs) in this study exhibited features similar to those of inorganic salts in depressing the freezing point of water. On the basis of the cryoscopic behavior recorded, the solid phases formed at higher IL contents were presumed to be hydrates of the form IL·nH$_2$O. The HOEtpyBr+H$_2$O and HOEtmimBr+H$_2$O systems formed simple eutectic systems. The eutectic points were found to be at a water mole fraction of 0.617 and 219.841 K in the first system and at a water mole fraction of 0.657 and 202.565 K in the second system. Water activities in aqueous IL solutions were predicted by COSMO-RS and COSMO-SAC and compared to water activities derived from the experimentally determined freezing points. The COSMO-RS predictions were closer to the experimental water activities than the COSMO-SAC predictions. The experimental results indicate that the freezing points of IL+H$_2$O systems are affected by the nature of both cations and anions. However, according to the COSMO-RS excess enthalpy prediction results, the anions have a relatively higher influence than cations on the IL+H$_2$O interaction.

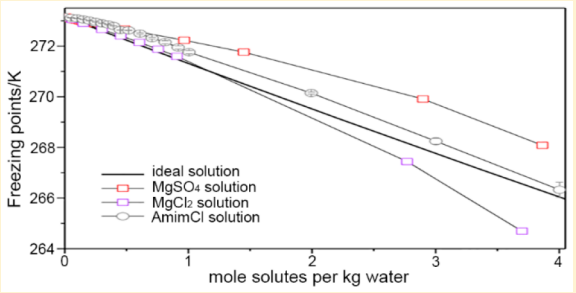

1. INTRODUCTION

In 2002, ionic liquids were introduced as new green solvents for cellulose dissolution.[1] This attracted interest for a range of applications.[2] ILs have many merits compared to conventional organic solvents, such as being less hazardous, having immeasurably low vapor pressure, having excellent chemical and thermal stability, being able to conduct electricity, and being nonflammable.[3] However, cost is still a key factor for the application of ILs in, for example, cellulose refining applications. Recovery and reuse of ILs is therefore crucial. In the cellulose regeneration process, water is commonly used as an antisolvent for the coagulation of cellulose, which is why it is urgent and necessary to develop good methods for IL recovery from IL+H$_2$O mixtures.

Several IL recovery methods from different IL−aqueous mixtures have recently been reported in the literature. Birdwell Jr. et al.[4] successfully separated hydrophobic ILs/hydrocarbon/aqueous systems using centrifugal solvent extraction contactors. Another treatment is evaporation of water in a rotary evaporator followed by vacuum drying. This method is based on the vapor pressures of the compounds and was considered a straightforward and efficient tool to recover ILs.[5] The addition of a phase has also been applied in recovery of ILs. Vergara et al.[6] investigated the recovery of ammonium-based ILs from aqueous solution after extraction of metal ions. This IL recovery was best achieved by adding a mixture of acetone and ethanol with the volume ratio of 1:1. These two solvents were selected by taking into account their refractive indices based on the study of Seki et al.[7] In that study, the refractive index was found to be related to the polarizability of the studied ILs. Lynam et al.[8] first illustrated an environmentally friendly, low temperature, and ambient pressure method of direct contact membrane distillation to separate water from EmimAc and Emim[HCOO]. Two membranes were used in this separation process, hydrophobic polytetrafluoroethylene (PTFE) and hydrophobic polyvinylidene fluoride (PVDF). It was found that the PTFE membrane has a higher flux than the PVDF membrane. The separation resulted in an increase in concentration from 5 wt % to 50 wt % IL.

Because of the lower energy cost of freezing water rather than evaporating, we hypothesized that freeze crystallization could be a feasible method for IL recovery from IL+H$_2$O mixtures. The main objective of this work was to determine the freezing points of selected ILs. The study included six selected

Received: March 17, 2017
Accepted: June 20, 2017
Published: July 6, 2017

DOI: 10.1021/acs.jced.7b00274
J. Chem. Eng. Data 2017, 62, 2374−2383

ILs and the measurement of their freezing points in the concentration range from pure water to pure IL. Freezing points were measured by freezing point depression equipment using ethanol and liquid nitrogen as refrigerants and with continuous data acquisition of the temperature.

The excess enthalpy and its three contributions of H-bonds (HB), misfits (MS), and van der Waals forces (VDW) of the six studied IL+H_2O systems were predicted by COSMO-RS. The experimental results were compared with COSMO-RS prediction results to evaluate the ability of COSMO-RS to predict the interaction of ILs with water.

2. EXPERIMENTAL DESCRIPTION

2.1. Materials. The structures of the six ILs studied in this work are shown in Figure 1. EimAc (99 wt %) was purchased

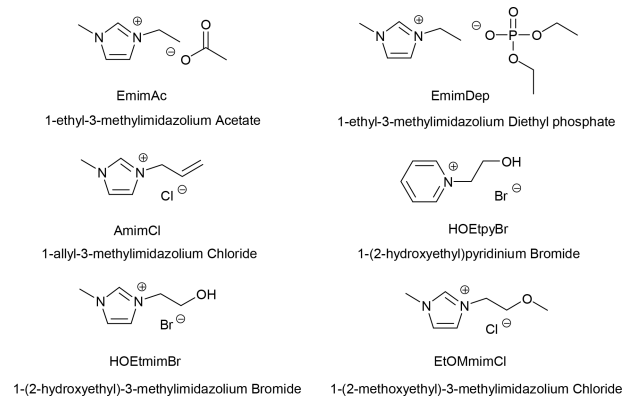

Figure 1. Structures of the ILs studied in this work.

from Shanghai Cheng Jie Chemical Co., Ltd. The other five ILs: HOEtpyBr, HOEtmimBr, AmimCl, EtOMmimCl, and EmimDep were synthesized in one step. The synthetic method and the purity analysis method for these five synthesized ionic liquids were explained in detail in the Supporting Information of our previous work with the same purities and water contents.[9] The structures of the five synthesized ILs were confirmed by their ^{1}H and ^{13}C NMR spectra using a Bruker 600 spectrometer. Characteristic peaks and ^{1}H and ^{13}C NMR data for these five ILs are shown in the Supporting Information. The sample information used in this study is given in Table 1.

2.2. The Freezing Point Measurement Method. The freezing point depression (FPD) measurements were performed with a modified Beckmann apparatus as described by Fosbøl et al.,[10] The FPD method was verified as an easy and accurate measurement for water activity in aqueous amine systems loaded with CO_2.[11] An illustration of the freezing point measurement equipment is shown in Figure 2.

The temperature was controlled by a Julaba FP 50 thermostatic bath. Ethanol was used as refrigerant and the lowest temperature obtainable from this thermostatic bath (A) is about 225 K. Samples with freezing points lower than this were cooled using liquid nitrogen as refrigerant. Approximately 5−10 g of IL solution was placed into the sample glass (C) at room temperature which was then cooled by the ethanol bath (F) or by liquid nitrogen. The temperature of the ethanol bath (F) was maintained by the cooling jacket (B) which was connected with the thermostatic bath (A). To ensure a homogeneous sample temperature during the measurement, a continuous magnetic stirrer in the bottom of the sample glass was used together with a device for manual stirring (E). The

Table 1. Samples Used in the Measurements

chemical name[a]	source	CAS No.	mass fraction purity	method purification	water content (mass fraction)	analysis method
EmimAc	Shanghai Cheng Jie Chemical Co., Ltd.	143314-17-4	0.99	none	$\leq 5.00 \times 10^{-3}$	none
EmimDep	synthesized	848641-69-0	0.996	extraction, rotary vacuum evaporation, vacuum drying	1.94×10^{-3}	NMR spectrum, elemental analysis, water content
AmimCl		65039-10-3	0.985		2.51×10^{-3}	
EtOMmimCl			0.993	extraction, filtration, vacuum drying	4.43×10^{-3}	
HOEtmimBr			0.987		9.33×10^{-3}	
HOEtpyBr			0.983		9.77×10^{-3}	

[a]The full name of EmimAc, EmimDep, AmimCl, EtOMmimCl, HOEtmimBr, and HOEtpyBr are displayed in Figure 1.

DOI: 10.1021/acs.jced.7b00274
J. Chem. Eng. Data 2017, 62, 2374−2383

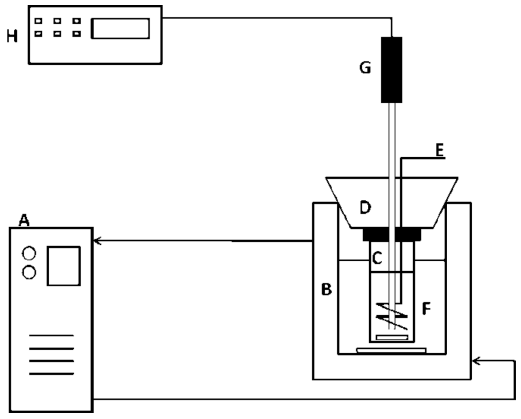

Figure 2. Illustration of the FPD equipment.[10,11] A, thermostatic bath with ethanol; B, cooling jacket; C, sample glass with magnetic stirrer; D, rubber stopper with sample glass lid; E, device for manual stirring; F, controlled temperature ethanol bath with magnetic stirrer; G, Pt100 thermometer; H, data acquisition unit.

sample temperature was recorded by a data acquisition unit, Agilent 34970A (H) using a Pt100 thermometer (G). The Agilent data acquisition unit was calibrated by seven different sodium chloride solutions of 0%, 2.5%, 5.0%, 7.5%, 10%, 15%, 17.5 wt %. Deionized water was used for preparation of sample solutions and as blank control. All the samples were weighed by an analytical balance with an accuracy of ±0.1 mg.

Every freezing point measurement of the calibration samples was repeated 10 times. The standard deviation did not exceed 0.02 K. The IL solution samples were measured 5 times each. The temperature curves showed that the temperature rose abruptly from the under-cooled condition due to the exothermal ice formation and then decreased slightly again. The maximum temperature measured in this region was treated as the freezing point.[10] With increasing IL concentration, the viscosity of the aqueous IL solutions increased gradually, making the measurements more difficult. At the same time, the freezing points of the concentrated solutions were lower than the cooling capacity of the FPD equipment. Liquid nitrogen was therefore introduced as refrigerant in these cases. The IL +H_2O solutions were first under-cooled by liquid nitrogen. Then they were held and stirred at room temperature until all crystals disappeared. At this point the freezing points were determined. The disappearance of crystals was monitored visually.

The freezing points of six IL+H_2O solutions were measured at concentrations from pure water to pure IL. The measured freezing points were plotted as a function of mole of solutes per kilogram of water. One mol of IL corresponds to 2 mol of solutes because of the dissociation. The measured freezing points were plotted together with the freezing points of $MgSO_4$ and $MgCl_2$ solutions in order to compare their properties (Figure 3 and Figure 4). In addition, the freezing point curve of an ideal solution was plotted. The ideal solution data in Figure 3 and Figure 4 were computed from eqs 2 and 3. The freezing point data of $MgCl_2$ solutions were cited from Loomis[12] and Rodebush.[13] The freezing point data of $MgSO_4$ solutions were quoted from Jones and Getman[14] and Jones.[15] The measured freezing points were also plotted as a function of mole fraction of water in order to show the whole range of measurements (Figure 5).

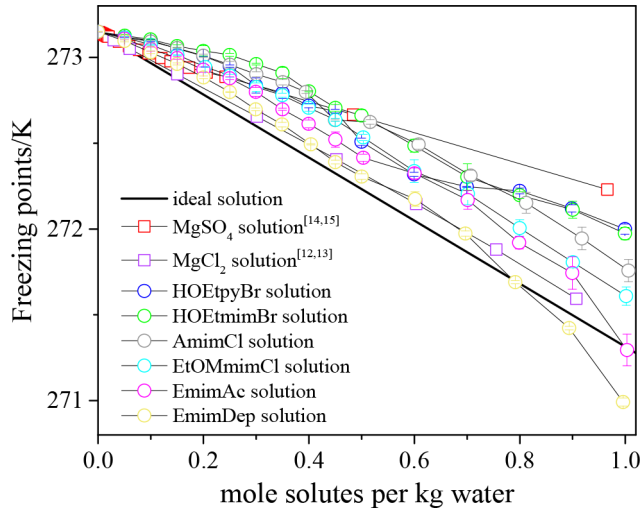

Figure 3. Freezing points of the studied IL solutions and of salt solutions compared at low concentrations. Error bars mark the experimental uncertainty. The black line of the ideal solution computed by using eqs 2 and 3 and the data displayed in Table 2. Measured data from Tables 3 and 4

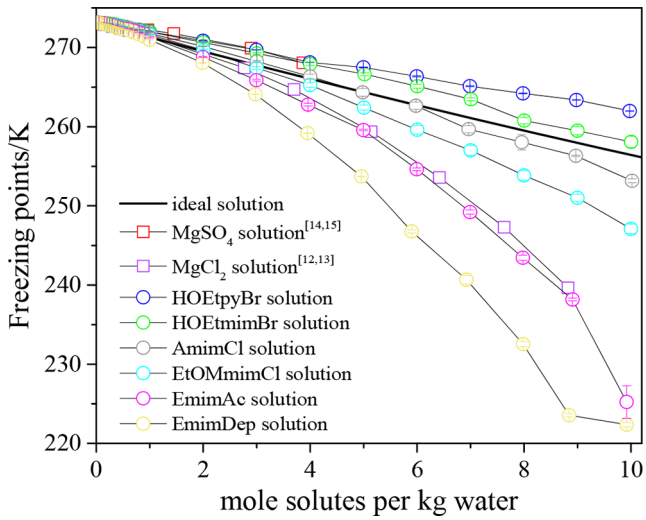

Figure 4. Freezing points of the studied IL solutions and of salt solutions compared at higher concentrations. Error bars mark the experimental uncertainty. The black line of the ideal solution computed by using eqs 2 and 3 and the data displayed in Table 2. Measured data from Tables 3 and 4

In the IL+H_2O separation process, water activity is an important parameter, if the water activity is high, less amount of energy will be consumed during the freezing process, which is conducive for IL recovery. Water activity (a_w) can be accurately acquired from freezing point data by considering that the equilibrium constant K_T is identical to the water activity a_w, $K_T = a_w$. The solid−liquid equilibrium is shown in eq 1. The equilibrium constant at reference temperature and pressure T_0 = 298.15 K and P_0 = 0.1 MPa was calculated from eq 2. The water activities of ideal solutions and of IL+H_2O solutions were obtained from eqs 2 and 3, introduced by Fosbøl et al.[10,16] and Arshad et al.,[11] the related correlation parameters of eq 3 are displayed in Table 2.[11] In the ideal solution, the water activity is equal to the water mole fraction.

$$H_2O(s) \rightleftarrows H_2O(l) \quad (1)$$

DOI: 10.1021/acs.jced.7b00274
J. Chem. Eng. Data 2017, 62, 2374−2383

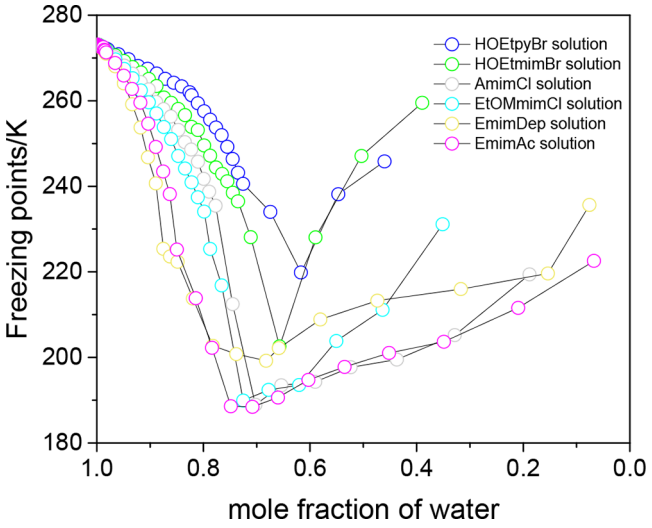

Figure 5. Measured freezing points of six IL solutions as a function of mole fraction of water. Error bars mark the uncertainty of the measurements. Measured data from Tables 3 to 6

$$\ln K_T = -\frac{\Delta_f G^0_w(T, P) - \Delta_f G^0_{ice}(T, P)}{RT} = \ln a_w \quad (2)$$

.

$$R \ln K_T = R \ln K_{T_0} - \Delta H^0_{T_0}\left(\frac{1}{T} - \frac{1}{T_0}\right) + \Delta a\left(\ln \frac{T}{T_0} + \frac{T_0}{T} - 1\right) + 0.5\Delta b\left(\frac{(T - T_0)^2}{T}\right) + \frac{\Delta c}{T_\Theta}\left(\frac{T - T_\Theta}{T} \ln \frac{T - T_\Theta}{T_0 - T_\Theta} - \ln \frac{T}{T_0}\right) \quad (3)$$

.

3. COSMO-RS COMPUTATION DETAIL

The interactions of water and ILs in this work were predicted by COSMO-RS calculations. In a recent report, Khan et al. have shown evidence that COSMO-RS can be efficiently applied to predict the interaction of pyridinium-, pyrrolidinium-, or piperidinium-based ionic liquids with water at 298.15 K.[17] The $Amim^+$ COSMOfile was determined in two steps. First, the quantum chemical Gaussian 09 package was used to optimize the $Amim^+$ at the B3LYP/6-31++G (d, p) level. Second, the COSMO files of $Amim^+$ were opened in Gaussian 03, and COSMO continuum solution models were calculated using the BVP86/TZVP/DGA1 level theory.

The other cations and anions studied in this work came from the COSMO-RS database. The σ-profiles were calculated using COSMOtherm. (implementation: COSMOtherm version C3.0 release 14.01, applied with parametrization BP_TZVP_C30_1401, COSMOlogic, Leverkusen, Germany).

The mole fractions of the cations and anions of the ILs were set equal; that is, $n_{cation} = n_{anion} = n_{IL}$.[18] The prediction temperature was set to 298.15 K. The activity coefficient calculation equation was previously described by Diedenhofen and Klamt,[19] and the excess enthalpy equation by Gonzalez-Miquel et al.[20]

The water activity coefficients were also predicted with COSMO-SAC[21] using the same σ-profiles. We modified the COSMO-SAC software provided by Virginia Tech[22] to include ternary systems (water plus two ions). The activity coefficients of water predicted by COSMO-RS and by COSMO-SAC at 298.15 K were converted to water activities and compared with water activities derived from the experimental freezing point data by eqs 2 and 3.

4. RESULTS AND DISCUSSION

4.1. Freezing Point Determination. The measured freezing point data of the IL+H_2O solutions are presented in Tables 3 to 6. In Tables 3 and 4, the concentrations of the ILs are given both as a function of mol solutes per kg water up to 10 molal and as the corresponding mole fraction of water. In Tables 5 and 6, the remaining data are given with concentrations in mole fraction of water up to 0.1 (liquid IL) or the solubility limit of IL (solid). The freezing point data acquired from experiments with liquid nitrogen cooling are marked gray in Tables 4 to 6. The high viscosities of the IL +H_2O solutions in the gray regions made it difficult to evaluate the freezing points. The standard deviations of five measurements obtained from liquid nitrogen cooling were more than 5 K as seen in the gray regions of the tables.

In Figures 3 and 4, the freezing points of the six IL+H_2O solutions, ideal solutions, $MgSO_4$ solutions, and $MgCl_2$ solutions are plotted against mol solutes/kg water. It can be seen that the freezing point curves of the six studied IL solutions were basically in the middle between the freezing point curves of $MgSO_4$ solutions and $MgCl_2$ solutions in the concentration range from 0 to 1 mol solutes/kg water (Figure 3). This shows that the ILs in this study exhibit features similar to those of inorganic salts with respect to depressing the freezing point of water. $MgCl_2$ is generally considered completely dissociated in aqueous solution. The freezing point curves of EmimDep+H_2O and $MgCl_2$+H_2O solutions follow each other closely in Figure 3, at least up to 0.91 mol solute/kg water. This indicates that most likely EmimDep is also completely dissociated in aqueous solutions at these concentrations. At higher concentrations, the freezing points of the IL solutions deviate from the ideal solution curve to different extents. It can be noticed in Figure 4 that the freezing point curves of HOEtpyBr and HOEtmimBr closely follow the freezing point curve of the $MgSO_4$ solutions at low concentrations and run above the ideal solution curve. This behavior differed from the freezing point curves of the other four IL solutions. The results may indicate that the bromide ILs are less dissociated than the remaining four ILs. If this is indeed the case, the data may infer that HOEtPyBr and HOEtmimBr

Table 2. Correlation Parameters for eq 3[a]

	$\Delta_f G^0$ kJ·mol^{-1}	$\Delta_f H^0$ kJ·mol^{-1}	a_i J·(mol·K)$^{-1}$	b_i J·(mol·K^2)$^{-1}$	c_i J·mol^{-1}
water	−237.129	−285.83	58.370	0.03896	523.88
ice	−236.538	−292.624	49.627	0	0

[a]The correlation parameters are cited from Arshad et al.[11] T_Θ = 200 K, T_0 = 298.15 K.

DOI: 10.1021/acs.jced.7b00274
J. Chem. Eng. Data 2017, 62, 2374−2383

Table 3. Freezing Points of the HOEtpyBr+H_2O, HOEtmimBr+H_2O, and AmimCl+H_2O Are Given at 0.1 MPa as a Function of mol Solutes/kg Water up to 10 molal and the Corresponding Mole Fraction of Water[a]

HOEtpyBr+H_2O					HOEtmimBr+H_2O					AmimCl+H_2O				
mol solutes/kg water	mole fraction of water	freezing point (K)	standard deviation (K)	solid phase	mol solutes/kg water	mole fraction of water	freezing point (K)	standard deviation (K)	solid phase	mol solutes/kg water	mole fraction of water	freezing point (K)	standard deviation (K)	solid phase
0	1	273.149	0.001	ice	0	1	273.149	0.001	ice	0	1.000	273.149	0.001	ice
0.050	0.999	273.118	0.004	ice	0.051	0.999	273.126	0.007	ice	0.050	0.999	273.117	0.002	ice
0.100	0.998	273.099	0.006	ice	0.100	0.998	273.104	0.002	ice	0.100	0.998	273.092	0.007	ice
0.150	0.997	273.050	0.006	ice	0.150	0.997	273.065	0.008	ice	0.150	0.997	273.054	0.003	ice
0.200	0.996	273.007	0.002	ice	0.200	0.996	273.038	0.030	ice	0.200	0.996	273.009	0.010	ice
0.250	0.995	272.949	0.007	ice	0.250	0.996	273.014	0.009	ice	0.250	0.996	272.957	0.019	ice
0.300	0.994	272.836	0.044	ice	0.300	0.995	272.960	0.005	ice	0.300	0.995	272.901	0.015	ice
0.350	0.993	272.793	0.031	ice	0.350	0.994	272.909	0.033	ice	0.350	0.994	272.855	0.017	ice
0.400	0.992	272.718	0.012	ice	0.400	0.993	272.802	0.004	ice	0.394	0.993	272.798	0.008	ice
0.450	0.991	272.687	0.011	ice	0.450	0.992	272.706	0.019	ice	0.449	0.992	272.634	0.005	ice
0.500	0.990	272.508	0.022	ice	0.500	0.991	272.661	0.034	ice	0.516	0.991	272.623	0.014	ice
0.600	0.988	272.318	0.012	ice	0.600	0.989	272.485	0.038	ice	0.608	0.989	272.492	0.029	ice
0.699	0.985	272.246	0.003	ice	0.700	0.988	272.303	0.077	ice	0.707	0.987	272.311	0.031	ice
0.800	0.983	272.222	0.017	ice	0.800	0.986	272.197	0.019	ice	0.812	0.986	272.152	0.060	ice
0.899	0.981	272.120	0.021	ice	0.900	0.984	272.112	0.049	ice	0.918	0.984	271.945	0.066	ice
0.999	0.979	272.000	0.030	ice	0.999	0.982	271.974	0.036	ice	1.006	0.982	271.758	0.065	ice
1.998	0.959	270.861	0.064	ice	2.000	0.965	270.636	0.021	ice	1.995	0.965	270.146	0.043	ice
2.996	0.940	269.710	0.014	ice	3.004	0.949	269.262	0.100	ice	3.003	0.949	268.241	0.122	ice
3.996	0.922	268.122	0.016	ice	4.000	0.933	267.903	0.174	ice	4.003	0.933	266.326	0.298	ice
4.995	0.905	267.495	0.028	ice	5.018	0.917	266.625	0.171	ice	4.981	0.918	264.339	0.498	ice
5.993	0.888	266.361	0.071	ice	6.003	0.902	265.102	0.251	ice	5.980	0.903	262.646	0.450	ice
6.988	0.871	265.121	0.044	ice	7.007	0.888	263.460	0.172	ice	6.965	0.889	259.679	0.439	ice
7.981	0.856	264.212	0.042	ice	8.005	0.874	260.772	0.394	ice	7.959	0.875	258.041	0.982	ice
8.980	0.841	263.373	0.033	ice	9.000	0.860	259.505	0.515	ice	8.969	0.861	256.324	0.079	ice
9.977	0.826	261.991	0.032	ice	10.002	0.847	258.083	0.709	ice	10.022	0.847	253.169	0.248	ice

[a]The standard uncertainty (u) for the mole fractions is $u(x) = 0.001$, for the pressure is $u(p) = 1$ kPa. The standard uncertainty in temperature is equal to either 0.02 K or the standard deviation of the mean reported in the table, whichever is greater.

have less interaction with water than the other ILs considered. EmimAc and EmimDep reduced the freezing point of water significantly more than the other ILs (Figure 4). From Figure 4, it can also be seen that the more concentrated solutions have increasingly lower freezing points on the order of HOEtpyBr (highest), HOEtmimBr, AmimCl, EtOMmimCl, EmimAc, and EmimDep (lowest) solutions.

Figure 5 shows the freezing points of the studied ILs as a function of mole fraction of water. All the freezing point values were measured in this work and are listed in Tables 3 to 6. Three of the ILs, which are solid at room temperature, were only studied from 0 to the solubility limit of the IL due to difficulties in dissolving these ILs in water.

The freezing point curves of HOEtpyBr and HOEtmimBr indicate simple eutectic systems with steep freezing point elevations as the IL concentrations increase (Figure 5). The shapes of the freezing point curves of aqueous AmimCl, EtOMmimCl, EmimDep, and EmimAc systems differ from this pattern by having more flat curves beyond the eutectic points (Figure 5). This latter type of curve indicates formation of hydrates with different amounts of water molecules attached. In the dilute region, ice starts forming when the solutions are cooled to their freezing points. A change in slope of the freezing point curve indicates a change in solid phase. The solid phases at high IL concentrations are expected to be pure, solid ILs or hydrates of the form IL·$n$$H_2O$. Some of the changes in slope of the freezing point curves might be caused by the high viscosities of the IL solutions.

For all the examined ILs, pure ice seems to be the stable solid phase at mole fractions of water from approximately 1 to 0.85 for EmimAc and EmimDep solutions, 1 to 0.75 for AmimCl and EtOmmimCl solutions, 1 to 0.67 for HOEtpyBr, and 1 to 0.71 for HOEtmimBr solutions. In these regions, it might be possible to separate the studied ILs from H_2O by freeze crystallization or by eutectic freeze crystallization.[23] The HOEtpyBr and HOEtmimBr freezing point curves are special because eutectic points can be clearly observed at a mole fraction of water around 0.617 with the freezing points of 219.841 K and 0.657 of 202.565 K, respectively. This indicates that the HOEtpyBr+H_2O system and the HOEtmimBr+H_2O system might be easier to recover from water by freezing separation than the other four ILs. Further investigations need to be conducted in order to verify that this separation is possible. Especially the high viscosity can be a hindrance for using eutectic freeze crystallization to separate these systems.

An analysis of the shapes of the freezing point curves results in the following conclusions: the two bromide ILs which have the same anion, same functional groups, but different cation types have freezing point curves close to each other. The two chloride ILs which have the same anions, same cation type, but different functional groups also have freezing point curves close to each other. However, EmimDep and EmimAc which have the same cation type and same functional groups have similar freezing points at the mole fraction of water between 0.8 and 1, but have larger differences in freezing points at lower mole fractions of water. All these observations indicate that the

DOI: 10.1021/acs.jced.7b00274
J. Chem. Eng. Data 2017, 62, 2374−2383

Table 4. Freezing Points of the EtOMmimCl+H_2O, EmimAc+H_2O, and EmimDep+H_2O Are Given at 0.1 MPa as a Function of mol Solutes/kg Water up to 10 molal and the Corresponding Mole Fraction of Water[a]

EtOMmimCl+H_2O					EmimAc+H_2O					EmimDep+H_2O				
mol solute/ kg water	mole fraction of water	freezing point (K)	standard deviation (K)	solid phase	mol solutes/ kg water	mole fraction of water	freezing point (K)	standard deviation (K)	solid phase	moe solutes/ kg water	mole fraction of water	freezing point (K)	standard deviation (K)	solid phase
0	1	273.149	0.001	ice	0	1	273.149	0.001	ice	0	1	273.149	0.001	ice
0.051	0.999	273.116	0.003	ice	0.050	0.999	273.109	0.006	ice	0.050	0.999	273.096	0.006	ice
0.100	0.998	273.073	0.004	ice	0.100	0.998	273.048	0.012	ice	0.100	0.998	273.029	0.007	ice
0.151	0.997	273.014	0.001	ice	0.150	0.997	272.997	0.007	ice	0.150	0.997	272.962	0.006	ice
0.203	0.996	272.944	0.003	ice	0.200	0.996	272.928	0.016	ice	0.200	0.996	272.884	0.007	ice
0.250	0.996	272.893	0.008	ice	0.250	0.996	272.878	0.008	ice	0.250	0.996	272.798	0.003	ice
0.300	0.995	272.826	0.025	ice	0.299	0.995	272.798	0.026	ice	0.299	0.995	272.697	0.007	ice
0.349	0.994	272.779	0.012	ice	0.350	0.994	272.697	0.006	ice	0.349	0.994	272.609	0.013	ice
0.399	0.993	272.707	0.021	ice	0.400	0.993	272.612	0.023	ice	0.404	0.993	272.494	0.003	ice
0.450	0.992	272.636	0.009	ice	0.450	0.992	272.521	0.044	ice	0.450	0.992	272.390	0.011	ice
0.503	0.991	272.533	0.018	ice	0.503	0.991	272.415	0.021	ice	0.500	0.992	272.306	0.016	ice
0.600	0.989	272.337	0.066	ice	0.600	0.989	272.324	0.032	ice	0.601	0.989	272.175	0.043	ice
0.701	0.988	272.206	0.064	ice	0.701	0.988	272.169	0.054	ice	0.697	0.988	271.974	0.015	ice
0.800	0.986	272.006	0.048	ice	0.799	0.986	271.921	0.036	ice	0.791	0.986	271.690	0.010	ice
0.901	0.984	271.806	0.032	ice	0.899	0.984	271.743	0.094	ice	0.893	0.984	271.423	0.010	ice
1.002	0.982	271.609	0.054	ice	1.003	0.982	271.295	0.092	ice	0.996	0.982	270.992	0.023	ice
2.007	0.965	269.667	0.127	ice	1.996	0.966	268.811	0.056	ice	1.987	0.965	268.065	0.018	ice
3.001	0.949	267.422	0.165	ice	2.995	0.949	265.872	0.110	ice	2.977	0.949	264.083	0.018	ice
4.000	0.933	265.253	0.314	ice	3.963	0.934	262.778	0.159	ice	3.951	0.934	259.182	0.036	ice
5.007	0.917	262.412	0.321	ice	4.995	0.918	259.583	0.101	ice	4.960	0.918	253.728	0.021	ice
6.002	0.902	259.614	0.557	ice	5.995	0.903	254.627	0.173	ice	5.901	0.904	246.774	0.198	ice
7.005	0.888	257.010	0.612	ice	6.994	0.889	249.218	0.270	ice	6.924	0.889	240.679	0.547	ice
8.000	0.874	253.857	0.608	ice	7.979	0.875	243.450	0.326	ice	7.983	0.875	**232.535**	0.332	ice
9.000	0.860	251.010	0.443	ice	8.908	0.863	238.181	0.172	ice	8.844	0.863	**223.565**	0.199	ice
10.001	0.847	247.099	0.598	ice	9.919	0.850	**225.226**	2.069	ice	9.918	0.848	**222.363**	0.270	ice

[a]The standard uncertainty (u) for the mole fractions is $u(x)$ = 0.001, for the pressure it is $u(p)$ =1 kPa. The standard uncertainty in temperature is equal to either 0.02 K or the standard deviation of the mean reported in the table, whichever is greater. The freezing point data acquired from experiments with liquid nitrogen cooling are in bold font.

Table 5. Remaining Freezing Points of HOEtpyBr+H_2O, HOEtmimBr+H_2O, and AmimCl+H_2O Are Given at 0.1 MPa as a Function of Mole Fraction of Water Continued from Table 3. The Value of n Used for Describing the Solid Phases Was Not Determined[a]

HOEtpyBr+H_2O				HOEtmimBr+H_2O				AmimCl+H_2O			
mole fraction of water	freezing point (K)	standard deviation (K)	solid phase	mole fraction of water	freezing point (K)	standard deviation (K)	solid phase	mole fraction of water	freezing point (K)	standard deviation (K)	solid phase
0.822	261.288	0.027	ice	0.834	256.614	0.239	ice	0.835	250.305	0.551	ice
0.810	259.410	0.057	ice	0.822	253.872	0.252	ice	0.823	248.595	0.344	ice
0.799	257.525	0.047	ice	0.810	253.135	0.622	ice	0.810	245.773	0.247	ice
0.787	255.584	0.566	ice	0.799	249.559	1.049	ice	0.799	241.756	0.539	ice
0.776	253.729	0.582	ice	0.787	247.161	0.378	ice	0.789	238.758	0.287	ice
0.766	251.950	0.597	ice	0.776	244.413	0.703	ice	0.777	**235.460**	0.294	ice
0.755	249.238	0.610	ice	0.765	242.901	1.273	ice	0.745	**212.452**	0.190	ice
0.745	246.373	0.623	ice	0.755	241.178	0.531	ice	0.703	**188.924**	1.503	ice
0.735	243.183	0.635	ice	0.745	238.483	0.431	ice	0.654	**193.472**	2.091	AmimCl·nH_2O
0.726	240.593	0.646	ice	0.735	236.474	0.260	ice	0.590	**194.280**	1.952	AmimCl·nH_2O
0.674	**234.007**	0.700	ice	0.711	**228.105**	1.299	ice	0.524	**197.672**	1.537	AmimCl·nH_2O
0.617	**219.841**	0.750	ice	0.657	**202.565**	3.222	ice	0.437	**199.502**	1.199	AmimCl·nH_2O
0.547	238.137	0.800	HOEtpyBr·nH_2O	0.590	**228.051**	1.457	HOEtmimBr·nH_2O	0.328	**205.221**	2.299	AmimCl·nH_2O
0.460	245.812	0.850	HOEtpyBr·nH_2O	0.503	247.104	5.637	HOEtmimBr·nH_2O	0.188	**219.401**	2.244	AmimCl·nH_2O
				0.390	259.511	4.707	HOEtmimBr·nH_2O				

[a]The standard uncertainty (u) for the mole fractions is $u(x)$ = 0.001, for the pressure is $u(p)$ = 1 kPa. The standard uncertainty in temperature is equal to either 0.02 K or the standard deviation of the mean reported in the table, whichever is greater. The freezing point data acquired from experiments with liquid nitrogen cooling are marked in bold font.

DOI: 10.1021/acs.jced.7b00274
J. Chem. Eng. Data 2017, 62, 2374−2383

Table 6. Remaining Freezing Points of EtOMmimCl+H_2O, EmimAc+H_2O, and EmimDep+H_2O Are Given at 0.1 MPa as Function of Mole Fraction of Water Continued from Table 4. The Value of n Used for Describing the Solid Phases Was Not Determined[a]

EtOMmimCl+H_2O				EmimAc+H_2O				EmimDep+H_2O			
mole fraction of water	freezing point (K)	standard deviation (K)	solid phase	mole fraction of water	freezing point (K)	standard deviation (K)	solid phase	mole fraction of water	freezing point (K)	standard deviation (K)	solid phase
0.835	244.137	0.804	ice	0.814	**213.829**	2.683	ice	0.820	**213.764**	3.503	ice
0.822	240.934	0.324	ice	0.784	**202.242**	2.410	ice	0.782	**202.703**	1.936	ice
0.810	237.454	0.644	ice	0.749	**188.584**	0.632	ice	0.738	**200.767**	0.587	ice
0.799	**234.077**	0.242	ice	0.708	**188.442**	0.479	ice	0.682	**199.221**	1.531	ice
0.787	**225.357**	2.299	ice	0.660	**190.615**	2.013	EmimAc·nH_2O	0.659	**202.147**	0.186	EmimDep·nH_2O
0.766	**216.813**	2.138	ice	0.603	**194.752**	2.843	EmimAc·nH_2O	0.580	**208.855**	0.353	EmimDep·nH_2O
0.725	**189.899**	2.305	ice	0.535	**197.768**	0.384	EmimAc·nH_2O	0.473	**213.277**	0.133	EmimDep·nH_2O
0.678	**192.393**	1.216	EtOMmimCl·nH_2O	0.452	**201.036**	1.208	EmimAc·nH_2O	0.317	**215.965**	0.970	EmimDep·nH_2O
0.620	**193.516**	0.634	EtOMmimCl·nH_2O	0.349	**203.643**	1.767	EmimAc·nH_2O	0.154	**219.617**	0.422	EmimDep·nH_2O
0.551	**203.837**	1.462	EtOMmimCl·nH_2O	0.209	**211.580**	4.589	EmimAc·nH_2O	0.076	**235.640**	0.327	EmimDep·nH_2O
0.464	**211.124**	2.497	EtOMmimCl·nH_2O	0.067	**222.545**	2.631	EmimAc·nH_2O				
0.351	**231.136**	3.070	EtOMmimCl·nH_2O								

[a]The standard uncertainty (u) for the mole fractions is $u(x) = 0.001$, for the pressure is $u(p) = 1$ kPa. The standard uncertainty in temperature is equal to either 0.02 K or the standard deviation of the mean reported in the table, whichever is greater. The freezing point data acquired from experiments with liquid nitrogen cooling are in bold font.

freezing points of these six IL solutions depend on the different types of IL cations and anions. It is likely that anions have a relatively larger effect on the formation of hydrates than cations, as evident by for example, comparing the curves of EmimDep and EmimAc in Figure 5 at water mole fractions between 0 and 0.8. From the decreasing tendency of the freezing point curves in Figure 4, it is found that in the concentration range studied, the anions influence the freezing points in the order Dep^- > Ac^- > Cl^- > Br^-. For the three latter ions, this order is in accordance with the Hofmeister series.[24] This can explain why EmimDep and EmimAc have stronger bonds with water than the two chloride ILs and the two bromide ILs.

4.2. The COSMO-RS and COSMO-SAC Prediction Results. A comparison of experimental and COSMO-RS predicted water activities are displayed in Figure 6a. From Figure 6a, a significant effect of ILs on the water activity can be seen. The higher water activity indicates a weaker interaction between ILs and water. The water activities from the freezing point measurements were computed according to eqs 2 and 3. These experimentally determined water activities are valid at the temperature they were measured. The predicted water activities were converted from water activity coefficients which were calculated by COSMO-RS at 298.15 K. Water activities are only weak functions of temperature. The water activity of an eutectic $MgCl_2$ solution is 0.700 at 239.65 K according to the freezing point data from Rodebush.[13] At 298.15 K, the water activity of the same solution is 0.715 according to isopiestic measurements by Robinson and Bower.[25] This corresponds to an increase in water activity of 2% over a span of 58.5 K.

Large deviations between experimental and predicted results are seen for all ILs, except for EmimDep. Generally, the predicted water activities are much lower than the corresponding experimental values. These deviations are far too large to be caused by the temperature difference. The observed deviation is in accordance with the accuracy of COSMO-RS predictions of logarithmic activity coefficients at infinite dilution of solutes in ionic liquids. These logarithmic infinite dilution activity coefficients are usually assumed to have an average standard deviation of 0.6 ln units, when predicted by COSMO-RS at the level of BP-—TZVP.[26] 0.6 natural logarithm units correspond to an average deviation of about a factor of 1.8 for the infinite dilution activity coefficients. Most of the predicted water activities approximately fall within this deviation range. However, the predicted trend is hard to interpret. In Figure 6b water activities predicted from COSMO-RS and COSMO-SAC are plotted together. The water activities predicted by COSMO-SAC have a tendency to be lower than the corresponding COSMO-RS values. This indicates that the COSMO-RS prediction results are closer to the experimental data reported in this work. Therefore, the following prediction work was based on the COSMO-RS model.

σ-Profiles calculated by COSMOtherm provide information on molecular interaction. The σ-profiles of water and anions studied in this work are shown in Figure 7. The σ-profiles can be divided into three main regions: the H-bond donor region ($\sigma < -0.0082$ e/Å^2), the H-bond acceptor region ($\sigma > +0.0082$ e/Å^2) and the nonpolar region ($-0.0082 < \sigma < +0.0082$ e/Å^2).[20] From Figure 7, it can be seen that the σ-profile of water is almost symmetric in the region from −0.019 to 0.021 e/Å^2. This illustrates that water has the feature of being a H-bond donor as well as a H-bond acceptor.

The σ-profiles of anions shown in Figure 7 are not symmetric like that of water. The σ-profiles of Ac^- and Dep^- cover a much wider range than the σ-profiles of Cl^- and Br^-. The peaks of Ac^- and Dep^- in the H-bond acceptor region are located on the right side of Cl^- and Br^-, indicating that Ac^- and Dep^- can form stronger H-bonds than Cl^- and Br^-. Therefore, ILs with Ac^- or Dep^- usually have a stronger interaction with water than the ILs with Cl^- or Br^-. Comparing the σ-profile curves of Ac^- and Dep^-, the 0.011 e/Å^2 peak of Ac^- in the positive region is more complementary than that of Dep^- and the nonpolar region of Ac^- is lower than that of Dep^-. This gives evidence that ILs with Ac^- have stronger interactions with water than ILs with Dep^-. In the positive range, the peak of Cl^- (0.019 e/Å^2) is to the right of Br^- (0.017 e/Å^2). This results in the bigger size and the lower charge density of bromide, which again results in bromide ILs having a lower interaction with water than chloride ILs. Consequently, it can be concluded that the interaction of IL anions and water predicted by COSMO-RS in this work can be ranked as Ac^- > Dep^- > Cl^- > Br^-.

DOI: 10.1021/acs.jced.7b00274
J. Chem. Eng. Data 2017, 62, 2374−2383

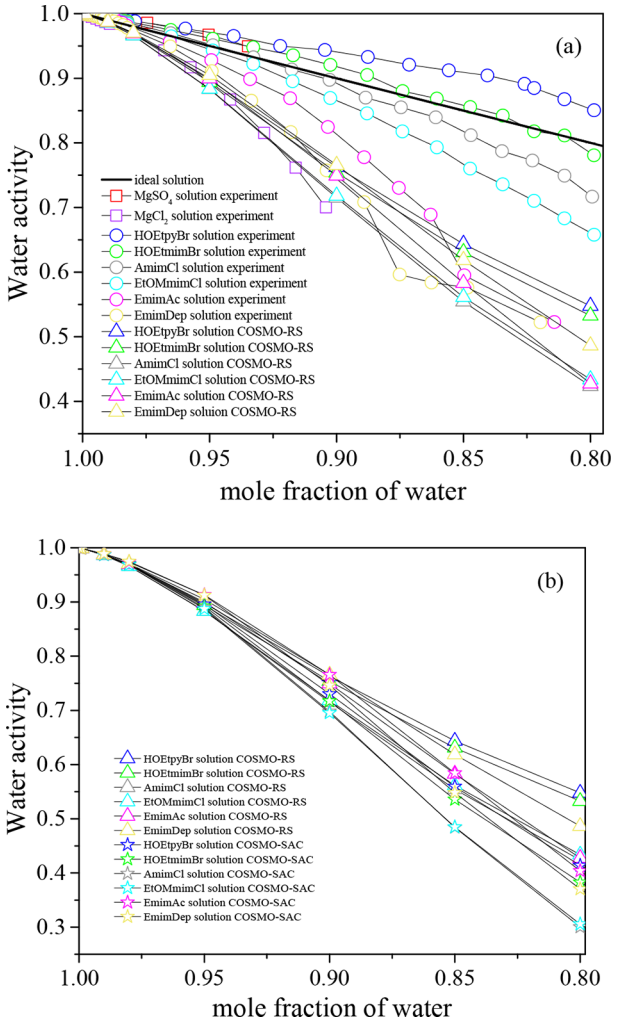

Figure 6. (a) Experimental (at the temperature of the experiment) and COSMO-RS predicted water activities (at 298.15 K). The black line of the ideal solution was computed by using eqs 2 and 3 and the data displayed in Table 2. The COSMO-RS values are generally lower than the experimental values. (b) COSMO-RS and COSMO-SAC predicted water activities (at 298.15 K). The COSMO-SAC values are generally lower than the COSMO-RS values.

Figure 8 and Figure 9 display the total excess enthalpy and the contribution of each interaction to the total excess enthalpy (H-bond, misfit, and van der Waals) of ILs and water. The contributions to the excess enthalpy of IL + H_2O systems at x_{H_2O} = 0.65 is shown in Figure 9. The 0.65 mol fraction was selected based on the minimum in excess enthalpy for EmimAc at this mole fraction (Figure 8). Figure 8 shows that solutions of the two bromide ILs and of the two chloride ILs pair wise have very similar excess enthalpies. EmimDep and EmimAc that share the same cation but have different anions display a big difference in excess enthalpy. Therefore, according to COSMO-RS, the anion of ILs is the key factor to control the water miscibility.[27,28] The number of complexes formed between water molecules and anions is largely dependent on the nature of different anions.[29,30] This result is also in agreement with the findings of Khan et al.[17] The contribution of excess enthalpy in Figure 9 indicates that H-bond is consistently the dominant interaction between ILs and water, followed by misfit and van der Waals. An analysis of the values of H-bond contribution to the excess enthalpy of the six IL

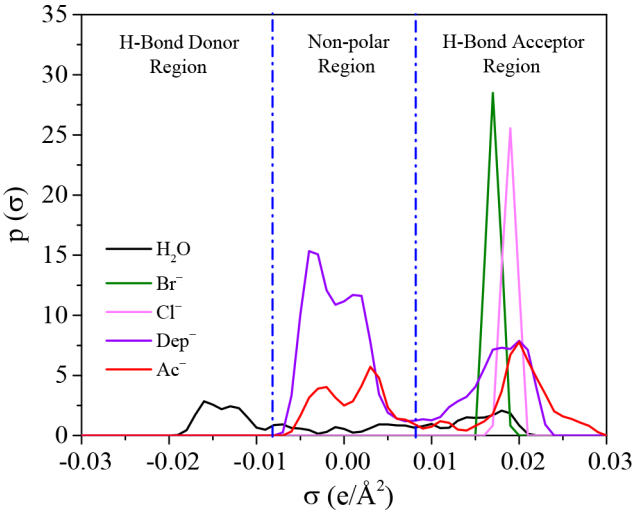

Figure 7. σ-Profile of water and anions studied in this work, COSMO-RS prediction.

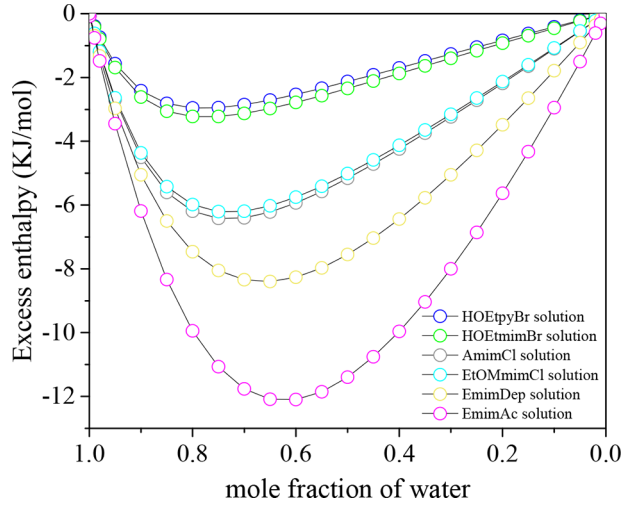

Figure 8. Excess enthalpy of IL+H_2O systems at 298.15 K estimated by COSMO-RS.

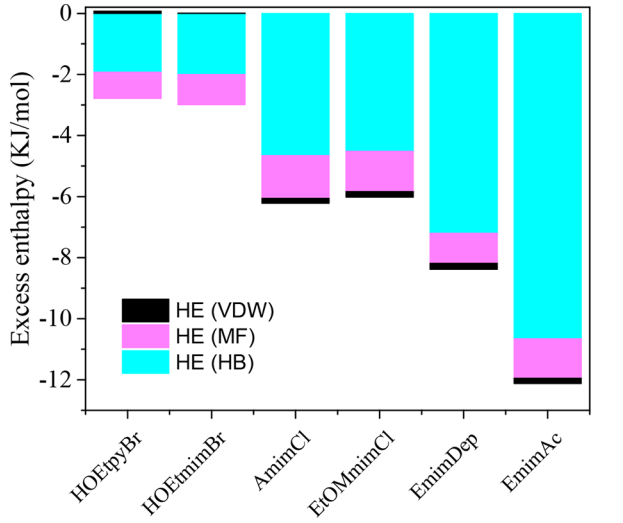

Figure 9. Contribution to the excess enthalpy of ILs+H_2O systems at 298.15 K predicted by COSMO-RS at x_{H2O} = 0.65.

DOI: 10.1021/acs.jced.7b00274
J. Chem. Eng. Data 2017, 62, 2374−2383

solutions also leads us to conclude that according to COSMO-RS, the anion is the key factor for the interaction of ILs and water. However, compared with the experimental results in Figure 4, it can be found that the experimental trend of freezing points of EmimDep and EmimAc is contrary to the σ-profiles and excess enthalpy prediction results. This result not only shows that the COSMO-RS is wrong in its prediction of the system of EmimDep+H_2O and EmimAc+H_2O,[25] but also illustrates that COSMO-RS is not able to predict freezing points of IL solutions as accurately as it predicts solubility.[31] Thermodynamically, excess enthalpy is the temperature derivative of activity coefficients. The uncertainty in the activity coefficient prediction for IL+H_2O systems is therefore naturally reflected in an uncertainty in excess enthalpy prediction for the same system.

Figure 10 shows a correlation of freezing points and the excess enthalpy predicted by COSMO-RS at a water mole fraction of approximately 0.85 corresponding to a mass percent around 50 wt %. Figure 10 indicates that a good agreement with a mean squared correlation coefficient of R^2 = 0.95 was obtained between freezing points and excess enthalpy, which can be used to conclude that low freezing points are accompanied by low excess enthalpy.

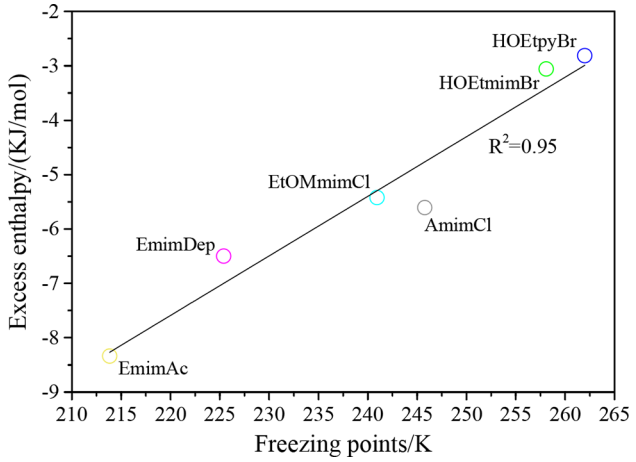

Figure 10. Freezing point values of six IL solutions plotted against excess enthalpy predicted by COSMO-RS at a water mole fraction of approximately 0.85.

5. CONCLUSION

Through measurement of freezing point curves, important data were obtained concerning the IL + water interactions. The data can be valuable for investigating if eutectic freeze crystallization is a possible route for separating ILs from water. Six ILs, HOEtpyBr, HOEtmimBr, AmimCl, EtOMmimCl, EmimAc, and EmimDep were selected for the freezing point measurements. These ILs were chosen because they are potential ILs for dissolving cellulose.[9,32,33] From the freezing point curves, Figures 3 and 4, it can be observed that the behavior of dilute solutions of ILs in water is very similar to that of dilute solutions of $MgSO_4$ and $MgCl_2$. From this it can be concluded that the considered aqueous IL solutions behave similarly to aqueous solutions of common salts. At high concentrations, the freezing point curves of four of the ILs (AmimCl, EtOMmimCl, EmimAc, and EmimDep) in water mixtures deviate increasingly from the ideal solution curve. The deviation increases through AmimCl, EtOMmimCl, EmimAc, and EmimDep. Apparently, the freezing points of IL solutions vary with the types of cations and anions.

Through COSMO-RS prediction of excess enthalpy, it was indicated that the H-bonds formed by IL anions are the dominant type of interaction between ILs with water. However, the COSMO-RS prediction of freezing point curves of the six IL solutions studied is not consistent with the experimental results. This result confirms that COSMO-RS prediction of the activity coefficients of IL+H_2O systems includes a significant uncertainty.

The mole fraction of water regions for possible separation of the six studied IL solutions were determined according to the shapes of the freezing points curves. If eutectic freeze crystallization can be used for recovery of the studied ILs from water in new cellulose processing applications, it is expected to save significant amounts of energy and contribute to qualify ILs as green solvents.

■ ASSOCIATED CONTENT

Supporting Information

The Supporting Information is available free of charge on the ACS Publications website at DOI: 10.1021/acs.jced.7b00274.

NMR spectral analysis of ILs (PDF)

■ AUTHOR INFORMATION

Corresponding Author

*E-mail: kth@kt.dtu.dk. Tel.: +45 4525 2860. Fax: +45 4588 2258.

ORCID

Kaj Thomsen: 0000-0003-1373-1630

Funding

This work was supported by the Department of Chemical and Biochemical Engineering, Technical University of Denmark and the National Key Projects for Fundamental Research and Development of China (Grant No. 2016YFB0600903), National Natural Science Funds for Distinguished Young Scholar (Grant No. 21425625), General Program of National Natural Science Foundation of China (Grant No. 21576262).

Notes

The authors declare no competing financial interest.

■ REFERENCES

(1) Swatloski, R. P.; Spear, S. K.; Holbrey, J. D.; Rogers, R. D. Dissolution of Cellulose with Ionic Liquids. *J. Am. Chem. Soc.* **2002**, *124*, 4974−4975.

(2) Li, X. J.; Li, N. K.; Xu, J. G.; Duan, X. Q.; Sun, Y. S.; Zhao, Q. Cellulose Fibers from Cellulose/1-Ethyl-3-Methylimidazolium Acetate Solution by Wet Spinning with Increasing Spinning Speeds. *J. Appl. Polym. Sci.* **2014**, *131*, 742−751.

(3) Zhao, Y. L.; Liu, X. M.; Wang, J. J.; Zhang, S. J. Insight into the Cosolvent Effect of Cellulose Dissolution in Imidazolium-Based Ionic Liquid Systems. *J. Phys. Chem. B* **2013**, *117*, 9042−9049.

(4) Birdwell, J. F., Jr; McFarlane, J.; Hunt, R. D.; Luo, H. M.; DePaoli, D. W.; Schuh, D. L.; Dai, S. Separation of Ionic Liquid Dispersions in Centrifugal Solvent Extraction Contactor. *Sep. Sci. Technol.* **2006**, *41*, 2205−2223.

(5) Alonso, L.; Arce, A.; Francisco, M.; Rodríguez, O.; Soto, A. Gasoline Desulfurization Using Extraction with [C_8mim][BF_4] Ionic Liquid. *AIChE J.* **2007**, *53*, 3108−3115.

(6) Vergara, M. A. V.; Lijanova, I. V.; Likhanova, N. V.; Xometl, O. O.; Vigueras, D. J.; Ramirez, A. J. M. Recycling and Recovery of Ammonium-Based Ionic Liquids after Extraction of Metal Cations from Aqueous Solutions. *Sep. Purif. Technol.* **2015**, *155*, 110−117.

DOI: 10.1021/acs.jced.7b00274
J. Chem. Eng. Data 2017, 62, 2374−2383

(7) Seki, S.; Tsuzuki, S.; Hayamizu, K.; Umebayashi, Y.; Serizawa, N.; Takei, K.; Miyashiro, H. Comprehensive Refractive Index Property for Room-Temperature Ionic Liquids. *J. Chem. Eng. Data* **2012**, *57*, 2211−2216.
(8) Lynam, J. G.; Chow, G. I.; Coronella, C. J.; Hiibel, S. R. Ionic Liquid and Water Separation by Membrane Distillation. *Chem. Eng. J.* **2016**, *288*, 557−561.
(9) Liu, Y. R.; Thomsen, K.; Nie, Y.; Zhang, S. J.; Meyer, A. S. Predictive Screening of Ionic Liquids for Dissolving Cellulose and Experimental Verification. *Green Chem.* **2016**, *18*, 6246−6254.
(10) Fosbøl, P. L.; Pedersen, M. G.; Thomsen, K. Freezing Point Depressions of Aqueous MEA, MDEA, and MEA−MDEA Measured with a New Apparatus. *J. Chem. Eng. Data* **2011**, *56*, 995−1000.
(11) Arshad, M. W.; Fosbøl, P. L.; von Solms, N.; Thomsen, K. Freezing Point Depressions of Phase Change CO_2 Solvents. *J. Chem. Eng. Data* **2013**, *58*, 1918−1926.
(12) Loomis, E. H. On the Freezing-Points of Dilute Aqueous Solutions. *Phys. Rev.* **1896**, *3*, 270−292.
(13) Rodebush, W. H. The Freezing Points of Concentrated Solutions and the Free Energy of Solution of Salts. *J. Am. Chem. Soc.* **1918**, *40*, 1204−1213.
(14) Jones, H. C.; Getman, F. H. Über das Vorhandensein von Hydraten in Konzentrierten Wässerigen Lösungen. *Z. Phys. Chem.* **1904**, *49*, 385−455.
(15) Jones, H. C. Über die Bestimmung des Gefrierpunktes sehr Verdünnter Salzlösungen. *Z. Phys. Chem.* **1893**, *11*, 529−551.
(16) Fosbøl, P. L.; Thomsen, K.; Stenby, E. H. Modeling of the Mixed Solvent Electrolyte System CO_2-Na_2CO_3-$NaHCO_3$-Monoethylene Glycol-Water. *Ind. Eng. Chem. Res.* **2009**, *48*, 4565−4578.
(17) Khan, I.; Taha, M.; Pinho, S. P.; Coutinho, J. A. P. Interactions of Pyridinium, Pyrrolidinium or Piperidinium based Ionic Liquids with Water: Measurements and COSMO-RS Modeling. *Fluid Phase Equilib.* **2016**, *414*, 93−100.
(18) Casas, A.; Omar, S.; Palomar, J.; Oliet, M.; Alonso, M. V.; Rodriguez, F. Relation Between Differential Solubility of Cellulose and Lignin in Ionic Liquids and Activity Coefficients. *RSC Adv.* **2013**, *3*, 3453−3460.
(19) Diedenhofen, M.; Klamt, A. COSMO-RS as a Tool for Property Prediction of IL Mixtures-A Review. *Fluid Phase Equilib.* **2010**, *294*, 31−38.
(20) Gonzalez-Miquel, M.; Massel, M.; DeSilva, A.; Palomar, J.; Rodriguez, F.; Brennecke, J. F. Excess Enthalpy of Monoethanolamine + Ionic Liquid Mixtures: How Good Are COSMO-RS Predictions? *J. Phys. Chem. B* **2014**, *118*, 11512−11522.
(21) Lin, S. T.; Sandler, S. I. A Priori Phase Equilibrium Prediction from a Segment Contribution Solvation Model. *Ind. Eng. Chem. Res.* **2002**, *41*, 899−913.
(22) Virginia Tech, VT Sigma Profile Databases: http://www.design.che.vt.edu/VT-Databases.html (accessed March 2017).
(23) Vaessen, R.; Seckler, M.; Witkamp, G. J. Eutectic Freeze Crystallization with an Aqueous KNO_3-HNO_3 Solution in a 100-L Cooled-Disk Column Crystallizer. *Ind. Eng. Chem. Res.* **2003**, *42*, 4874−4880.
(24) Yang, Z. Hofmeister Effects: an Explanation for the Impact of Ionic Liquids on Biocatalysis. *J. Biotechnol.* **2009**, *144*, 12−22.
(25) Robinson, R. A.; Bower, V. E. Properties of Aqueous Mixtures of Pure Salts. Thermodynamics of the Ternary System: Water-Calcium Chloride-Magnesium Chloride at 25°C. *J. Res. Natl. Bur. Stand., Sect. A* **1966**, *70*, 305−311.
(26) COSMOlogic white papers, Quality Evaluation and Method Comparison (DMol3, TZVP and TZVPD-FINE level) of the Prediction of Infinite Dilution Activity Coefficients in Ionic Liquids: http://www.cosmologic.de/files/downloads/white-papers/WP_IL_gamma_results.pdf (accessed March 2017).
(27) Huddleston, J. G.; Willauer, H. D.; Swatloski, R. P.; Visser, A. E.; Rogers, R. D. Room Temperature Ionic Liquids as Novel Media for 'Clean' Liquid-Liquid Extraction. *Chem. Commun.* **1998**, *16*, 1765−1766.
(28) Bonhôte, P.; Dias, A.-P.; Papageorgiou, N.; Kalyanasundaram, K.; Grätzel, M. Hydrophobic, Highly Conductive Ambient-Temperature Molten Salts. *Inorg. Chem.* **1996**, *35*, 1168−1178.
(29) Cammarata, L.; Kazarian, S. G.; Salter, P. A.; Welton, T. Molecular States of Water in Room Temperature Ionic Liquids. *Phys. Chem. Chem. Phys.* **2001**, *3*, 5192−5200.
(30) Niazi, A. A.; Rabideau, B. D.; Ismail, A. E. Effects of Water Concentration on the Structural and Diffusion Properties of Imidazolium-Based Ionic Liquid-Water Mixtures. *J. Phys. Chem. B* **2013**, *117*, 1378−1388.
(31) Kahlen, J.; Masuch, K.; Leonhard, K. Modelling Cellulose Solubilities in Ionic Liquids Using COSMO-RS. *Green Chem.* **2010**, *12*, 2172−2181.
(32) Wang, H.; Gurau, G.; Rogers, R. D. Ionic Liquid Processing of Cellulose. *Chem. Soc. Rev.* **2012**, *41*, 1519−1537.
(33) Sun, N.; Rodríguez, H.; Rahman, M.; Rogers, R. D. Where Are Ionic Liquid Strategies Most Suited in the Pursuit of Chemicals and Energy from Lignocellulosic Biomass? *Chem. Commun.* **2011**, *47*, 1405−1421.

DOI: 10.1021/acs.jced.7b00274
J. Chem. Eng. Data 2017, 62, 2374−2383

Paper III

Yanrong Liu, Anne S. Meyer, Yi Nie, Suojiang Zhang, Kaj Thomsen

Low energy recycling of ionic liquids via freeze crystallization during cellulose spinning

Green Chemistry, 2017, DOI: 10.1039/C7GC02880F.

Green Chemistry

PAPER

View Article Online
View Journal

Cite this: DOI: 10.1039/c7gc02880f

Low energy recycling of ionic liquids *via* freeze crystallization during cellulose spinning†

Yanrong Liu,[a,b,c] Anne S. Meyer,[c] Yi Nie,[a] Suojiang Zhang *[a] and Kaj Thomsen *[b]

A new method for recycling ionic liquids (ILs) from a cellulose spinning process is suggested. The method involves the combination of freeze crystallization and evaporation of H_2O from IL + H_2O mixtures to recycle the ILs. Processes with EmimAc and EmimDep were used as references to develop this IL recycling method. EmimAc + 12.5 wt% H_2O and EmimDep + 4 wt% H_2O were selected for a quantitative mass and energy analysis of the cellulose spinning and IL recycling process (the maximal initial H_2O levels in the ILs + H_2O mixtures for cellulose dissolution were determined experimentally). The energy requirement for the freeze crystallization + evaporation method was compared to evaporation only for recycling of EmimAc and EmimDep. To produce 1 kg dry cellulose fiber, 45.4 MJ and 62.6 MJ are required for recycling EmimAc and EmimDep respectively by the freeze crystallization + evaporation recycling method. Using evaporation only, 66.9 MJ is required for EmimAc recycling and 99.9 MJ for EmimDep recycling per kg cellulose fiber produced. Thus, to fabricate 1 kg dry cellulose fiber using freeze crystallization + evaporation rather than evaporation, 21.5 MJ can be saved for EmimAc and 37.3 MJ for EmimDep recycling. We also show that compared to a classical Lyocell fiber production method using *N*-methylmorpholine-*N*-oxide (NMMO) as solvent, use of ILs is energy saving in itself. Hence, significantly less H_2O is required in the cellulose spinning process with ILs than with NMMO, and in turn less H_2O has to be evaporated for the solvent recycling.

Received 22nd September 2017,
Accepted 18th December 2017

DOI: 10.1039/c7gc02880f

rsc.li/greenchem

1. Introduction

The demand for textile fibers is increasing with the growth of the global population and the improvement of living standards. As commonly known, cellulose fibers, notably in the form of cotton, are crucially important for textile manufacturing all over the world. The classical industrial methods for producing cellulose fibers include the viscose process, the cuprammonium hydroxide process, and the NMMO process.[1] However, these processes have the drawbacks of being far from eco-friendly.[2]

Ionic Liquids (ILs) can be considered green solvents for cellulose dissolution, and certain ILs have been shown to function well as solvents for spinning of cellulose fibers.[1] Water is commonly used as an anti-solvent for coagulation of cellulose and for washing of the fibers to remove the IL after spinning. Hong *et al.*[3] introduced an air-gap spinning process to spin cellulose fibers in EmimAc using distilled water as coagulation solvent. Sun *et al.*[4] prepared the cellulose fiber with raw pulp in BmimCl based on dry-jet and wet-spun methods and washing of the BmimCl by tap water. Luo *et al.*[5] and Zhu *et al.*[6] investigated wet-spinning of electrically conductive cellulose fibers in AmimCl and EmimAc respectively using deionized water to remove the solvents. However, in none of these studies, recycling of ILs from IL + H_2O mixtures after the fiber spinning was investigated. Despite the merits of ILs compared to organic solvents, including non-flammability and low vapor pressure,[7] their cost is still a key inhibitory factor for their application in the cellulose fiber industry. Therefore, it is urgent and necessary to develop methods for IL recycling including feasible recovery of ILs from IL + H_2O systems in cellulose spinning processes.

Several IL recycling methods have been reported in the literature including membrane separation,[8] evaporation,[9] liquid–liquid extraction,[10] centrifugal solvent-extraction,[11] and

[a]*Beijing Key Laboratory of Ionic Liquids Clean Process, Key Laboratory of Green Process and Engineering, State Key Laboratory of Multiphase Complex Systems, Institute of Process Engineering, Chinese Academy of Sciences, P. O. Box 353, Beijing, 100190, China. E-mail: sjzhang@ipe.ac.cn*
[b]*Center for Energy Resources Engineering (CERE), Department of Chemical and Biochemical Engineering, Technical University of Denmark, Søltofts Plads 229, 2800 Lyngby, Denmark. E-mail: kth@kt.dtu.dk*
[c]*Center for Bioprocess Engineering, Department of Chemical and Biochemical Engineering, Technical University of Denmark, Søltofts Plads 227, 2800 Lyngby, Denmark. E-mail: am@kt.dtu.dk*

†Electronic supplementary information (ESI) available: EmimAc and EmimDep recycling processes by evaporation method. See DOI: 10.1039/c7gc02880f

Supercritical CO_2 extraction.[12] Membrane separation usually results in low IL recovery due to the high viscosity of IL mixtures, which is a barrier for industrial implementation.[13] Evaporation of H_2O from IL + H_2O mixtures has been used for recycling of the ILs, but this method is obviously energy consuming and the large energy requirement is a constraint for practical implementation. Liquid–liquid extraction by use of conventional organic solvents has also been suggested for recycling of ILs, but the use of organic solvents is not compatible with the "green" aspect of employing ILs.[13]

Based on our recent study determining the freezing points of a series of IL + H_2O mixtures,[14] we hypothesized that freeze crystallization could be a feasible method for recovering ILs from dilute IL + H_2O solutions. Previous studies have shown that eutectic freeze crystallization is technically and economically feasible in cases where high product quality was required. Energy costs can be reduced by about 70% for certain systems by use of freeze crystallization compared to a three-stage evaporative crystallization.[15] The present study was therefore undertaken to test the workability of this hypothesis in relation to minimizing energy use by employing freeze crystallization of H_2O in the separation and recycling of ILs during a cellulose spinning process. The study included 1. Cellulose solubility measurements for two selected ILs in mixtures with different water contents to identify the cellulose solubility in IL + H_2O mixtures. 2. Determination of the optimal initial water content from the cellulose solubility data. 3. Cellulose regeneration after spinning. 4. Prediction of the energy requirement for the IL recycling process. In addition, we included scanning electron microscopy (SEM) to assess the morphology of the cellulose fibers after spinning. Lastly, we compared the energy requirement of spinning using the ILs as solvents to the energy required in a classical cellulose spinning process employing NMMO as solvent.

2. Computational details

The heat capacities (C_p) of ILs were obtained from published experimental values: EmimAc (298.15 K to 393.22 K)[16,17] and EmimDep (298 K to 343 K).[18] These values can also be found in the Ionic Liquids Database-IL Thermo (V2.0).[19] A linear temperature dependency of heat capacity was calculated from these data for EmimAc and EmimDep as following: the slope, a, for the temperature dependency was calculated using eqn (1). The heat capacities of EmimAc and EmimDep at the temperature T were calculated by eqn (2). This equation was assumed to be valid at temperatures up to 393.15 K for EmimDep. The heat capacity of the cellulose, microcrystalline cellulose, (MCC) was measured by Blokhin *et al.*[20] Their C_p data show an almost linear function of temperature in the temperature range relevant to our work. We used these data to fit parameters for MCC with eqn (2). The specific enthalpy of EmimAc, EmimDep, and MCC at the temperature T was calculated with eqn (3) using a reference temperature (T_{ref}) of 298.15 K.

$$a = \frac{C_{p,T_2} - C_{p,T_1}}{T_2 - T_1} \quad (1)$$

$$C_p = C_{p,298.15\ K} + a(T - 298.15) \quad (2)$$

$$H = \int_{T_{ref}}^{T} C_p dT \quad (3)$$

The specific enthalpy of water (liquid and vapor) was calculated using the NIST/ASME steam properties program (NIST standard reference database 10, version 3.0). For each step of the process (see later) the enthalpy of water vapor was calculated at the relevant temperature and pressure. A COSMO-RS evaluation of the water activity coefficient of the liquid solution leaving the evaporator at 393.15 K was used to predict the required pressure in the evaporator. The water activities (a_w) of the EmimAc + H_2O and EmimDep + H_2O mixtures were determined from the water mole fraction of these mixtures and the predicted water activity coefficient. In each case, this water activity was multiplied with the saturation pressure of water, 0.199 MPa at 393.15 K to get the required pressures of the evaporators. The specific enthalpies of water and water vapor at these conditions were calculated by the NIST/ASME steam properties program.

The heat capacity of liquid water cannot easily be measured below 273.15 K. The heat capacity of liquid water in the freezing step was therefore set as the approximate value of 4.2 kJ kg^{-1} K^{-1}. The water enthalpy in the freezing step was calculated by eqn (3) with a reference temperature of 273.16 K (the triple point temperature of water). The value used for the heat of fusion of ice in this study was 333.55 kJ kg^{-1}.[21] The heat capacity of ice was cited from Arshad *et al.*,[22] the value is 49.627 J mol^{-1} K^{-1}, which corresponds to 2.76 kJ kg^{-1} K^{-1}. Thus, the specific enthalpy of ice was calculated from eqn (4). T_{ref} in eqn (4) is the reference temperature for water enthalpy, 273.16 K.

$$H_{ice} = \int_{T_{ref}}^{T} 2.76 dT - 333.55 = 2.76(T - T_{ref}) - 333.55 \quad (4)$$

3. Results and discussion

3.1 MCC solubility in IL + H_2O mixture

By increasing the water content in mixtures with EmimAc and EmimDep, the MCC solubility decreases significantly (Table 1). At 12.5 wt% water in EmimAc, the solubility of MCC is 12 wt% at 363.15 K. At 4 wt% water in EmimDep the solubility of MCC is 8 wt% at 363.15 K. A sudden decrease in MCC solubility takes place when this threshold water content is exceeded (Fig. 1). The data are in agreement with previous reports showing that water influences cellulose solubility in ILs.[23–25] It was shown earlier that EmimAc with 15 wt% water can dissolve less than 1 wt% cellulose.[23] Olsson *et al.* reported that EmimAc is still an acceptable solvent for cellulose when mixed with certain amounts of water.[25] Thus, solutions of

Table 1 MCC solubility in total mixtures at 363.15 K

EmimAc (1) + H_2O (2) + MCC (3)		EmimDep (1) + H_2O (2) + MCC (3)	
w_2	w_3	w_2	w_3
0.005	0.27[26]	0.0019	0.15[26]
0.025	0.23	0.025	0.11
0.05	0.16	0.04	0.08
0.075	0.15	0.045	0.003
0.10	0.14		
0.125	0.12		
0.13	0.004		

w_2: weight fraction of H_2O in solvent. w_3: weight fraction of MCC in total mixture. The standard uncertainty of the weight fraction is 0.001.

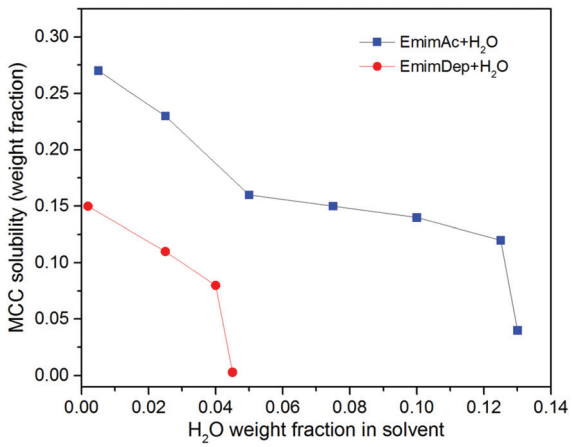

Fig. 1 Experimental values of MCC solubility plotted against H_2O weight fraction in solvent at 363.15 K.

EmimAc with 12.5 wt% H_2O and solutions of EmimDep with 4 wt% H_2O can be used as initial solvents for MCC in a cellulose spinning process.

3.2 EmimAc and EmimDep recycling processes

Fig. 2 and 3 illustrate spinning processes using EmimAc and EmimDep as solvents and with recycling of IL. The initial spinning solution derived from the measured solubility data are EmimAc (87.5 kg) + H_2O (12.5 kg) + MCC (13.6 kg) in Fig. 2 and EmimDep (96 kg) + H_2O (4 kg) + MCC (8.7 kg) in Fig. 3. By increasing the water content to 13 wt% in the case of EmimAc and to 4.5 wt% in the case of EmimDep, MCC will precipitate. However, the cellulose fiber (MCC) cannot be regenerated with these small amounts of excess water. In the spinning process, it was chosen to use an amount of deionized water corresponding to the mass of the spinning solution as coagulation bath in the regeneration process. After the cellulose fiber regeneration, the same quantity of washing water was used for washing EmimAc and EmimDep away from the wet fiber.

It was assumed that no cellulose was lost or recycled in the process. With a known amount of fiber, the water evaporated from the wet fiber could therefore be determined by the weight loss during the vacuum drying. According to the experiment, 48.0 kg water evaporated from the wet fibers in the EmimAc recycling process, and 48.2 kg in the EmimDep recycling process. The vacuum drying step took place at 353.15 K corresponding to a water saturation pressure of 0.0474 MPa. The experimental pressure was set to 0.015 MPa. Under these conditions, the fiber would be dried to a water activity, a_w of approximate 0.32. It is assumed that this water activity is a result of the interaction of water with IL rather than the interaction of water with fiber. According to COSMO-RS, a water activity of 0.32 is obtained for a solution with 0.68 mole fraction water in EmimAc. For EmimDep + H_2O the corresponding water mole fraction is 0.6. After drying, the mass of the dry fiber was 2.3 kg higher than the original mass of MCC in the EmimAc recycling process. In the EmimDep recycling process the same number was 3.6 kg. To obtain these water mole fractions, the final amounts of IL and water in the dry fiber product were determined to be 1.6 kg EmimAc + 0.7 kg H_2O in the EmimAc process and 3.0 kg EmimDep + 0.6 kg H_2O in the EmimDep process.

The EmimAc and EmimDep concentrations in the regenerated solvent (solution 1, Fig. 2 and 3) and in the washing water (solutions 2 and 3, Fig. 2 and 3) were determined by electrical conductivity measurements. The EmimAc and EmimDep electrical conductivity standard curves are given in Fig. 4. The measured electrical conductivities of solutions 1, 2, and 3 diluted 100 times are listed in Table 2. The concentrations and quantities of EmimAc and EmimDep in solutions 1, 2, and 3 were calculated from these calibration curves and are listed in Table 2. The amount of EmimAc recycled from these three solutions is 82.5 kg, corresponding to 94.2% of the amount of IL used as solvent. For EmimDep 91 kg is recycled, corresponding to 94.8% of the initial amount of EmimDep.

The amounts of IL and water remaining with the dry fiber was also determined from a mass balance assuming that the dry fiber corresponds to the initial amount of MCC. These values are given in Fig. 2 and 3. These amounts are not in complete agreement with the amounts of IL recovered in solutions 1, 2, and 3 from Fig. 2 and 3. The difference is partly caused by the uncertainty in calculating the water activity using COSMO-RS. This water activity was used for calculating the mole fraction of water in the solvent remaining with the dry fiber.

The mole fraction of water in the EmimAc + H_2O solution, Fig. 2, box (d) is 0.944. In our previous study it was concluded that a solution with a water mole fraction below 0.708 is not suitable for recycling EmimAc by freeze crystallization of water.[14] A water mole fraction of 0.708 corresponds to 85.9 kg EmimAc + 44.0 kg H_2O. Thus, 260.6 kg water can theoretically be removed as ice from a solution of 85.9 kg EmimAc + 304.6 kg H_2O. In order to further reduce the water content to 12.5 kg (Fig. 2), box (g), 31.5 kg of water needs to be evaporated. Similarly for the EmimDep recycling process in Fig. 3, the water mole fraction can be reduced from 0.957 to 0.682 by freezing of 254.1 kg water. Subsequently, 23.2 kg water has to be evaporated in the EmimDep recycling process. The amounts of components in each step of the EmimAc and EmimDep recycling processes are given in Fig. 2 and 3.

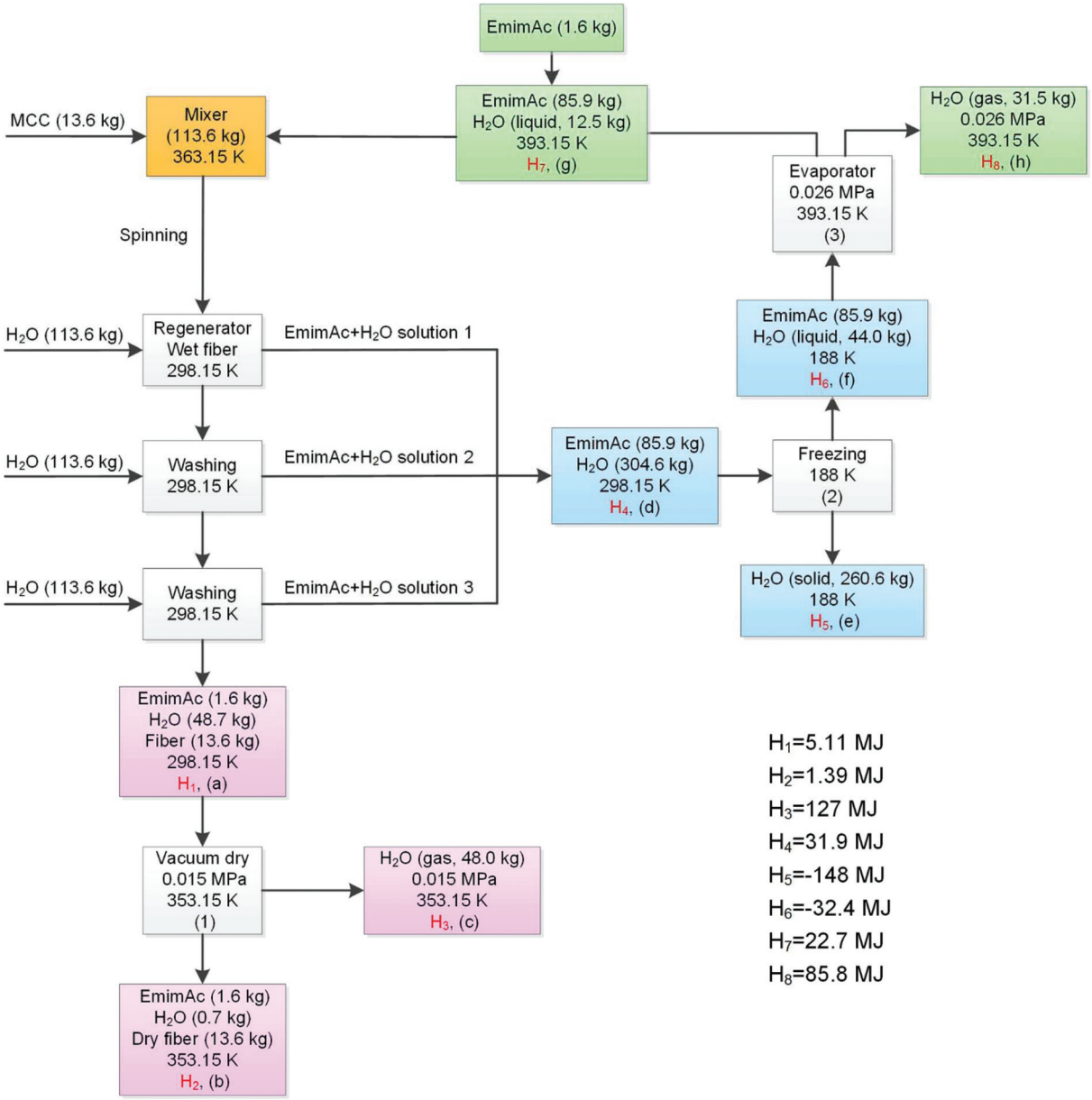

Fig. 2 EmimAc recycling in a cellulose spinning process. H_1–H_8 are the enthalpies of the mixtures described in box (a) to box (h).

3.3 Energy requirement for EmimAc and EmimDep recycling processes

Table 3 gives the values of the heat capacity parameters and the specific enthalpy of EmimAc, EmimDep, and MCC valid in temperature ranges relevant for Fig. 2 and 3. Based on these values, the specific enthalpy of EmimAc and EmimDep in box (a), (b), (d), (f) and (g) in Fig. 2 and 3 were calculated using eqn (3). A reference temperature of 298.15 K was used for ILs and MCC. The enthalpies of EmimAc, EmimDep, and MCC in box (a) and (d) are therefore 0. Specific enthalpy values for water and ice relevant for the processes in Fig. 2 and 3 are listed in Table 4.

Process diagrams for recycling processes for EmimAc (Fig. 6†) and EmimDep (Fig. 7†) using only evaporation are given in the ESI.† Key numbers for the energy requirement of this process are given together with key numbers for the freeze crystallization + evaporation process in Table 5.

The main energy requiring steps in the freeze crystallization + evaporation recycling processes in Fig. 2 and 3 include the vacuum drying, the freeze crystallization, and the evaporation processes. For the cellulose spinning process using EmimAc as solvent, Fig. 2, the energy consumption in the vacuum drying process is 123 MJ. The freeze crystallization process requires 212 MJ. The energy consumption of the evaporation process is 141 MJ. When EmimDep is used as solvent (Fig. 3), the energy

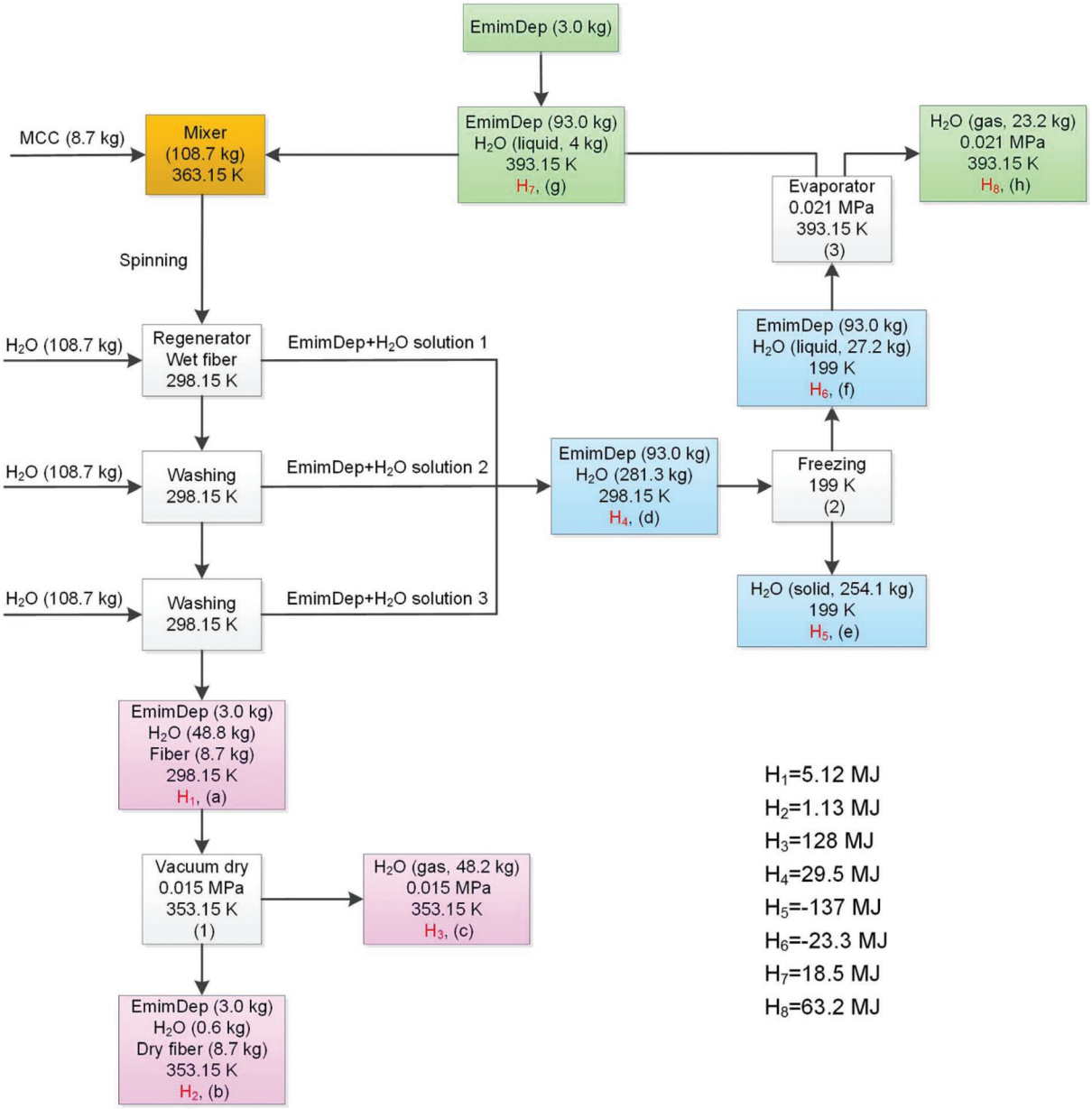

Fig. 3 EmimDep recycling in a cellulose spinning process. H_1–H_8 are the enthalpies of the mixtures described in box (a) to box (h).

usage in the vacuum drying process is 124 MJ, the freezing process requires 190 MJ, and the evaporation process uses 105 MJ. The efficiency of a freezing process is typically 60%.[27] The energy supplied to the freezing process in Fig. 2 could therefore be as high as 354 MJ, and in Fig. 3 the corresponding number could be 316 MJ. The total energy requirement for the vacuum drying process, the freezing process, and the evaporation process with EmimAc as solvent (Fig. 2) is 618 MJ, which is equal to 45.4 MJ kg^{-1} cellulose fiber. The total energy requirement for EmimDep recycling in Fig. 3 is 545 MJ corresponds to 62.6 MJ kg^{-1} cellulose fiber.

If recycling of EmimAc and EmimDep are performed by the evaporation method, the energy usage in the vacuum drying process is the same as calculated for the freeze crystallization + evaporation method. To remove water from the solvent by evaporation, the energy requirement is 787 MJ for EmimAc. For EmimDep the corresponding number is 745 MJ. Thus, the total energy usage for the EmimAc recycling process by evaporation is 910 MJ corresponding to 66.9 MJ kg^{-1} cellulose fiber. The EmimDep recycling process by evaporation requires 869 MJ corresponding to 99.9 MJ kg^{-1} cellulose fiber.

According to the energy balances, 21.5 MJ per kg cellulose fiber can be saved by using the combined freeze crystallization + evaporation process rather than evaporation only for recycling of EmimAc. The corresponding number is 37.3 MJ per kg cellulose fiber that can be saved if EmimDep is recycled using freeze crystallization + evaporation. The energy balances

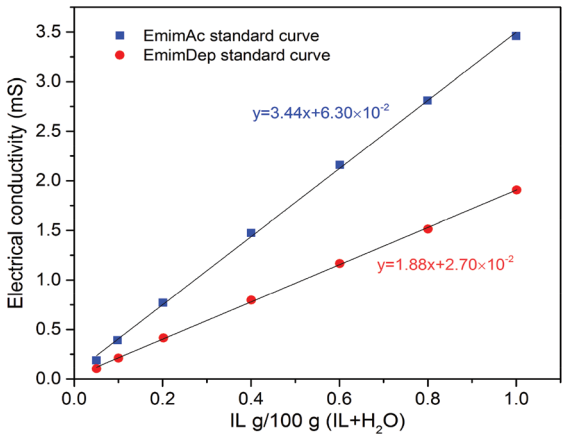

Fig. 4 EmimAc and EmimDep electrical conductivity standard curves. The standard uncertainty of the electrical conductivity is 0.07 mS.

therefore verify the hypothesis behind this work, namely that freeze crystallization + evaporation rather than evaporation for IL recycling will save a significant amount of energy.

In the EmimAc recycling process using freeze crystallization + evaporation (Fig. 2), the total quantity of water used in the regeneration and washing steps is 340.8 kg. 260.6 kg water is recovered as ice and only 79.5 kg water is evaporated. The amount of cellulose fiber produced is 13.6 kg. To produce 1 kg cellulose fiber requires the evaporation of 5.8 kg water in the drying and the recycling process when using EmimAc as solvent. When using EmimDep as solvent (Fig. 3), 8.2 kg water needs to be evaporated per kg fiber in the drying and recycling process. It is therefore clear that the energy requirement of the IL recycling process depends on the type of IL.

Cai *et al.*[28] indicated that recycling of the amount of NMMO solvent required for producing 1 kg Lyocell fiber requires evaporation of 15–40 kg water. This amount only includes the recycling of solvent, not the drying of fiber. It therefore seems like using IL as solvent, and recovering the IL by freeze crystallization + evaporation will save a large amount of energy also compared to traditional cellulose processing.

Our previous work,[14] shows that in the dilute region of aqueous solutions of ILs, ice starts forming when the solutions are cooled to their freezing points. A change in slope of the

Table 2 Electrical conductivity, quantity and recycling yield of EmimAc and EmimDep in solutions 1, 2 and 3

EmimAc	Solution 1	Solution 2	Solution 3
Electrical conductivity[a] (mS)	1.50	0.498	0.203
EmimAc g per 100 g (EmimAc + H_2O)	42.0	12.7	4.08
Quantity in solution (kg)	63.3	14.3	4.88
Recycling yield (wt%)	72.3	16.3	5.57
EmimDep	**Solution 1**	**Solution 2**	**Solution 3**
Electrical conductivity[a] (mS)	0.914	0.408	0.168
EmimDep g per 100 g (EmimDep + H_2O)	47.2	20.3	7.50
Quantity in solution (kg)	56.7	25.2	9.13
Recycling yield (wt%)	59.1	26.2	9.51

[a] Electrical conductivity (mS). Values were measured after diluting solutions 1, 2, and 3 100 times.

Table 3 Values of heat capacity, temperature slope *a*, and specific enthalpy of EmimAc, EmimDep, and MCC in Fig. 2 and 3

Name	$C_{p,\ 298.15\ K}$ kJ kg^{-1} K^{-1}	*a* kJ kg^{-1} K^{-2}	Box (b) kJ kg^{-1}	Box (f) kJ kg^{-1}	Box (g) kJ kg^{-1}
EmimAc	1.89[16]	2.40×10^{-3}	108	−194	190
EmimDep	1.74[18]	2.75×10^{-3}	99.9	−159	178
MCC	1.20[19]	4.29×10^{-3}	72.5		

a was calculated by eqn (1). Specific enthalpies were calculated with eqn (3). The specific enthalpies of EmimAc, EmimDep, and MCC in box (a) and (d) are 0.

Table 4 Specific enthalpy of water and ice relevant for Fig. 2 and 3

Process	H_2O (l) Box (a) and (d) kJ kg^{-1}	H_2O (l) Box (b) kJ kg^{-1}	H_2O (gas) Box (c) kJ kg^{-1}	H_2O (l) Box (f) kJ kg^{-1}	H_2O (l) Box (g) kJ kg^{-1}	H_2O (gas) Box (h) kJ kg^{-1}	H_2O (ice) Box (e) kJ kg^{-1}
Fig. 2	105	335	2649	−358	504	2724	−569
Fig. 3	105	335	2649	−311	504	2725	−538

The specific enthalpy of water was calculated by NIST/ASME steam properties program. The water enthalpy in box (f) was calculated by eqn (3). The ice enthalpy was calculated by eqn (4).

Table 5 Energy requirements for recycling EmimAc and EmimDep using a freeze crystallization + evaporation process and a process in which all water is removed by evaporation

Freeze crystallization + evaporation	Vacuum drying (MJ)	Freezing (MJ)	Evaporation (MJ)	Total (MJ)	Energy consumption per kg cellulose (MJ)
EmimAc	123	354[a]	141	618	45.4
EmimDep	124	316[a]	105	545	62.6

Evaporation	Vacuum drying (MJ)	Freezing (MJ)	Evaporation (MJ)	Total (MJ)	Energy consumption per kg cellulose (MJ)
EmimAc	123	—	787	910	66.9
EmimDep	124	—	745	869	99.9

[a] The freezing process is assumed to have an efficiency of 60% while the vacuum drying and the evaporation processes are assumed to have efficiencies of 100%. The total energy requirement for recycling EmimAc corresponds to producing 13.6 kg cellulose fiber. The total energy requirement for recycling EmimDep corresponds to producing 8.7 kg cellulose fiber.

freezing point curve at increased concentration of IL indicates a change in solid phase which might be IL·nH$_2$O. Therefore, ILs with a potential to dissolve cellulose can be partly regenerated by freeze crystallization in the concentration range where pure ice is the stable solid phase.

3.4 The morphology and crystallinity analysis of regenerated MCC

The morphologies of the original MCC (dry) and regenerated MCC (dry) were observed by SEM (Fig. 5). Fig. 5(a) shows the original MCC used in the experiment. Fig. 5(b) is MCC regenerated after dissolution in EmimAc with a water mole fraction of approximately 0.2 (EmimAc + 5 wt% H$_2$O). Fig. 5(c) is MCC regenerated after dissolution in EmimAc with a water mole fraction of approximately 0.3 (EmimAc + 7.5 wt% H$_2$O). Fig. 5(d) is MCC regenerated after dissolution in EmimDep with a water mole fraction of approximately 0.2 (EmimDep + 2.5 wt% H$_2$O). With increasing water mole fraction in EmimAc + H$_2$O mixtures, the surface morphology of the regenerated MCC changes distinctly (Fig. 5). With the same water mole fraction of approximately 0.2 in EmimAc (with 5 wt% H$_2$O) and in EmimDep (with 2.5 wt% H$_2$O) the surface morphologies of the regenerated MCC were also different. The SEM result indicates that the water content and the type of IL significantly affect the morphology and the properties of the fibers.

The X-ray diffraction (XRD) analysis is given in Fig. 6. The original MCC displays a strong peak around 2θ = 22.8°, corresponding to the (002) crystal plane of cellulose, as well as a composite peak corresponding to the (101) and (10$\bar{1}$) crystal planes at 2θ = 15° and 15.5° approximately. The intensity of the (002) plane decreases dramatically for MCC treated with EmimAc + H$_2$O and EmimDep + H$_2$O. No distinct peak remains for the (101) and (10$\bar{1}$) planes, which illustrates that the crystallinity of cellulose is greatly disrupted after the dissolution and regeneration from EmimAc + H$_2$O and EmimDep + H$_2$O. This disruption ability is diminished with the addition of water in EmimAc. These results are in agreement with the results obtained in the study by Doherty *et al.*[29]

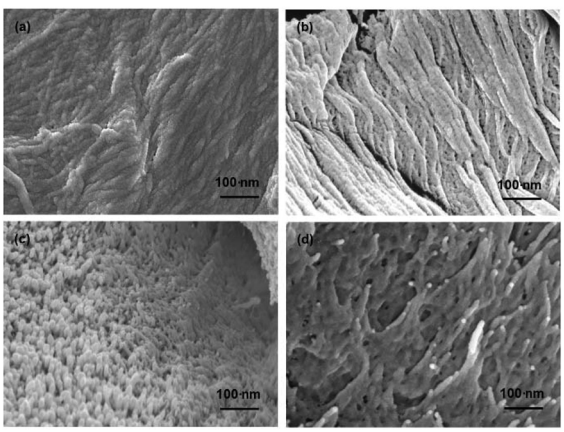

Fig. 5 (a) Morphology of original MCC, (b) MCC regenerated from EmimAc with water mole fraction of 0.2 (5 wt% H$_2$O), (c) MCC regenerated from EmimAc with water mole fraction of 0.3 (7.5 wt% H$_2$O), (d) MCC regenerated from EmimDep with water mole fraction of 0.2 (2.5 wt% H$_2$O).

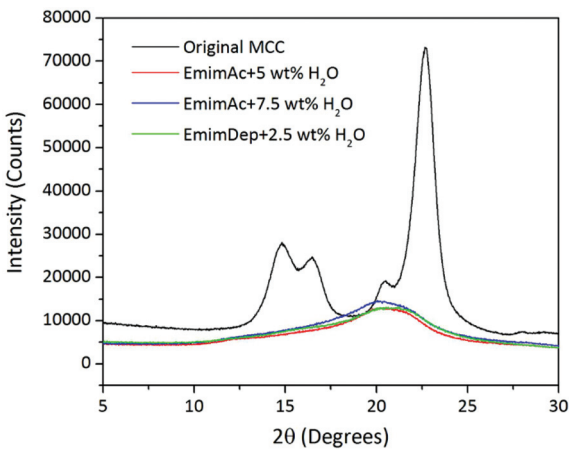

Fig. 6 XRD of original MCC and regenerated MCCs.

4. Experimental

4.1 Chemical reagents

1-Ethyl-3-methylimidazolium Acetate (EmimAc, 170.21 g mol^{-1}) and 1-ethyl-3-methylimidazolium Diethyl phosphate (EmimDep, 264.26 g mol^{-1}) which have the same cation and different anions were selected for this study. In our previous work it has been verified that these two ILs have a high capacity for cellulose dissolution.[26] EmimAc (99 wt%), was purchased from Shanghai Cheng Jie Chemical Co. Ltd (Shanghai, China), and EmimDep was synthesized in one step. The synthetic method and the purity analysis of EmimDep was given in the ESI† of our previous work.[26] The structures of EmimDep was confirmed by its ^{1}H and ^{13}C NMR spectra using a Bruker 600 spectrometer. Characteristic peaks and ^{1}H and ^{13}C NMR data of EmimDep was shown in the ESI† of our previous work.[14] Cellulose was microcrystalline cellulose (MCC) purchased from Sinopharm Chemical Reagent Co. Ltd (Shanghai, China).

4.2 Cellulose dissolution and IL recycling procedures

EmimAc and EmimDep were mixed with different amounts of water for assessing the solubility of MCC at 363.15 K. The MCC was dried at 353.15 K under vacuum for 48 h before use. An initial amount of MCC of approximately 0.05 g was added to the IL + H_2O mixtures (5 g) at the beginning. Subsequently, MCC was added stepwise in 0.05 g portions until the solubility limit was reached. When the MCC start solubility is less than 0.05 g, the stepwise added amount of MCC was changed to 0.005 g portions until the solubility limit was reached. An OLYMPUS BX 51 optical microscope was used to assess the dissolution of MCC in the different IL + H_2O mixtures. When MCC could be observed under the optical microscope without dissolving after 12 hours[26,30,31] the solubility limit had been exceeded.

The recycling process was performed at laboratory scale, and then scaled-up proportional to the experimental amounts. The recycling process included the following steps: 1. Different amounts of MCC was dissolved in IL + H_2O mixtures at 363.15 K to form the spinning solution. 2. The spinning solution was placed into a spinning equipment (Longer Pump, LSP01-1A) to make the cellulose fiber. A single hole spinneret needle was connected to a coagulation bath using deionized water as the regeneration solvent. After the cellulose regeneration, the cellulose fiber + IL + H_2O mixture was separated into wet cellulose fiber and aqueous IL solution. 3. The wet cellulose fiber was washed twice using deionized water to remove IL. 4. The amounts of IL in the solutions were determined by measuring the electrical conductivity. The three solutions were mixed and cooled to remove water as ice by freezing (prediction). Remaining water was evaporated to make the IL ready for recycling (prediction). 5. Finally, the wet fiber was dried in vacuum drying oven at the temperature of 353.15 K and the pressure of 0.015 MPa to remove water from it. The recycling procedures of EmimAc and EmimDep are illustrated in Fig. 2 and 3.

In step 2 and 3, the electrical conductivities of the regenerated solvent and two batches of wash solutions were measured. A conductivity meter (Orion, 136S) with automatic data logging was used. Electrical conductivity calibration curves of aqueous EmimAc and EmimDep solutions were first determined. The amounts of EmimAc and EmimDep used for measuring the electrical conductivity calibration curve were approximately 0.05, 0.1, 0.2, 0.4, 0.6, 0.8 and 1 g per 100 g solution. The aqueous EmimAc and EmimDep solutions in step 2 and 3 were diluted 100 times in order to be within the concentration range of the calibration curves. The quantities of EmimAc and EmimDep in the regenerated solvent and in the washing solutions were determined according to these calibration curves. The electrical conductivity of each sample was measured more than 15 minutes until a consistent value was reached.

4.3 SEM and XRD analysis for regenerated MCC

The morphology of the original MCC and the selected regenerated MCCs obtained after using EmimAc + H_2O and EmimDep + H_2O as solvents were observed by SEM (JSM 6700F, Japan, 5.0 kV). The sample was sputtered with platinum for better observation using JEC-3000FC auto fine coater. The current and the sputtering time were set to 20 mA and 150 s respectively. XRD of the original MCC and of the regenerated MCC was employed to examine the crystalline structures of original MCC and regenerated MCC. Data were obtained using a Bruker D8 Focus instrument, and the X-ray tube was operated at 40 kV and 200 mA with 2θ ranging from 5° to 30° at a scan speed of 0.05 s^{-1}.

5. Conclusion

In this study, the solubility of MCC in two selected ILs (*i.e.* in IL + H_2O mixtures) as a function of water content was measured at 363.15 K. The MCC solubility decreases gradually as water is added and then suddenly reaches a solubility limit. The viscosity of the IL + H_2O mixtures were also taken into account, hence EmimAc with 12.5 wt% H_2O and EmimDep with 4 wt% H_2O were chosen as solvents for cellulose spinning with IL recycling. The energy usage of two processes: freeze crystallization + evaporation *versus* evaporation of H_2O from ILs + H_2O mixtures was evaluated for recycling of the ILs. A higher initial amount of H_2O was used in practice for the cellulose solubilisation and spinning using EmimAc as compared to using EmimDep as solvent. Still, the higher solubility of cellulose (MCC) in EmimAc meant that less energy was required for freeze crystallization + evaporation of H_2O to recover and recycle the IL from EmimAc + H_2O mixtures than from EmimDep + H_2O mixtures (45.4 MJ *vs.* 62.6 MJ per kg dry cellulose fiber). Using electrical conductivity measurement, it was verified that 94.2 wt% of EmimAc and 94.8 wt% of EmimDep could be recovered after cellulose spinning.

It was found that using freeze crystallization + evaporation for recycling of EmimAc and EmimDep, respectively, can save

a significant amount of energy compared to a process where all water is removed by evaporation, namely 21.5 MJ for EmimAc and 37.3 MJ for EmimDep per kg dry cellulose produced. This new IL recycling method not only saves energy for IL recycling compared to evaporation, but is also much more energy efficient than conventional cellulose fiber production methods, such as the NMMO process. The freeze crystallization + evaporation method may also be applied to other processes requiring separation of IL + H_2O mixtures and thus potentially result in energy saving in multiple cellulose processing applications.

Conflicts of interest

There are no conflicts of interest to declare.

Acknowledgements

We would like to sincerely thank Liangyu Ma and Wenjun Wang for helping with the MCC solubility and MCC morphological properties study. This work was supported by the Department of Chemical and Biochemical Engineering, Technical University of Denmark and CAS/SAFEA International Partnership Program for Creative Research Teams (Grant No. 20140491518), General Program of National Natural Science Foundation of China (Grant No. 21576262 and 2157060191).

References

1 X. J. Li, N. K. Li, J. G. Xu, X. Q. Duan, Y. S. Sun and Q. Zhao, *J. Appl. Polym. Sci.*, 2014, **131**, 742–751.
2 A. R. Xu, J. J. Wang and H. Y. Wang, *Green Chem.*, 2010, **12**, 268–275.
3 J. H. Hong, M. K. Ku, Y. Ahn, H. J. Kim and H. Kim, *Fibers Polym.*, 2013, **14**, 2015–2019.
4 L. F. Sun, J. Y. Chen, W. Jiang and V. Lynch, *Carbohydr. Polym.*, 2015, **118**, 150–155.
5 Z. Q. Luo, A. Q. Wang, C. Z. Wang, W. C. Qin, N. N. Zhao, H. Z. Song and J. G. Gao, *J. Mater. Chem. A*, 2014, **2**, 7327–7336.
6 C. Zhu, J. Chen, K. K. Koziol, J. W. Gilman, P. C. Trulove and S. S. Rahatekar, *eXPRESS Polym. Lett.*, 2014, **8**, 154–163.
7 Y. L. Zhao, X. M. Liu, J. J. Wang and S. J. Zhang, *J. Phys. Chem. B*, 2013, **117**, 9042–9049.
8 J. G. Lynam, G. I. Chow, C. J. Coronella and S. R. Hiibel, *Chem. Eng. J.*, 2016, **288**, 557–561.
9 X. Liu, Y. Nie, X. L. Meng, Z. L. Zhang, X. P. Zhang and S. J. Zhang, *RSC Adv.*, 2017, **7**, 1981–1988.
10 T. Fukuyama, M. Shinmen, S. Nishitani, M. Sato and I. Ryu, *Org. Lett.*, 2002, **4**, 1691–1694.
11 J. F. Birdwell Jr., J. McFarlane, R. D. Hunt, H. M. Luo, D. W. DePaoli, D. L. Schuh and S. Dai, *Sep. Sci. Technol.*, 2006, **41**, 2205–2223.
12 L. A. Blanchard and J. F. Brennecke, *Ind. Eng. Chem. Res.*, 2001, **40**, 287–292.
13 B. Wu, W. W. Liu, Y. M. Zhang and H. P. Wang, *Chem. – Eur. J.*, 2009, **15**, 1804–1810.
14 Y. R. Liu, A. S. Meyer, Y. Nie, S. J. Zhang, Y. S. Zhao, P. L. Fosbøl and K. Thomsen, *J. Chem. Eng. Data*, 2017, **62**, 2374–2383.
15 R. Vaessen, M. Seckler and G. J. Witkamp, *Ind. Eng. Chem. Res.*, 2003, **42**, 4874–4880.
16 M. G. Freire, A. R. R. Teles, M. A. A. Rocha, B. Schröder, C. M. S. S. Neves, P. J. Carvalho, D. V. Evtuguin, L. M. N. B. F. Santos and J. A. P. Coutinho, *J. Chem. Eng. Data*, 2011, **56**, 4813–4822.
17 C. Su, X. Y. Liu, C. Y. Zhu and M. G. He, *Fluid Phase Equilib.*, 2016, **427**, 187–193.
18 C. M. Tenney, M. Massel, J. M. Mayes, M. Sen, J. F. Brennecke and E. J. Maginn, *J. Chem. Eng. Data*, 2014, **59**, 391–399.
19 IL Thermo: Ionic Liquids Database. http://ilthermo.boulder.nist.gov/ (accessed December 2017).
20 A. V. Blokhin, O. V. Voitkevich, G. J. Kabo, Y. U. Paulechka, M. V. Shishonok, A. G. Kabo and V. V. Simirsky, *J. Chem. Eng. Data*, 2011, **56**, 3523–3531.
21 Enthalpy of fusion. https://en.wikipedia.org/wiki/Enthalpy_of_fusion (accessed August 2017).
22 M. W. Arshad, P. L. Fosbøl, N. von Solms and K. Thomsen, *J. Chem. Eng. Data*, 2013, **58**, 1918–1926.
23 K. A. Le, R. Sescousse and T. Budtova, *Cellulose*, 2012, **19**, 45–54.
24 D. L. Minnick, R. A. Flores, M. R. DeStefano and A. M. Scurto, *J. Phys. Chem. B*, 2016, **120**, 7906–7919.
25 C. Olsson, A. Idström, L. Nordstierna and G. Westman, *Carbohydr. Polym.*, 2014, **99**, 438–446.
26 Y. R. Liu, K. Thomsen, Y. Nie, S. J. Zhang and A. S. Meyer, *Green Chem.*, 2016, **18**, 6246–6254.
27 Liquid air energy network, Chapter 2: An introduction to liquid air: http://liquidair.org.uk/full-report/report-chapter-two (accessed August 2017).
28 J. Cai and Z. Q. Han, *CN* 103046167A, 2013.
29 T. V. Doherty, M. Mora-Pale, S. E. Foley, R. J. Linhardt and J. S. Dordick, *Green Chem.*, 2010, **12**, 1967–1975.
30 A. Casas, S. Omar, J. Palomar, M. Oliet, M. V. Alonso and F. Rodriguez, *RSC Adv.*, 2013, **3**, 3453–3460.
31 L. Liu, M. T. Ju, W. Z. Li and Q. D. Hou, *Carbohydr. Polym.*, 2013, **98**, 412–420.

Paper IV

Yanrong Liu, Yi Nie, Kaj Thomsen, Suojiang Zhang, Anne S. Meyer

Wet-spinning conductive cellulose fiber base on ionic liquids as solvent and enzymatic modification

Yet to be submitted

Wet-spinning conductive cellulose fiber base on ionic liquids as solvent and enzymatic modification

Yanrong Liu,[a,b,c] Yi Nie,[a] Kaj Thomsen[b] Suojiang Zhang*[a] and Anne S. Meyer*[c]

[a]*Beijing Key Laboratory of Ionic Liquids Clean Process, Key Laboratory of Green Process and Engineering, State Key Laboratory of Multiphase Complex Systems, Institute of Process Engineering, Chinese Academy of Sciences, P. O. Box 353, Beijing, 100190, China, E-mail: sjzhang@ipe.ac.cn.*

[b]*Center for Energy Resources Engineering (CERE), Department of Chemical and Biochemical Engineering, Technical University of Denmark, Søltofts Plads 229, 2800, Lyngby, Denmark, E-mail: kth@kt.dtu.dk.*

[c]*Center for Bioprocess Engineering, Department of Chemical and Biochemical Engineering, Technical University of Denmark, Søltofts Plads 227, 2800, Lyngby, Denmark, E-mail: am@kt.dtu.dk.*

ABSTRACT

MWCNTs-cellulose conductive fiber was fabricated by wet-spinning using EmimDep as solvent. The effects of spinning parameters of extrusion flow, spinneret diameters and mass ratios of MWCNTs respect to cellulose were studied in this work. Rheological analysis, electrical conductivity, TGA, surface area, SEM and electrochemical property were applied for measurement the properties of the spinning solution and the studied fiber. The rheological analysis result indicates that the spinning solution has a spinning potential feature with the non-Newtonian of 0.6. The fiber electrical conductivity increase with the increasing of mass ratio of MWCNTs. The largest electrical conductivity acquired is 760 S/m at the spinning extrusion flow of 1 mL/min, spinneret diameter of 0.46 mm and 5:1 of MWCNTs respect to cellulose. TGA and surface area results evidenced that the fiber more stable at the spinneret diameter of 0.46 mm than 0.98 mm. The surface area of the conductive fiber can reach to 188 m^2/g. SEM result illustrated that a pore structure could be observed in the fiber surface and alignment MWCNTs in the fiber will decrease the fiber electrical conductivity. Tensile strength result shown that the fiber tensile strength will be increased after the phenol and enzyme solution treatment, especially has a significant increase for the studied cellulose fiber.

Keywords: Conductive cellulose fiber; Carbon nano tubes; Ionic liquids; Wet spinning.

1. Introduction

Electrically conductive polymer fiber may bring desirable applications to electrochemical and biomedical fields, such as electronic devices, capacitor electrode, neural probes, biosensors and bio-actuators, and shielding materials.[1-3] The recently attracted conductive fillers are carbon black (CB), carbon nanotubes (CNTs) and graphene nanoplatelets (GNP). CB was found to be superior to GNP in conductive fiber preparation by wet spun.[3] CNTs has a good electrical conductivity than CB, which makes CNTs to be a remarkable candidate as conductive filler. Moreover, CNTs has many merits of unique tubular structures, nanometer diameter, a large length/diameter ratio,[4] high mechanical property and excellent thermal stability.[5]

The previous methods on the use of CNTs for conductive fiber are mainly focus on spinning and dipping–drying,[6] and it has been reported that wet spinning is a flexible method to fabricate conductive fiber from use any types of CNTs.[7] Cellulose-based composites are of great importance because of the low cost of cellulose and its biodegradability. Cellulose is combined with CNTs can offer a good biocompatibility, electrical conductivity, and the ability to be easily spinning to fiber.[8] However, there are three challenges to achieving excellent conductivity cellulose/CNTs fiber: (1) Dissolve cellulose by green solvent. (2) Avoid the CNTs entanglement in solvent. (3) Disperse CNTs uniformly in cellulose solution.[9] This potential and desirable green solvent is ionic liquids (ILs), which have the outstanding properties of immeasurably low vapour pressure, excellent chemical and thermal stability, electrical conductivity, and nonflammability.[10] ILs are capable to dissolve cellulose at a low temperature, and to disperse CNTs through non-covalent cation-π interactions to prevent their entanglement. And more importantly, ILs also can act as a binder between CNTs and the cellulose for providing a stronger interaction with each other.[11]

Several studies of using ILs as solvent to produce CNTs conductive fibers by spinning have been reported. Zhang et al[12] investigated the conductive fiber preparation by dry-jet wet spinning using 1-allyl-3-methylimidazolium chloride (AmimCl) as solvent. The

proportion of multiwall carbon nanotubes (MWCNTs) respect to cellulose (wood pulp) were from 0~9 wt% with an interval of 1 wt% respectively. It was found that the fiber tensile strength increase from 204±6 MPa to 335±14 MPa with the MWCNTs mass percentages of 0~4 wt%, then decrease to 210±13 MPa from 4~9 wt% MWCNTs. And the fiber contains 4 wt% MWCNTs showed the highest electrical conductivity of 0.83 S/m. Rahatekar et al[8] using 1-ethyl-3-methylimidazolium acetate (EmimAc) as solvent to fabricate cellulose/MWCNTs fiber. The result illustrated that the fiber electrical conductivity could not be measured below 0.07 mass fraction of MWCNTs in MWCNT/cellulose. The electrical conductivity at 0.07 mass fraction of MWCNTs is 19 S/m. Xiao et al[13] using binary ILs of 1-butyl-3-methylimidazolium chloride (BmimCl) and 1-H-3-methylimidazolium chloride (HmimCl) to prepare chitosan/cellulose/MWCNTs fiber. The ratio of chitosan to cellulose was 1:3. The characterization results showed that the incorporation of MWCNTs could improve the comprehensive performances of the fiber, and the best loading of MWCNTs was 4 wt %. Zhu et al[9] were developed an electrically conductive fibers from carboxymethyl cellulose (CMC), EMIMAc and MWCNTs composition by dry-jet wet spinning. The spinning fiber was coagulated in water under the proportion of 10 wt% MWCNTs with respect to cellulose. The fiber highest electrical conductivity in this study is 0.24 S/m at the extrusion speed of 2.65×10^{-3} m/s with no winding speed. This study also evidenced that increase the winding speed, the fiber electrical conductivity will decrease.

On the basis of the previous studies, the aims of this work were to spun excellent electrical conductivity and high tensile strength cellulose conductive fiber using ILs as solvent. Meanwhile, the spinning solution and fiber characteristics were investigated by the analysis of rheological behavior, electrical conductivity, thermogravimetric analysis (TGA), surface area, scanning electron microscopy (SEM), tensile strength , and cyclic voltammetry. More importantly, the conductive fiber finally treatment by enzymatic modification to improve the tensile strength.

2. Experimental description

2.1 Materials

MWCNTs were selected as the conductive material because of their cost advantage compared to single-walled carbon nanotubes (SWCNTs). The MWCNTs were purchased from Cnano Technology (Zhenjiang) Ltd., which have the length of <10 μm and diameter between 10–15 nm. The purity of the MWCNTs is 98 wt% approximately with the iron amount less than 350 ppm. Cellulose (cotton pulp) was provided by Henan Dingda biological technology co., Ltd. with a polymerization degree of 720. 1-ethyl-3-methylimidazolium diethyl phosphate (EmimDEP, ＞99 wt%) was determined as the solvent for dissolving the cellulose and dispersing MWCNTs. This IL has been verified to be a potential solvent to disperse MWCNTs in our previous study,[14] and a super solvent to dissolve cellulose to acquire high modulus regenerated cellulose fiber by spinning.[15] The EmimDep was synthesized in one step at lab scale. The synthetic method, the purity analysis method and the NMR analysis of EmimDep was detailed explanation in the supporting information of our previous work.[16,17] Phenol was purchased from Riedel-de Haën. 2; 2′-azino-bis (3-ethylbenzthiazoline-6-sulfonic acid) (ABTS) was purchased from The Laccase, Myceliophthora thermophila (protein 78.59 mg/g) was provided by our group.

2.2 Cellulose conductive fiber manufacture procedures

The experimental procedures for manufacturing the cellulose and MWCNTs-cellulose conductive fiber were as follows:

1. Cotton pulp (0.3 g) with EmimDep (30 g) was heated in a thermostatic oil bath at 90 ℃ by mechanical mixing for 30 minutes to give clear liquid of 1 wt% cellulose. This 1 wt% cellulose solution was used as the blank control experiment.

2. Cotton pulp (0.3 g) with EmimDep (15 g) was heated in a thermostatic oil bath at 90 ℃ by mechanical mixing for 30 minutes to give clear liquid of solution 1. Four amounts of MWCNTs (0.6 g, 0.9g, 1.2g and 1.5g) were suspended in EmimDep (15 g) independently and ground in an agate mortar for 30 minutes at room temperature to get the mixtures. These four mixtures were added to solution 1 respectively at 90 ℃ by mechanical mixing for 2 hours to acquire the cellulose-MWCNTs mixtures. The ratios of MWCNTs respect to cellulose in these four conductive mixtures were 2:1, 3:1, 4:1 and 5:1.

3. The 1 wt% cellulose solution and these four cellulose-MWCNTs mixtures were placed in a vacuum drying oven to deaerate at 35 ℃ for 12 hours before using.

4. After the deaeration, the 1 wt% cellulose solution and these four cellulose-MWCNTs mixtures were transferred into a syringe, respectively. The syringe was fixed in a lab-built wet-spinning equipment, which consisted of a syringe pump, a regeneration bath (water is coagulation) and a winding shift, was used for fiber spinning. These above spinning solutions were spun into the regeneration bath directly at room temperature at varying extrusion flows of 0.01, 0.1, 0.4, 0.8, and 1.0 mL/min through a single hole spinneret needle with no winding, respectively. Two different diameters of the spinneret needle were used in this work. The inner diameters of spinneret needle were 0.46 mm and 0.98 mm. The length-diameter ratio of the spinneret needle was set as 2, which has been verified by Hauru et al[18] that this value gives a better strength property for cellulose spinning.

5. After the wet-spinning and the regeneration, the wet fibers were soaked into deionized water overnight and washed 5 times to remove the EmimDep away.[19]

6. Partly of the washed wet fiber was treated by 50 ml enzymatic solution at room temperature for 30 minutes. The enzymatic solution including approximately 10 wt% phenol and 0.5 wt% Myceliophthora thermophila of the cellulose weight in the fiber.[20] After the enzymatic treatment, the fiber was rinsed thoroughly by deionized water. Before the enzymatic treatment, the influence of the remaining EmimDep in the last time wash solution on the enzyme activity was investigated. 0.5 mM ABTS[21] and 10 mg/ml Myceliophthora thermophila solution were prepared in deionized water and EmimDep wash solution respectively. The absorbance was measured at 420 nm for the reaction of 240 μL 0.5 mM ABTS and 10 μL Myceliophthora thermophila solution (10 mg/ml, 1000 time dilute) at the room temperature with the increase of time (every point repeat 3 times). Then the slops of absorbance plotted against time of these two reaction were compared to

determine the influence of the EmimDep on enzyme activity.

7. The untreated and treated wet fibers from step 6 were first rolled at room temperature, and then sent them to vacuum drying oven at 35 ℃ for 48 hours for further characteristic analysis.

2.3 Characterization of cellulose and cellulose-MWCNTs fibers

Rheological analysis. The rheological properties of the 1 wt% cellulose solution and the four cellulose-MWCNTs mixtures were measured by TA instrument of Discovery HR-2 hybrid rheometer. The measurement temperature was set as 25 ℃, and the shear rate (r) was 0~500 s^{-1}. The non-Newtonian index is the degree of the non-Newton fluid deviating from the Newton fluid. As is known, the power law relationship of the Ostwald de Waele model is a useful form of expressing the flow behavior. The non-Newtonian index of n can be expressed by equation 1, where σ (pascal) indicates the shear stress, and K is the consistency index. The non-Newtonian index, n, is the slope of $\log\sigma = f(\log r)$.

$$\sigma = K r^n \qquad (1)^{22,23}$$

Electrical Conductivity. The electric conductivity was measured by a two-probe method (3 times repeat for each sample). The resistance (R) of the cellulose-MWCNTs fibers was measured by a precision voltmeter (LINI-T, UT58A). The voluresistivity ρ of the fibers was calculated by taking into account the section area (A) of the cellulose-MWCNTs fibers and the length (L) between the contacts: $\rho = R \times A/L$. Then, the conductivity γ (S/m) of the fibers was acquired from the reciprocal of the resistivity, that is $\gamma = L/R \times A$.[3,7,24]

Thermogravimetric analysis (TGA). The thermal stability of the cellulose and cellulose-MWCNTs fibers was investigated *via* TGA (Q5000 V3.15 Build 263).The heating rate of the TGA measurement is 10 ℃/min under nitrogen atmosphere. The gas flow rate was 30 mL/min. The dry fiber weight was given at the weight of 100 ℃.[14,22] The fiber decomposition temperature (T_d) was determined according to the 5 wt% loss weight of the dry fiber.[25]

Surface area. The surface area of cellulose-MWCNTs fibers was studied by an accelerated surface area and porosimetry system (ASAP 2460). Approximately 100 mg sample was placed into a long neck flask. The long neck flask together with the sample was sent to deaerate at 120 ℃ under the Nitrogen atmosphere for 6 h. After the deaeration, the long neck flask was connect with the equipment for surface area measurement using liquid nitrogen as cooling.

Mechanical property. The mechanical properties of cellulose and cellulose-MWCNTs fibers were measured by Dynamic Mechanical Analyzer (DMA Q800 V20.26 Build 45) at 30 ℃ (3 times repeat for each sample). The rate force and the upper force limit were 0.05 N/min and 18 N, respectively.

Scanning Electron Microscopy (SEM) Characterization. The SEM of cellulose and cellulose-MWCNTs fibers were observed by scanning electron microscopy (SU8000, Japan, 5.0 kV). The sample was sputtered with platinum for better observation using JEC-3000FC auto fine coater. The current and sputtering time were set to 20 mA and 30 s respectively.

Electrochemical property. The electrochemical property of cyclic voltammetry was characterized using a three electrodes cell. This setup is composed of a working electrode (Cellulose-MWCNTs fiber), a counter electrode (Pt filament) and a reference electrode (Ag filament). The electrodes were then immersed into an aqueous NaCl (0.1 M) and connected to an electrochemical workstation (CH Instruments, model CHI660E). The fiber was immersed in NaCl aqueous solution is about 2 cm. Cyclic voltammetry measurements were performed from −0.4 to +0.8 V at 10 mV/s scan rate.[7] The specific volumetric capacitance (C_{sp}) of the cellulose-MWCNTs fibers in a three-electrode cell was determined according to $C_{sp} = C_{electrode}/V_{fibre}$. The $C_{electrode}$ is the measured capacitance in the three-electrode configuration and V_{fibre} is the volume of the fiber used as the working electrode. The fiber is considered to be a cylinder to calculate its volume. $C_{electrode}$ was also can be calculated using the voltammetric charge integrated from cyclic voltammetry curves according to the formula 2.[26]

$$C_{electrode} = \frac{Q}{2V} = \frac{1}{2V\upsilon}\int_{V_-}^{V_+} i(V)dV \qquad (2)$$

where Q is the total voltammetric charge obtained by integrating the positive and negative sweeps (i(V) is the current) of a cyclic voltammetry curve, υ is the scan rate, and V ($V=V_+-V_-$) represents the scanned potential window.

3. Results and discussion

The rheological property of the cellulose solution and cellulose-MWCNTs mixtures is a significant parameter in the spinning. Figure 1 was indicated that the viscosity of spinning solutions increased with the increasing of MWCNTs quality. The spinning solutions were exhibited the shear thinning behavior, which is the typical property of non-Newtonian fluid. Figure 2 illustrated that the logarithmic curves of the shear stress (σ) and shear rate (r) show a good linear relationship. The non-Newtonian of n all about 0.6, which indicates an excellent potential for spinning.

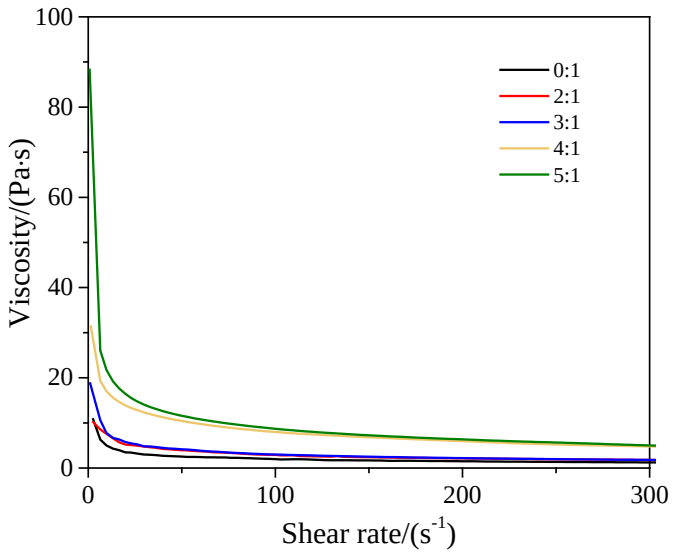

Figure 1 Dependence of apparent viscosity on shear rate of cellulose solution and cellulose-MWCNTs mixtures. 0:1 is the 1 wt% cellulose solution. 2:1, 3:1, 4:1 and 5:1 are the mass ratios of MWCNTs respect to cellulose.

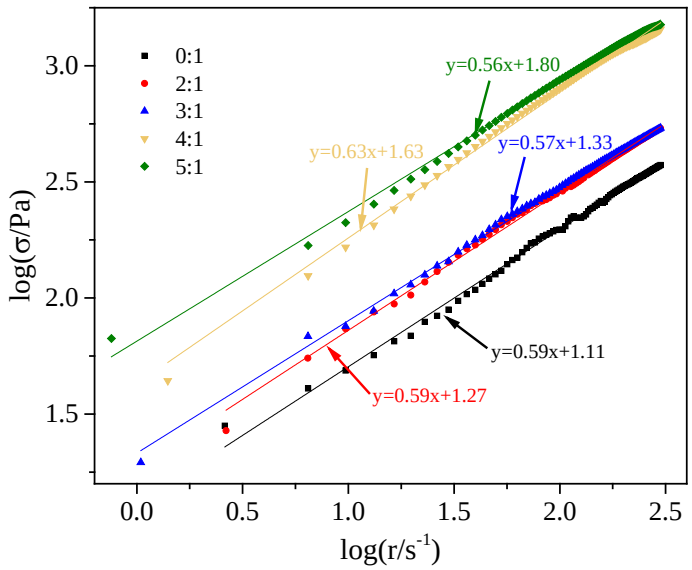

Figure 2 Dependence of logarithmic plots of shear stress vs shear rate of cellulose solution and cellulose-MWCNTs mixtures. 0:1 is the 1 wt% cellulose solution. 2:1, 3:1, 4:1 and 5:1 are the mass ratios of MWCNTs respect to cellulose.

The effects of MWCNTs amount, spinneret diameter and extrusion flow on the electrical conductivities of cellulose-MWCNTs fibers were shown in Figure 3(a) and 3(b). The conductivity cannot be measured by the used precision voltmeter at the ratio of MWCTs respect to cellulose of 1:1. Therefore, the ratio of the MWCNTs and cellulose start from 2:1 in this work. The electrical conductivity result indicate that with the increasing of MWCNTs amount, the conductivity increased obviously. The electrical conductivity range in this study is from 0.5 to 760 S/m approximately. The effect of the extrusion flow was investigated. The electrical conductivity has a significant increase from 0.01 to 0.4 ml/min at the ratio of 2:1 and 3:1 approximately, and an increase range from 0.01 to 0.2 ml/min at the ratio of 4:1 and 5:1. Then, the electrical conductivity has a relatively small variation. The spinneret diameter result illustrated that the diameter at 0.98 mm has a larger effect than 0.46 mm with the increase of extrusion flow at mass ratios of 2:1 and 3:1. When the mass ratios increased to 4:1 and 5:1, the smaller diameter makes a higher electrical conductivity.

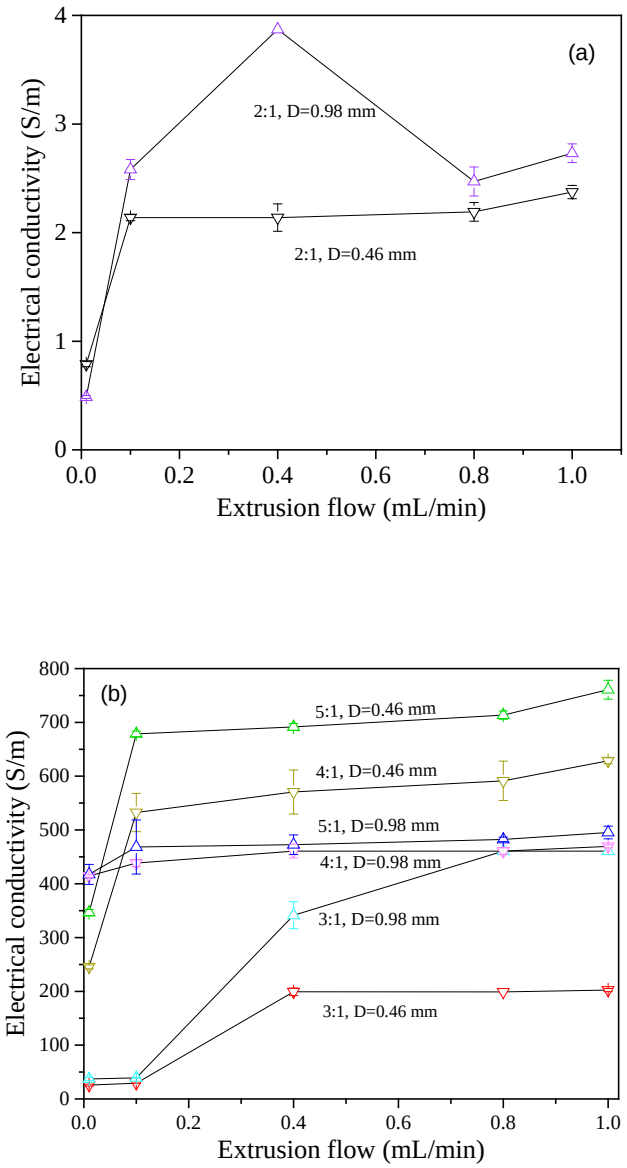

Figure 3 Electrical conductivities of MWCNTs-cellulose fibers at different MWCNTs amount, spinneret diameter and extrusion flow. (a) Electrical conductivities at the mass ratio of MWCNTs respect to cellulose of 2:1. (b) Electrical conductivities at the mass ratios of MWCNTs respect to cellulose of 3:1, 4:1 and 5:1.

The thermal stability of the cellulose solution and cellulose-MWCNTs mixtures were investigated via TGA. The extrusion flow in this TGA study was selected 1 mL/min under the excellent electrical conductivity. From Figure 4, it can be seen that at 500 ℃ and the spinneret needle diameters of 0.46 mm and 0.98 mm, the char yield of the

cellulose fiber was about 18 wt%, whereas those of the composite materials with the mass ratios of 2:1, 3:1, 4:1, and 5:1 of MWCNTs respect to cellulose were approximately of 63 wt%, 74 wt%, 79 wt% and 82%, respectively. This indicated that the char yield of the MWCNTs-cellulose fibers increased significantly with increasing appropriate amount of MWCNTs. This result was agree with xiao et al.[13] Figure 5 was the decomposition temperature of the studied fiber. It is the onset temperature at a 5 wt% weight loss of dry fibers. In the case of cellulose fiber, it can be found that the T_d was about 271 ℃ at the spinneret needle diameter of 0.98 mm, and about 281 ℃ at the spinneret needle diameter of 0.46 mm. On the other hand, the T_d of different ratios of MWCNTs-cellulose fibers at the spinneret needle diameter of 0.46 mm also higher than that of 0.98 mm, which evidenced that the fibers were more stable with a smaller spinneret needle parameter in the wet-spinning.

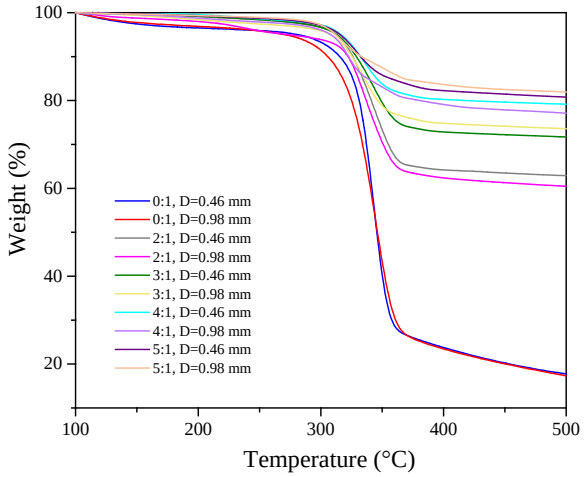

Figure 4 TGA of cellulose and MWCNTs-cellulose fibers. Extrusion flow of the TGA study is 1 mL/min. 0:1 is the 1 wt% cellulose solution. 2:1, 3:1, 4:1 and 5:1 are the ratios of MWCNTs respect to cellulose.

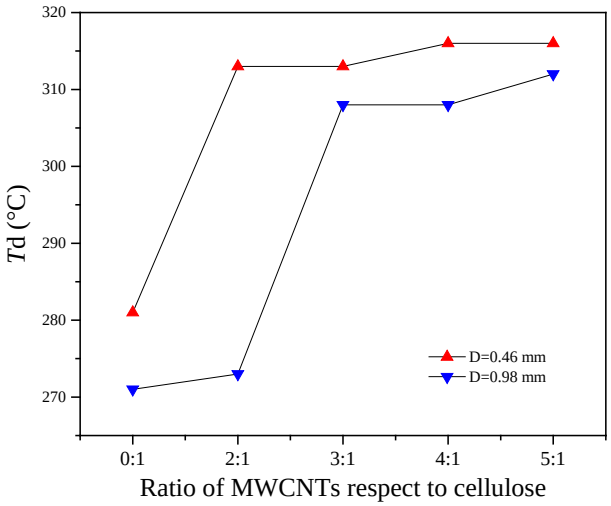

Figure 5 Decomposition temperature of cellulose and MWCNTs-cellulose fibers. Extrusion flow of the TGA study is 1 mL/min. 0:1 is the 1 wt% cellulose solution. 2:1, 3:1, 4:1 and 5:1 are the ratios of MWCNTs respect to cellulose.

Because the surface area of the cellulose fiber was difficult to measure in this work. The surface area only studied based on MWCNTs-cellulose fibers. Figure 6 is the surface area of MWCNTs-cellulose fibers at the extrusion flow of 1mL/min and different spinneret needle diameters. The result indicated that the fibers surface area increased with the increasing of the amount of MWCNTs. And the surface area was higher at the spinneret needle diameter of 0.98 mm than that of 0.46 mm. This result was consist with the TGA result that the fiber was more stable at the spinneret needle diameter of 0.46 mm. The previous surface area investigations of carbon fibers have been shown that carbon microfiber (<10 m^2/g) and CNTs-coated carbon fiber (34.6 m^2/g),[27] dry-spun MWCNTs fiber (100 m^2/g),[28] and wet-spun SWCNTs fiber (160 m^2/g).[29] In this work, the best surface area at spinneret needle diameters of 0.46 mm and 0.98 mm almost the same. It was approximately 188 m^2/g at the ratio of 5:1 of MWCNTs respect to cellulose. This result was better than the above previous studies.

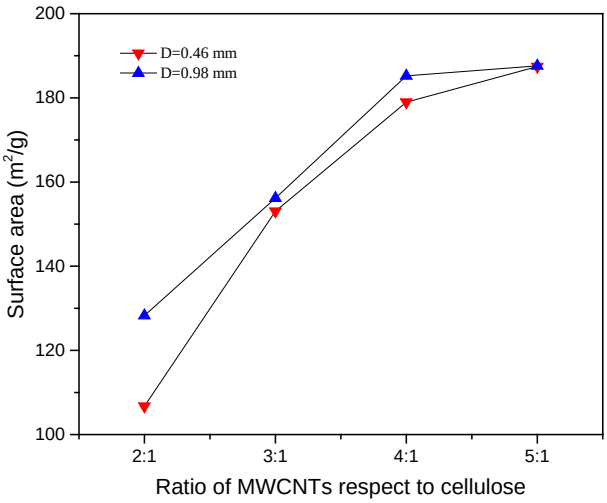

Figure 6 Surface area of MWCNTs-cellulose fibers at different extrusion flow of 1 mL/min and spinneret needle diameters of 0.46 mm and 0.98 mm. 2:1, 3:1, 4:1 and 5:1 are the mass ratios of MWCNTs respect to cellulose.

SEM images of original materials and spinning fibers were given in Figure 7 (a)-(h). Figure 7 (a) is the morphology of original MWCNTs. It is can be seen that the MWCNTs stacking and winding together with each other before the dispersion. After dispersion, the stacking of the MWCNTs in the surface of the MWCNTs-cellulose fiber almost disappear, and uniform winding with each other (e) or alignment in the fiber surface ((g)and (h)), which indicates that the selected EmimDep can promote MWCNTs dispersion and cellulose dissolution. The morphology original cotton pulp was shown in Figure 7 (b). After the cotton pulp (1 wt%) dissolved in EmimDep and with the spinning extrusion flow of 1 mL/min and spinneret diameter of 0.46 mm, the obvious creasing morphology can be seen in the surface of the cellulose fiber. This morphology was similar with the study of Qi et al.[30] When the mass ratio is 5:1, extrusion flow is 0.01 mL/min and spinneret diameter of 0.46 mm, some flat area (such as the blue square area in Figure 7 (f)) were formed in the surface of the fiber. These flat areas were contribute to two alignment MWCNTs morphology (Figure 7 (g) and (h)). According to the investigation of Zhu et al.[9] This alignment of the MWCNTs will decrease the fiber conductivity, which can be used to explain that the electrical conductivity is lower in the extrusion flow of 0.01 mL/min than 1 mL/min. The surface morphology of Figure

7 (e) shown that the pore structure was observed under SEM. This pore structure could be contribute to the surface area of the studied fiber.

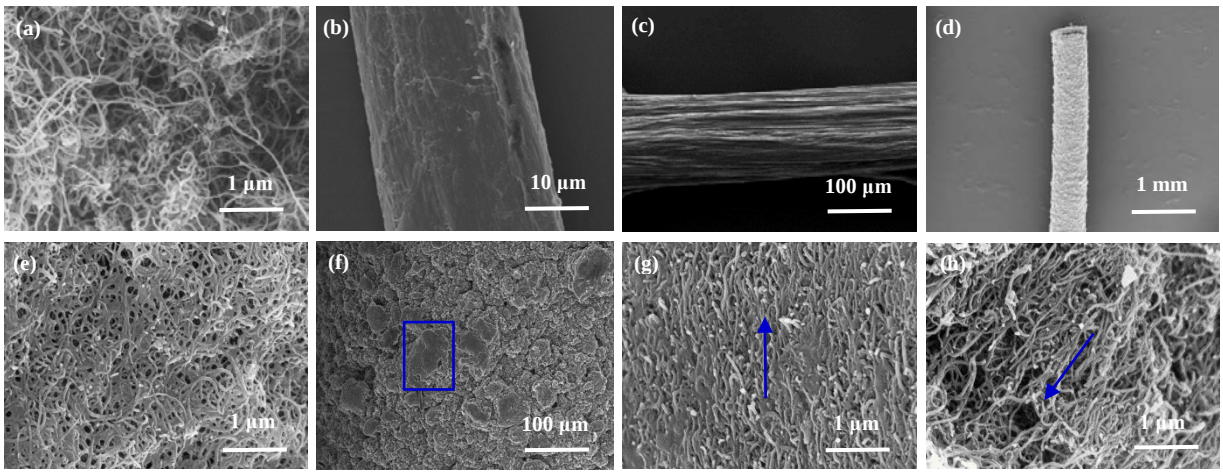

Figure 7 SEM of original material and spinning fiber. (a) Original MWCNTs. (b) Original cotton pulp. (c) 1 wt% cellulose fiber. Extrusion flow is 1 mL/min, diameter is 0.46 mm. (d) 5:1 MWCNTs-cellulose fiber (low magnification). Extrusion flow is 1 mL/min, spinneret diameter is 0.46 mm. (e) Morphology of 5:1 MWCNTs-cellulose fiber. Extrusion flow is 1 mL/min, diameter is 0.46 mm. (f), (g) and (h) Morphology of 5:1 MWCNTs-cellulose fiber. Extrusion flow is 0.01 mL/min, spinneret diameter is 0.46 mm.

Cyclic voltammetry curves of the investigated fibers are shown in Figure 8. The fibers were measured in aqueous NaCl 0.1 M at the scan rate of 10 mV/s. The extrusion flow for fabricating the fiber is 0.8 mL/min, the spinneret diameter is 0.46 mm. Figure 8 indicated that with the increase of the MWCNTs amount, the cyclic voltammetry curves were presented from spindle shape (2:1 and 3:1) to rectangular shape (4:1 to 5:1). The change shapes of the cyclic voltammetry curves illustrated that 4:1 and 5:1 MWCNTs-cellulose fibers have a good capacitive behavior than 2:1 and 3:1 MWCNTs-cellulose fibers.[31] The size of the cyclic voltammetry curve area was proportional to specific capacitance. Combining with the equation 2, the specific volumetric capacitances were acquired and shown in Figure 9. The result evidenced that the specific volumetric capacitances of the studied fibers were increased from 0.036 to 1.48 F/cm^3. However, comparing with the report of Qin et al,[31] the specific volumetric capacitance in this work is not so satisfactory.

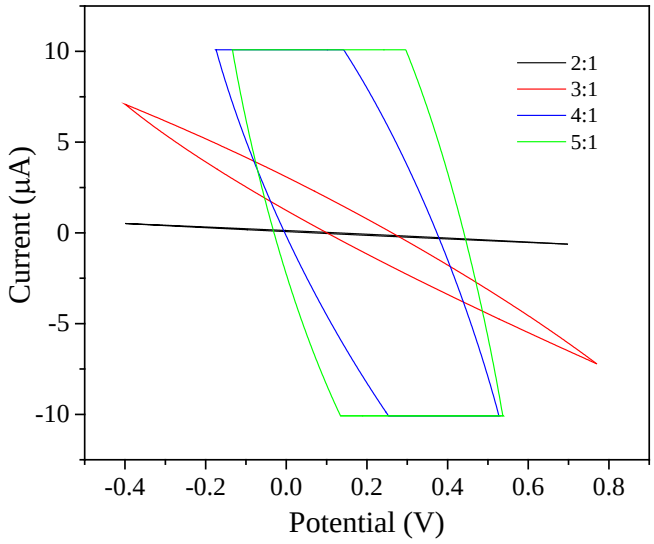

Figure 8 Cyclic voltammetry curves in aqueous NaCl 0.1 M at the scan rate of 10 mV/s. 2:1, 3:1, 4:1 and 5:1 are the mass ratios of MWCNTs respect to cellulose.

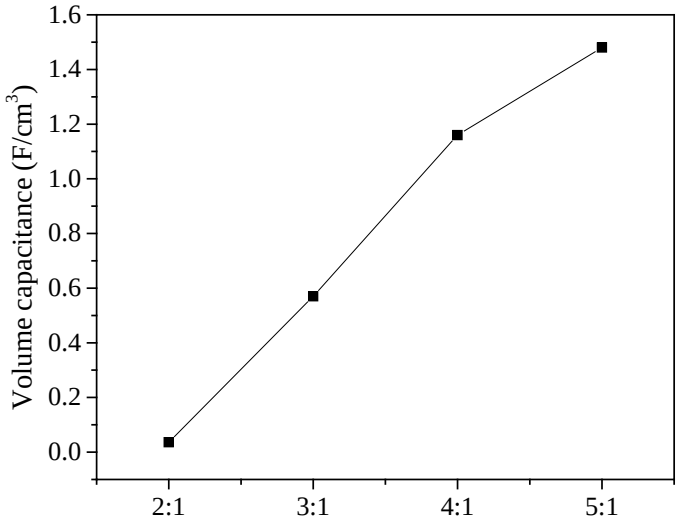

Figure 9 Specific volumetric capacitances of the studied fibers. 2:1, 3:1, 4:1 and 5:1 are the mass ratios of MWCNTs respect to cellulose.

Figure 10 indicates the slope of absorbance plotted against time of two reaction solution. The results shown that the ABTS and Myceliophthora thermophila which

prepared in deionized water has a slope of 2.1×10^{-4}. The ABTS and Myceliophthora thermophila prepared in EmimDep wash solution has a slope of 1.7×10^{-4}. This slope is close to 2.1×10^{-4}, which evidence that the remaining EmimDep is hardly affects the enzyme activity after 5 times washing of the fiber. The tensile strength of the studied fiber before and after the enzyme treated were given in Figure 11 (a and b). The results illustrated that the tensile strength was decreased with the increasing of MWCNTs on the fiber. And after the phenol and Myceliophthora thermophila treated, the fiber tensile strength was increased. This result was particularly significant for the 1 wt% cellulose fiber. This finding was agree with Ming et al[20]. In the report of Ming indicated that the tensile strength will be increased after hemp fiber treated by the composition which include the enzyme of Laccase. Although the mainly composition of the pulp is the cellulose, the phenol in this enzyme treatment solution might be play an important role for making the bridge of cellulose and enzyme.[32]

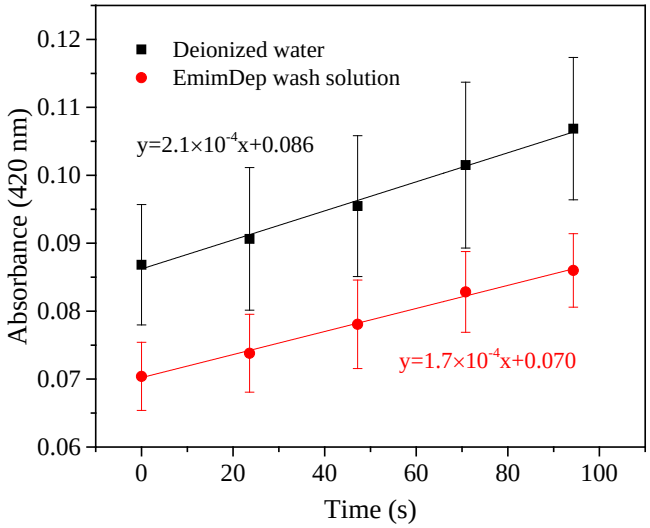

Figure 10 Absorbance plotted against time of two reaction solution of ABTS with enzyme prepared in deionized water and EmimDep wash solution.

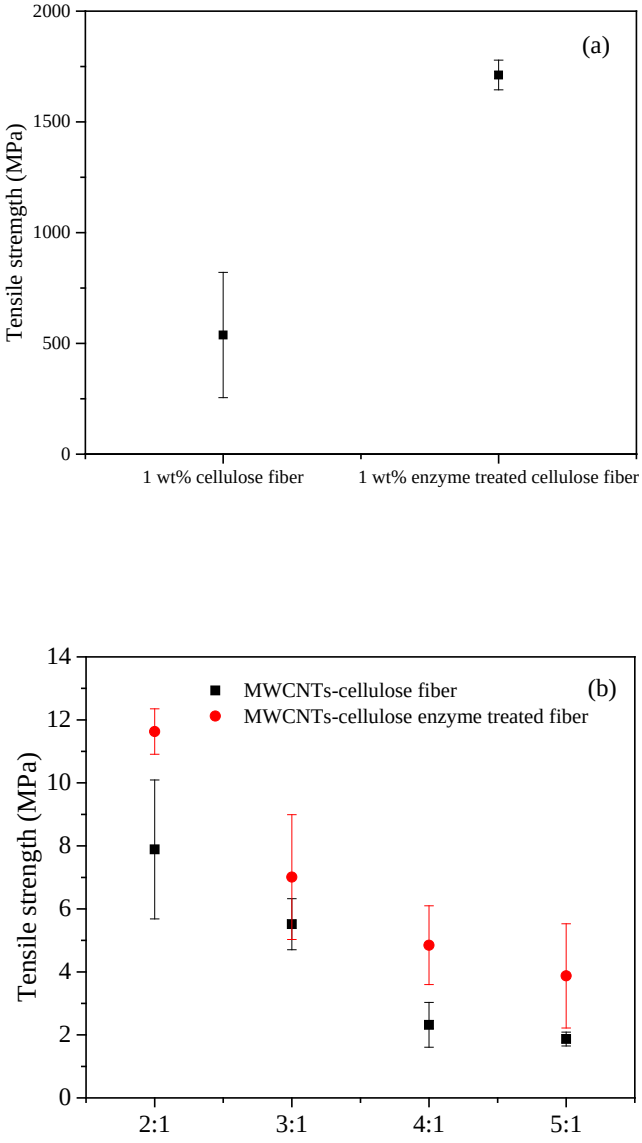

Figure 11 Tensile strength of cellulose and MWCNTs-cellulose fiber. (a) 1 wt% cellulose fiber and 1 wt% enzyme treated cellulose fiber. (b) MWCNTs-cellulose fiber and MWCNTs-cellulose enzyme treated fiber.

Conclusion

In this work, wet-spinning method was used for fabricating cellulose and conductive fibers. The studied material are cotton pulp, MWCNTs and EmimDep, together with the spinning parameters of extrusion flows in 0.01, 0.1, 0.4, 0.8 and 1 mL/min, and the

spinneret diameters at 0.46 mm and 0.98 mm. In the spinning solution, the mass percentage of cotton pulp in EmimDep is 1 wt% and the mass ratios of MWCNTs respect to cellulose are 2:1, 3:1, 4:1 and 5:1. The rheological analysis, electrical conductivity, TGA, surface area, SEM and electrochemical property were applied for measurement the properties of the spinning solution and the studied fiber. The results shown that the non-Newtonian of the spinning solutions are all about 0.6, which indicates a potential feature for spinning. The electrical conductivity measurement indicated that the extrusion flow, spinneret diameter and the mass ratio of MWCNTs can influence the fiber conductivity. The largest electrical conductivity acquired in this study is 760 S/m at the spinning parameters of 1 mL/min, 0.46 mm and 5:1 of MWCNTs respect to cellulose. TGA and surface area analyzed results illustrated that the fiber more stable at the spinneret diameter of 0.46 mm than 0.98 mm. The fiber surface area range is 107-188 m^2/g. SEM result shown that a pore structure can be observed in the surface of conductive fiber, and an alignment MWCNTs can be formed at the extrusion flow of 0.01 mL/min. This alignment MWCNTs will decrease the fiber electrical conductivity. Attribute to the lower specific volumetric capacitance of the fiber, it might be not suitable for energy storage. Based on the study of Neimark et al. This fiber might has the capable of absorbing liquids and vapors, [29] or applied in the cable field.

Acknowledgements

This work was supported by the Department of Chemical and Biochemical Engineering, Technical University of Denmark and General Program of National Natural Science Foundation of China (Grant No. 2157060191and 21776276).

References

1. Rapiphun Janmanee, Sopis Chuekachang, Saengrawee Sriwichai, Akira Baba, and Sukon Phanichphant. Functional Conducting Polymers in the Application of SPR Biosensors. *J. Nanotech.*, 2012, 2012, 1–7.
2. Tae-Won Lee, MiJeong Han, Sang-Eui Lee, Young Gyu Jeong. Electrically conductive and strong cellulose-based composite fibers reinforced with multiwalled

carbon nanotube containing multiple hydrogen bonding moiety. *Compos. Sci. Technol*., 2016, 123, 57–64.

3. Linda Hardelin, Bengt Hagstrom. Wet Spun Fibers from Solutions of Cellulose in an Ionic Liquid with Suspended Carbon Nanoparticles. *J. Appl. Polym. Sci.* 2015, 132, 41417–414113.

4. Farbod Alimohammadi, Mazeyar Parvinzadeh Gashti, Ali Shamei. A novel method for coating of carbon nanotube on cellulose fiber using 1,2,3,4-butanetetracarboxylic acid as a cross-linking agent. *Prog. Org. Coat*., 2012, 74, 470–478.

5. Ray H. Baughman, Anvar A. Zakhidov, Walt A. de Heer. Carbon Nanotubes--the Route Toward Applications. *Science*, 2002, 297, 787–792.

6. Farbod Alimohammadi, Mazeyar Parvinzadeh Gashti, Ali Shamei. Functional cellulose fibers via polycarboxylic acid/carbon nanotube composite coating. *J. Coat. Technol. Res*., 2013, 10, 123–132.

7. Anne-Sophie Michardière, Cintia Mateo-Mateo, Alain Derré, Miguel A. Correa-Duarte, Nicolas Mano, and Philippe Poulin. Carbon Nanotube Microfiber Actuators with Reduced Stress Relaxation. *J. Phys. Chem. C*, 2016, *120*, 6851−6858.

8. Rahatekar S. S., Rasheed A., Jain R., Zammarano M., Koziol K. K., Windle A. H., Gilman J. W., Kumar S.: Solution spinning of cellulose carbon nanotube composites using room temperature ionic liquids. *Polymer*, 2009, 50, 4577−4583.

9. C. Zhu, J. Chen, K. K. Koziol, J. W. Gilman, P. C. Trulove, S. S. Rahatekar. Effect of fibre spinning conditions on the electrical properties of cellulose and carbon nanotube composite fibres spun using ionic liquid as a benign solvent. *Express Polym. Lett*., 2014, 8, 154−163.

10. Zhao, Y. L.; Liu, X. M.; Wang, J. J.; Zhang, S. J. Insight into the Cosolvent Effect of Cellulose Dissolution in Imidazolium-Based Ionic Liquid Systems. *J. Phys. Chem. B*, 2013, 117, 9042−9049.

11. Ali K. Ghamsari, Scott Wicker, Eyassu Woldesenbet. Bucky syntactic foam; multi-

functional composite utilizing carbon nanotubes-ionic liquid hybrid. *Composites: Part B*. 2014, 67, 1–8.

12. Hao Zhang, Zhigang Wang, Zhinan Zhang, Jin Wu, Jun Zhang, and Jiasong He. Regenerated-Cellulose/Multiwalled-Carbon-Nanotube Composite Fibers with Enhanced Mechanical Properties Prepared with the Ionic Liquid 1-Allyl-3-methylimidazolium Chloride. *Adv. Mater.* 2007, 19, 698–704.
13. Wenjun Xiao, Tinghua Wu, Jiajian Peng, Ying Bai, Jiayun Li, Guoqiao Lai, Ying Wu, Lizong Dai. Preparation, Structure, and Properties of Chitosan/Cellulose/Multiwalled Carbon Nanotube Composite Membranes and Fibers. *J. Appl. Polym. Sci*. 2013, 128, 1193–1199.
14. Wenjun Wang, Yi Nie, Yanrong Liu, Lu Bai, Jinsen Gao, Suojiang Zhang, Preparation of Conductive Membranes by Ionic Liquids. *Fiber Polym.*, 2017, 18, 1780–1789.
15. Chenchen Zhu, Robert M. Richardson, Kevin D. Potter, Anastasia F. Koutsomitopoulou, Jeroen S. van Duijneveldt, Sheril R. Vincent, Nandula D. Wanasekara, Stephen J. Eichhorn, and Sameer S. Rahatekar. High Modulus Regenerated Cellulose Fibers Spun from a Low Molecular Weight Microcrystalline Cellulose Solution. *ACS Sustainable Chem. Eng.*, 2016, 4, 4545−4553.
16. Yan Rong Liu, Kaj Thomsen, Yi Nie, Suo Jiang Zhang and Anne S. Meyer. Predictive screening of ionic liquids for dissolving cellulose and experimental verification. *Green Chem.*, 2016, 18, 6246–6254.
17. Yanrong Liu, Anne S. Meyer, Yi Nie, Suojiang Zhang, Yongsheng Zhao, Philip L. Fosbøl, and Kaj Thomsen. Freezing point determination of water-ionic liquid mixtures. *J. Chem. Eng. Data*, 2017, 62, 2374−2383.
18. Lauri K. J. Hauru, Michael Hummel, Anne Michud, Herbert Sixta. Dry jet-wet spinning of strong cellulose filaments from ionic liquid solution. *Cellulose*, 2014, 21, 4471–4481.
19. Zhiqiang Luo, Aiqing Wang, Chunzheng Wang, Weichao Qin, Ningning Zhao, Hongzan Song and Jungang Gao. Liquid Crystalline Phase Behavior and Fiber

Spinning of Cellulose/Ionic Liquid/Halloysite Nanotubes Dispersions. *J. Mater. Chem. A*, 2014, 2, 7327–7336.

20. Ming Liu, Andreas Baum, Jürgen Odermatt, Jens Berger, Liyun Yu, Birgitte Zeuner, Anders Thygesen, Jesper Holck, Anne S. Meyer. Oxidation of lignin in hemp fibres by laccase: Effects on mechanical properties of hemp fibres and unidirectional fibre/epoxy composites. *Composites: Part A*, 2017, 95, 377–387.

21. Airong Li, Yue Zhu, Liang Xu, Wenqing Zhu and Xingjun Tian. Comparative study on the determination of assay for laccase of Trametes sp. *Afr. J. Biochem. Res.*, 2008, 2, 181–183.

22. Xue Liu, Yi Nie, Xianglei Meng, Zhenlei Zhang, Xiangping Zhang and Suojiang Zhang. DBN-based ionic liquids with high capability for the dissolution of wool keratin. *RSC Adv.*, 2017, 7, 1981–1988.

23. Y. Zhang , X. Tu , D. Li, H. Wang. Effect of Polymerization Conditions on the Rheological Behavior of Acrylic Polymer Solutions with 1-Butyl-3-Methylimidazolium Tetrafluoroborate as Solvent. *Polymer-Plastics Technol. Eng.*, 2008, 47, 688–691.

24. A. I. S. Neves, T. H. Bointon, L. V. Melo1, S. Russo, I. de Schrijver, M. F. Craciun & H. Alves. Transparent conductive graphene textile fibers. *Sci. Rep.*, 2015, 5, 9866; doi: 10.1038/srep09866.

25. Shuangshuang Zheng, Yi Nie, Suojiang Zhang, Xiangping Zhang and Lijun Wang. Highly Efficient Dissolution of Wool Keratin by Dimethylphosphate Ionic Liquids. *ACS Sustainable Chem. Eng.*, 2015, 3, 2925−2932.

26. Dingshan Yu, Kunli Goh, Hong Wang, Li Wei, Wenchao Jiang, Qiang Zhang, Liming Dai and Yuan Chen. Scalable synthesis of hierarchically structured carbon nanotube–graphene fibres for capacitive energy storage. *Nat. nanotechnol.*, 2014, 9, 555–562.

27. Xueyan Zhao, Xin Lu, William T.Y. Tze, Ping Wang. A single carbon fiber microelectrode with branching carbon nanotubes for bioelectrochemical processes. *Biosens. Bioelectron*., 2010, 25, 2343–2350.

28. Xuli Chen, Longbin Qiu, Jing Ren, Guozhen Guan, Huijuan Lin, Zhitao Zhang, Peining Chen, Yonggang Wang, and Huisheng Peng. Novel Electric Double-Layer Capacitor with a Coaxial Fiber Structure. *Adv. Mater.* 2013, 25, 6436–6441.

29. Alexander V. Neimark, Sigrid Ruetsch, Konstantin G. Kornev, and Peter I. Ravikovitch. Hierarchical Pore Structure and Wetting Properties of Single-Wall Carbon Nanotube Fibers. *Nano Lett.*, 2003, 3, 419–423.

30. Haisong Qi, Jianwen Liu and Edith Mäder. Smart Cellulose Fibers Coated with Carbon Nanotube Networks. *Fibers*, 2014, 2, 295–307.

31. Tianfeng Qin, Shanglong Peng, Jiaxin Hao, Yuxiang Wen, Zilei Wang, Xuefeng Wang, Deyan He, Jiachi Zhang, Juan Hou, and Guozhong Cao. Flexible and Wearable All-Solid-State Supercapacitors with Ultrahigh Energy Density Based on a Carbon Fiber Fabric Electrode. *Adv. Energy Mater.*, 10.1002/aenm.201700409.

32. Jacob Podschun, Alexander Stücker, Rosanna I. Buchholz, Martina Heitmann, Andreas Schreiber, Bodo Saake, and Ralph Lehnen. Phenolated Lignins as Reactive Precursors in Wood Veneer and Particleboard Adhesion. *Ind. Eng. Chem. Res.*, 2016, 55, 5231−5237.